Uncertainty Quantification in Dynamical System Design using Reduced Order Models

By

Matthew Scott Bonney

A dissertation submitted in partial fulfillment of the requirements for the degree of

Doctor Of Philosophy

(Engineering Mechanics)

at the

University of Wisconsin-Madison

2017

Date of final oral examination: 5/31/2017
The dissertation is approved by the following members of the Final Oral Committee:

Daniel Kammer, Professor, Engineering Physics

Michael Plesha, Professor Emeritus, Engineering Physics

Matthew Allen, Associate Professor, Engineering Physics

Roderic Lakes, Professor, Engineering Physics

Roxann Engelstad, Professor, Mechanical Engineering

ABBREVIATIONS

ROM	Reduced Order Model
MC	Monte-Carlo
UQ	Uncertainty Quantification
LHC	Latin Hypercube
CB	Craig-Bampton
DOF	Degree of Freedom
CC	Craig-Chang
POD	Principal Orthogonal Decomposition
SVD	Singular Value Decomposition
MCMC	Markov-Chain Monte-Carlo
SROM	Stochastic Reduced Order Model
PC	Polynomial Chaos
PROM	Parameterized Reduced Order Model
FE	Finite Element
HD	Hyper-Dual
HDM	Hyper-Dual Meta-Model
MEA	Non-Parametric Maximum Entropy Approach
CMS	Component Mode Synthesis
BRB	Brake-Reuß Beam
RMS	Root-Mean-Square
GTMS	Glass-to-Metal Seal
EL	Empirical Negative log-likelihood
KLE	Karhunen-Loève Expansion
DIC	Digital Image Correlation

LIST OF FIGURES

LIST OF TABLES

CONTENTS

EXECUTIVE SUMMARY

During the traditional aerospace design process, large variability is commonly experienced due to design optimization techniques. These changes can have a large effect on both the system design and the production. One particular aspect of interest is the effect of machining precision on the desired output. Large aerospace systems tend to have thin components, thus making the machining tolerance more important. Machining tolerance build-up can lead to possible failures and thus requires the quantification of the uncertainty to ensure a safe design and to determine the probability of possible failure.

One way to characterize and quantify the uncertainty of the design is in the use of numerical models. Using these numerical models utilize both physical parameters as well as mathematical adjustment factors to account for the unknown physics of the system. One possible method to increase the accuracy is to perform a model calibration for the particular system for a physically testable case. These types of tests include modal characterization and ground vibration tests. One commonly used algorithm in this model calibration is the use of gradient based optimization. The calculation of these gradients is a very computationally expensive procedure. Using hyper-dual numbers to determine these numerical derivatives is able to calculate these exactly with a single code evaluation. This is compared to the approximation of the finite difference, which introduces multiple types of errors through the use of multiple code evaluations. Three of the most commonly used methods to generate numerical derivatives are compared for a simple mathematical function as well as a simple finite element model. The mathematical function shows that the hyper-dual

step is the most accurate method among those tested for the first two derivatives. This trend is expected to be true for higher order derivatives but was not tested. Due to the novelty of the hyper-dual step, some special considerations are needed when implemented into a finite element model. These considerations are shown and the results are also shown for both material variations and geometric variations.

In order to perform uncertainty quantification, typically multiple code evaluations is required. One way to reduce this large computational burden is with the used of parameterized reduced order models, or surrogate models. These models are able to provide accurate results at a fraction of the time. Typically, these are generated with high-fidelity code evaluations that incorporate information about the response space in order to be parameterized. This is done by including information about the derivatives or by the use of multiple evaluations in the design space. One novel model of interest is the hyper-dual meta-model. This uses the exact derivative information at multiple design space locations to provide an information rich surrogate model with very few model evaluations. These methods are compared for three different systems with both material variations as well as geometric variation, and are also very useful for model calibration. In addition to calibration, the methods are useful for uncertainty distribution propagation to greatly reduce the computational cost for these models.

During the design process, many engineering judgments are introduced. One of the major considerations is the type of numerical model to use. These choices can include type of finite element or how to model the material or joints. Since these choices can lead to very different results, a quantitative measure on how the choices affect the accuracy is desired. One possible method to characterize this model form error is presented and utilized. This method incorporates random matrices into the mechanical system to produce a stochastic model that has physically significant bounds, such as positive mass. These random matrices are generate non-parametrically

by a maximum entropy approach. The determination of these matrices are only constricted to physical bounds, such as positive mass, and the assumption that the nominal model is the mean of the random matrix. Using experimental data, the variance of the random matrix can be calibrated to give an estimate on the model form error. The more accurate the model, the lower the expected value of the variance for the random matrices. This method to determine the model form error is performed on four systems: one is a concentric glass-to-metal seal, while the other three are related to a substructured system with two components. The glass-to-metal seal uses temperature dependent, linear elastic material properties and is compared to experimentally derived material properties. This analysis uses the residual stress profile on the surface as validation data. The substructuring system uses the first 11 natural frequencies as validation data. This analysis is used to investigate the model reduction/synthesis technique and modal truncation.

Using the non-parametric maximum entropy approach can determine both the model form error along with a separate determination for parametric errors. This requires a large amount of computational resources due to the multiple MC simulations required. In order to reduce this burden, the use of a surrogate model is almost necessary. This final chapter implements the hyper-dual meta-model for the panel system to determine both parametric variance and model form error. The main difficulty is the additional truth data that is required. Independent data sets are required and can be either a scalar value or a vector of scalars. For this analysis, the Frobenius norm of the stiffness matrix and the first ten natural frequencies are used. This analysis shows a preliminary attempt of this specific analysis. Further work must be done on this analysis to ensure validity of the results.

1. INTRODUCTION

1.1 Motivation

Aerospace systems undergo a very long design cycle that can span many years. During this design process, individual components and as well as the entire system are dependent on computer modeling in order to test new designs and environments. This is due to the fact that typical environments, such as zero gravity, are impossible or very expensive to test physically. The use of a computational model allows for these such situations to be tested, ensuring the safety of the system and passengers. These models are used throughout the entire design process. A typical aerospace design process can be visualized in the flow chart in Figure 1.1. This flow chart is primarily focused on the analysis of a given design.

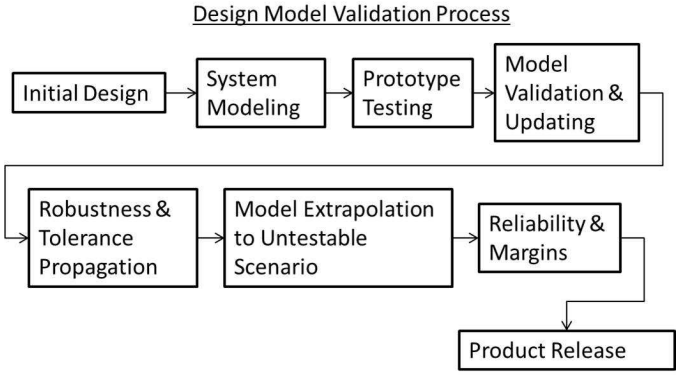

Figure 1.1: Typical Aerospace Design/Verification Process

Within the initial design phase, there can be large changes to the system, either to ensure performance or to reduce total cost of the system. This is predominate in a design analysis such as topology optimization [1], which adjusts the geometry automatically to produce a more optimal

design. Due to this optimization, large changes in the geometry can be introduced. This causes a highly nonlinear response surface that must be optimized. Even when the response is nonlinear, the models used in the analysis are typically linear models that are quick to compute since many evaluations are required.

Once an initial design is selected, a more in depth analysis is performed to ensure that the model is accurate. This further analysis typically involves nonlinear elements within the model. These elements can be based on nonlinear physics or material characteristics. This is important since the typical materials used in aerospace components, in recent designs, are composites. These can exhibit non-homogeneous, non-orthotropic, or nonlinear material behavior, such as elastic-plastic or stress relaxation.

Since the systems of interest are typically very large, performing the nonlinear analysis on the entire system, and still maintaining all the important physics, is usually infeasible or impracticable. A common strategy when designing aerospace systems is to hire contractors to build specific components, such as an engine. Doing so reduces the design time-line and overall costs. While this reduces cost, the contractors typically do not provide the component model in full form for one of several reasons: proprietary information/materials, too large for data transfer, or the use of custom software that is unavailable outside the contracting firm. When a system is built like this, the method of substructuring and reduced order models (ROMs) are used. Using these techniques allow for quick and accurate system level evaluations. However, the steps in substructuring produce errors compared to the physical system. A flow chart of the step of substructuring and the induced errors at each step is pictured in Figure 1.2.

Another advantage that substructuring introduces is the ability to validate the models at the component level. Performing these tests and validating the model is very important for safety and to ensure that the predictions are accurate. This can also give an estimate of parametric errors that can

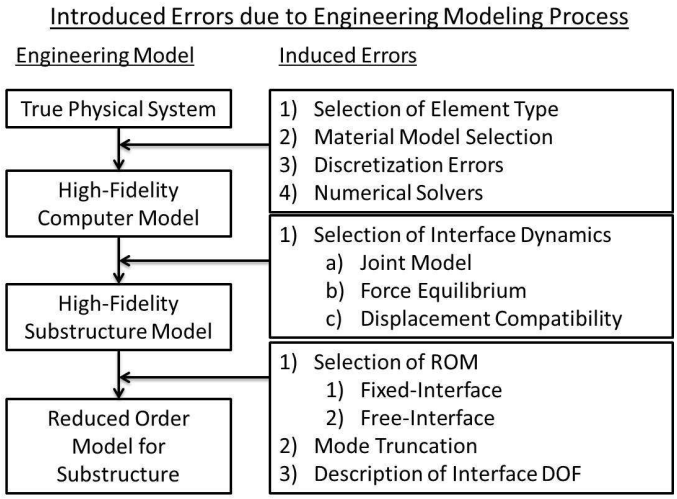

Figure 1.2: The Induced Errors of Substructuring

be used to propagate into the full system to get evidence based reliability information. During this validation process, the computational model can be adjusted to give a more accurate result. This change can be due to small variability in the material properties or the machining precision. During this updating process, large changes in the response can occur due to the nonlinear behavior of the system or the model. Since there are many inputs into a computational model, this calibration can be computationally expensive. In order to reduce the computational time, a surrogate model can be used. A surrogate model is similar to a ROM, but typically is based purely on the mathematics of the response and does not incorporate any physics of the system, which ROMs often do.

The calibration of the computational model can be classified into one of two categories, deterministic or stochastic. This is important during the consideration of the model inputs and is typically driven by the experimental data available. If a component can be made and tested multiple times, this will lead to a distribution of the output parameters due to known and unknown variabilities. When a distribution is available on the output, a stochastic calibration can lead to a more accurate model since it considers the variability of the physical system, due to factors such as machining tolerances. This is not always available and thus a deterministic calibration can give

reasonable results for a nominal or mean system. Since the components in aerospace systems are expensive and complicated to build, the deterministic calibration is typically performed.

Once the model has been properly updated and validated, the next step in the design process is to evaluate the robustness of the model. Since a machine cannot measure to infinite precision, there are slight differences that can result in an unsafe system due to tolerance build-up. Doing this on the component level and propagating this build-up into the full system can produce unintended, sometimes unsafe, results. There are several methods of doing this analysis, but for ease of use, a Monte-Carlo (MC) analysis is typically used along with a validated surrogate model or ROM.

While looking at the effects of robustness in the model, the type of the major error should be investigated and possible reduced. There are many types of errors that come from two main types of uncertainty. A visualization of one classification of these errors can be found in Figure 1.3. The first type of error is the variability on the measurements during the testing of the system. This occurs from signal processing, uncertain forcing, and human errors. Model form errors comes the choices that the engineer makes in the creation of the model used. This error can be reduced by using a physics appropriate model. While this is not always possible, a nonlinear model will typically produce less model form error as compared to a linear model since it better represents the physical system. Parametric error comes from the variability of the inputs of the model. This can be due to environmental factors, like temperature and humidity, or from uncertain material properties. The predictive error is associated with the errors that come from extrapolation or interpolation of the model. Since the validation is done on testable scenarios, when the model is used to predict untested events, such as cycle failure, there is an error that occurs. Each of the errors discussed arise from two types of uncertainty: aleatoric and epistemic. Aleatoric is the un-reducible uncertainty since it contains the natural variability of the system. Epistemic is the reducible uncertainty that comes from lack of knowledge. Examples of this uncertainty would be

using a linear model as compared to a nonlinear model, or poor instrumentation locations.

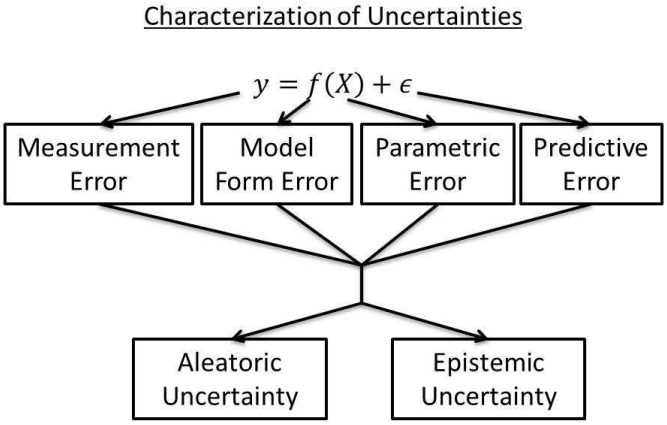

Figure 1.3: Characterization of Multiple Sources of Error

The understanding of these errors is very important for aerospace systems. One of the main reasons why this quantification and knowledge is important is due to the high cost of failure. Since many of the aerospace systems contain human passengers or required supplies, a failure in operation can cost lives if the system is not designed properly. This is why the aerospace field heavily relies on the computational models and Uncertainty Quantification (UQ) techniques in the design process. Different industries, such as the automobile industry, might have a different dependence on computational model. This is done by incorporating historical data or simple prototypes that can be tested for all expected environments.

The remainder of this chapter is organized as follows. Section 1.2 describes several methods of reducing the computational burden of running a code evaluation. This describes the fixed-interface reduction, the free-interface reduction, and the principal orthogonal decomposition (POD). Section 1.3 describes different methods to represent a distribution and how to sample it. This section describes the basic MC analysis, a reduced sampling method Latin Hypercube (LHC), and a method to select an optimal subset of samples to best represent the distribution. Section 1.4 describes a variety of state-of-the-art UQ methods that are not utilized in this dissertation. The

organization of the remainder of the dissertation is described in Section 1.5.

The work that is presented in this dissertation presents a collection of work that introduces novel advancements to established techniques and discovers new methodologies. This work utilizes hyper-dual (HD) numbers for the use in uncertainty quantification (UQ) of structural dynamics. These have been used for various other topics by other researchers, but the use within structural dynamics is novel and unique. The main new technique introduced in this work is the hyper-dual meta-model (HDM). This takes the advantages of other various parameterized reduced order modeling techniques and combines them into a single method to greatly increase the accuracy over a large variability range. Along with the parametric uncertainty, the study of model form error is also investigated. This study looked at the modeling choices of a reduced order model and in particular for substructuring type analysis. To the author's knowledge, no previous study has been done to propagate this model form error from a substructures into a synthesized system using the characterization used in this dissertation. Along with the propagation, this work also introduces the use of the empirical likelihood function into the determination of the optimal dispersion parameter in order to increase the repeatability and reduce the effect of the sampling technique.

1.2 Background and Theory - Reduced Order Models

Performing system level analysis on aerospace systems can be very computationally expensive. One commonly used technique to reduce this burden is to use a ROM or surrogate model. Both of these techniques are used in almost exactly the same way but with some nomenclature differences. A ROM refers to a reduction that uses the physics of the system to reduce the size of the system. Two examples of ROMs are presented in Sections 1.2.1 and 1.2.2. A surrogate model refers to a mathematical reduction of the system. These type of reductions do not depend on the type of system and is studied primarily in data science and electronic systems, but can be very useful for

model calibration and UQ techniques. One example is presented in Section 1.2.3.

1.2.1 Craig-Bampton/Fixed-Interface Reduction

The Craig-Bamption (CB) representation is a mixed coordinate system that contains fixed-interface modal degrees of freedom (DOF) and physical interface DOF together [2]. The method presented in this section is called the primal formulation in [3]. There are two different approaches to forming the ROMs. In [3], Rixen uses a Lagrange multiplier technique and in [4], Craig uses a more physical approach. This section uses the more physical approach taken by Craig. The displacement vector takes the form of $u = [\eta \;\; u_j]^T$ where η is the fixed-interface modal DOF and u_j are the physical interface displacement DOF. This representation allows for a truncation of the fixed-interface modal DOF according to frequency or desired mode shapes [5]. Performing this truncation can greatly decrease the size of the subsystem if there are only a few interface DOF. The transformation of the displacement from the full subsystem to the CB representation is given by

$$\begin{bmatrix} u_i \\ u_j \end{bmatrix} = \begin{bmatrix} \hat{\Phi} & \Psi_c \\ 0 & I \end{bmatrix} \begin{bmatrix} \eta \\ u_j \end{bmatrix} = T_{cb}\, u_{cb}, \tag{1.1}$$

where u_i are the interior physical DOF and $\hat{\Phi}$ are the kept fixed-interface modes that are mass normalized. Ψ_c is the constraint modes, which is the displacement of the interior DOF due to a unit deflection at one of the interface DOF and maintaining zero deflection at the other interface DOF, 0 is a matrix of zeros, and I is an identity matrix. The constraint modes are generated geometrically by

$$\Psi_c = -K_{ii}^{-1} K_{ij}, \tag{1.2}$$

with the subscript i corresponds to the interior DOF and the subscript j corresponds to the interface DOF. This transformation matrix, T_{cb}, is a non-square transformation that can be applied to the equations of motion by the mass and stiffness matrix, given by

$$\hat{M} = T_{cb}^T \, M \, T_{cb}. \tag{1.3}$$

This transformation is applied for both substructures individually. Once the mass and stiffness matrices are generated, the uncoupled full system matrices are generated and take the form of

$$M_{uncoupled} = \begin{bmatrix} \hat{M}^\alpha & 0 \\ 0 & \hat{M}^\beta \end{bmatrix}, \tag{1.4}$$

where the superscripts α and β corresponds to an individual substructure. At this point, the full system is not formed yet, so a coupling synthesis matrix must be applied. The simplicity of this synthesis matrix is one of the strengths of the CB representation. This coupling synthesis matrix is given in terms of a coordinate system transformation

$$\begin{bmatrix} \eta^\alpha \\ u_j^\alpha \\ \eta^\beta \\ u_j^\beta \end{bmatrix} = \begin{bmatrix} I & 0 & 0 \\ 0 & 0 & I \\ 0 & I & 0 \\ 0 & 0 & I \end{bmatrix} \begin{bmatrix} \eta^\alpha \\ \eta^\beta \\ u_j \end{bmatrix} = S_{cb} \, u_{cbs}, \tag{1.5}$$

where S_{cb} is the coupling synthesis matrix. The synthesis enforces displacement compatibility, such that $u_j^\alpha = u_j^\beta = u_j$. This coupling synthesis matrix is then applied to the uncoupled equations of motion and takes the form

$$M_{system} = S_{cb}^T \, M_{uncoupled} \, S_{cb}. \tag{1.6}$$

This coupling technique is performed on all of the system matrices. For the linear undamped systems, the equations of motion of the synthesized system is written as

$$M_{system}\,\ddot{u}_{cbs} + K_{system}\,u_{cbs} = 0. \tag{1.7}$$

1.2.2 Craig-Chang/Free-Interface Reduction

The CB method uses fixed-interface modes as the DOF that are reduced. In the Craig-Change (CC) formulation, free-interface modes are the modal DOF that are used. Using free-interface modal DOF can also be used for method such as the ones used by MacNeal [6] and Rubin [7]. These use physical displacement interface DOF while the CC method [8] uses the interface forces. The same DOF are used in the dual formulation of CB substructures introduced by Rixen in [9] while only enforcing force equilibrium at the interface. CC enforces force equilibrium and displacement compatibility at the interface.

While the coupling synthesis matrix is simple for CB synthesis, the interface still has each physical DOF that it originally had before the synthesis. If there are a large number of interface DOF, then the CB representation will still have a large computational burden. The CC representation eliminates the interface DOF in the synthesized system. This representation is produced with the free-interface modes along with residual attachment modes as presented in [8]. The transformation from physical DOF to a CC DOF set is given by

$$\begin{bmatrix} u_i \\ \\ u_j \end{bmatrix} = \begin{bmatrix} \Phi_k & \Psi_d \end{bmatrix} \begin{bmatrix} P_i \\ \\ P_j \end{bmatrix} = T_{cc}\,u_{cc}, \tag{1.8}$$

where Φ_k are the kept free-interface modes that are mass normalized, Ψ_d are the residual attachment modes, P_i are the free-interface modal coordinates, and P_j are the interface generalized coordinates

that correspond to the force at each DOF on the interface. The free-interface modes are the normal modes when the interface is unconstrained. These modes contain the rigid body motion. The residual attachment modes are the response to a unit force at a single interface DOF and are linearly independent of the free-interface modes. To ensure linear independence, the residual attachment modes are derived based on the residual flexibility matrix which can be expressed as

$$G^d = K^{-1} - \Phi_k \Lambda_k^{-1} \Phi_k^T, \tag{1.9}$$

where G^d is the residual flexibility matrix, K is the physical stiffness matrix, and Λ_k^{-1} is a diagonal matrix containing the inverse of the eigenvalues of the free-interface modes. One complication of this method is the inverse of the stiffness matrix. For a system that contains rigid body motion, this stiffness matrix is singular, which implies that the inverse of the matrix does not exist. One method to eliminate this effect is with the use of oblique projectors [10]. These project the stiffness matrix onto a non-singular domain, allowing the inverse to exist. Mathematically, this is expressed in [11] and the implementation for structural dynamics is expressed in [12]. The residual attachment modes can be written in terms of the residual flexibility matrix via

$$\Psi_d = \begin{bmatrix} \\ G_{ij}^d \\ \\ \\ G_{jj}^d \\ \\ \end{bmatrix}. \tag{1.10}$$

With this transformation matrix, the equations of motion can be transformed into the new coordinates by

$$\hat{M} = T_{cc}^T \, M \, T_{cc}. \tag{1.11}$$

This can then be performed for both substructures and then combined using the same method as the CB representation. The only difference is the coupling synthesis matrix. The coupling synthesis matrix is given by

$$\begin{bmatrix} P_j^\alpha \\ P_j^\beta \\ P_i^\alpha \\ P_i^\beta \end{bmatrix} = \begin{bmatrix} -(\Psi_{dj}^\alpha + \Psi_{dj}^\beta)^{-1}\, \Phi_{kj}^\alpha & (\Psi_{dj}^\alpha + \Psi_{dj}^\beta)^{-1}\, \Phi_{kj}^\beta \\ (\Psi_{dj}^\alpha + \Psi_{dj}^\beta)^{-1}\, \Phi_{kj}^\alpha & -(\Psi_{dj}^\alpha + \Psi_{dj}^\beta)^{-1}\, \Phi_{kj}^\beta \\ I & 0 \\ 0 & I \end{bmatrix} \begin{bmatrix} P_i^\alpha \\ P_i^\beta \end{bmatrix} = S_{cc}\, u_{ccs}, \tag{1.12}$$

where the subscript j refers to the row partition of the matrix to the interface DOF. The CC synthesis enforces both displacement compatibility and force equilibrium. This coupling synthesis matrix is then applied to the uncoupled equations of motion in the form of

$$M_{system} = S_{cc}^T\, M_{uncoupled}\, S_{cc}. \tag{1.13}$$

The advantage of using this method compared to the CB is that the synthesized system only contains DOF in the modal domain, with no interface DOF. The disadvantage is that the formulation of the attachment modes is more complicated since it requires taking the inverse of the stiffness matrix, which can be computationally expensive.

Both the CC and CB methods are able to produce accurate results. The accuracy of each method is varied based on the system of interest. For example, fixed-interface methods produce the best results when substructures are flexible and are rigidly connected together. The free-interface reduction can still produce accurate results but can require more kept modes for the same system. Using the CC method can effective for systems that have little mass at the interface or a large interface area.

1.2.3 Principal Orthogonal Decomposition

The POD is a mathematical tool to represent data in a way that is able to be truncated and reduced. A review of this method using some geometric representations and example systems can be seen in [13]. In essence, POD is a method to represent data as a collection of orthogonal vectors. The discrete version of this is called the singular value decomposition (SVD), with the literature interchanging these names at will.

POD decomposes an array of information into a collection of three matrices of the form

$$A = \Sigma D V^T, \tag{1.14}$$

where A is a collection of information such as a state matrix or responses, Σ and V are collections of orthonormal vectors, and D is a diagonal matrix of singular values. These singular values corresponds to the importance of each vector to the reconstruction of the full matrix. There is a lot of information that can be gathered from this decomposition as well as being able to reduce the system. The first piece of information observed is that the number of non-zero terms in the diagonal matrix D corresponds to the rank of the matrix A. Along with the rank, the D matrix can be truncated based on the non-zero terms. These terms can be neglected and thus the vector that the value represents can be removed. Doing this decreases the memory requires to store the information. The SVD can also give a simplified method to determine the inverse of the matrix A.

Another interesting aspect of the SVD is that if the matrix A is a symmetric real matrix, such as the mechanical stiffness matrix. For this type of matrix, the collection of vectors, Σ and V, are the same and corresponds to the eigenvectors of the matrix. When parameterizing a POD system, it is possible to only parameterize the singular values. If the parameterization does not affect the orthogonal vectors, or similarly in a dynamic system's mode shapes, then the parameterization can

be performed only on the singular values [14]. This is a potentially large reduction in computational cost in a perturbation analysis and is demonstrated in [15] and in Chapter 3.

While this method is useful for parameterizations, it is also used in other engineering practices. One particular use of recent interest is for interface reduction in substructuring methods, such as CB formulations. This particular method is called characteristic constrain modes. This takes the interface DOF and performs a POD for the specific partition. Examples of this method is found in [16] and [17]. This work is also a current area of research at the Nonlinear Mechanics and Dynamics workshop at Sandia National Laboratories.

1.3 Background and Theory - Sampling Techniques

One commonly used technique in many UQ methods is to represent a stochastic process by using multiple deterministic simulations. This allows for a simple transition between a deterministic design and a stochastic design, which is able to quantify the uncertainty of the system. There are many different types of sampling techniques including pseudo-random and deterministic selection. Three different methods are described in detailed in this section. This is not an exhaustive list, but gives some commonly used methods, in particular the methods used in this dissertation.

1.3.1 Monte-Carlo Sampling

The first sampling technique is the most simple and straightforward of the three techniques, MC sampling. This idea was originally proposed in [18] and named after the famous casino in Monte-Carlo, France. This technique is based on the pseudo-random number generator that is programmed in computer software. These pseudo-random numbers are on the range of $[0, 1]$ with an uniform distribution. This distribution can be transformed into any desired distribution via algebraic expressions.

The basic concept of this technique is to perform a large number of deterministic simulations with varied input parameters then to describe the output statistics of the simulation. In order to use this method, several engineering decisions must be made. The first decision is the input distribution of the parameters. This must be chosen based on the physical characteristics and previous knowledge of these parameters. One example of this could be a machining tolerance that is specified, setting the bounds of the distribution, or using previous test data for material properties.

Another decision that must be made is the number of simulations that can be performed. This is a very important decision since the method requires a large number of simulations in order to produce accurate results, but the computational burden must also be considered. This number of possible simulations can be increased by using a less accurate model such as ROMs or surrogate models. One study, presented in [19], shows that the convergence of a MC simulation is exponential but very slow, requiring a large number of samples for the desired accuracy accuracy.

In this type of analysis, each simulation is treated as equally probable and each simulation is treated as independent. This leads to a very simple continuation into parallel computing. The output distribution is generated based on the assumption that the more probable input parameter will have more simulations than the less probable parameter values. There are several variations on this method. This particular method involves random numbers generated independently from the computer list of quasi-random numbers. Other methods, such as Markov chain MC (MCMC) sampling, have some dependencies of previous values in the sequence. This complexity can better represent certain systems or UQ methods with fewer samples. Some variants of this technique require a burn-in period, where the first values do not go into the simulation and are used to eliminate the sensitivity to the initial design point in the conditional probability.

The major strength of this method is its simplicity that requires almost zero code modification

in order to perform. This allows an engineer without much UQ experience to perform this type of analysis. One of the major weaknesses is the computational burden of the method. This burden can be reduced via parallel computing or surrogate modeling.

1.3.2 Latin Hypercube

The LHC sampling technique is a stratification of the traditional MC technique. This was originally introduced in [20] to improve on the number of required samples to converge to a solution. This is done by dividing the probability density function into equally probable sections. Within each of the sections, one design point is selected. Then the deterministic simulations are performed at each of the selected values, and are treated as equally probable. Extensive use of LHC for various distributions and data sets is studied in [21].

The selection of the value within the equally probable section can be determined via two different ways: deterministically or randomly. The deterministic approach uses the mid-point within the section as the selected value. A random approach is to assign a uniform distribution to the section and choose a value based on this distribution. As the number of samples increase, the difference between these two selection methods decreases. This is due to the range of each section decreasing, and the difference between the mid-point and a random point becomes small.

This technique is very effective on bounded distributions such as beta or uniform distributions. There are several numerical issues that can arise for semi-bounded or non-bounded distributions such as normal or exponential distributions. The main numerical instability involves the tails of the distribution. As the number of samples increases, the last equal probable section contains very large values. These values can create bit resolution issues when comparing to small values. Another issue is the memory requirements to use this sampling technique. All the values have to be determined before the simulations are performed. These values must be stored in global memory.

This issue is not a large problem for systems that only have low dimensionality for the stochastic variables but can become important for higher dimensionality or random matrices.

Using the LHC is especially useful for systems that require a large amount of computational power to evaluate. The LHC is able to give an accurate representation with far less number of samples. This difference is about an order of magnitude less samples that traditional MC sampling as studied in [22].

1.3.3 Stochastic Reduced Order Model

The previous two sampling methods treat each simulation calculation with the same probability. Not all sampling methods require equal probability for each simulation point. The stochastic reduced order model (SROM) technique adds another layer of complexity such that each simulation run is not treated with the same probability. The calculation of the parameter values and probabilities at each value are based on an optimization technique that originally was proposed in [23] and further expanded in [24].

The basic optimization technique is to select an optimal subset of the distribution to best match the statistical moments of the distribution. In order to perform this type of sampling method, several inputs must be selected. The first input is the total number of simulations that can be performed. This number is typically very small compared to the MC approach. The next input is the number of possible subsets to evaluate. This is selected based on the memory and computational power available.

This technique requires a large amount of computational power to evaluate all the possible subsets to get the optimal evaluation points. However, this part does not require any of the model information; it only requires the distribution of each of the input parameters. The determination can be performed prior to the actual simulations runs. This allows for a separation in the work

performed and creates an effective computational reduction. Using these SROMs is a new area of research and some generalities still have to be explored, but shows some promising results when only a couple high-fidelity calculations are available.

1.4 Alternative Uncertainty Quantification Methods

UQ is the merging of statistics and engineering design. This merging allows for a large amount of resources and varying methods that can describe the stochastic characteristics of an engineering system. Several reviews of these methods are previously studied, especially in [25, 26, 27]. These papers review many of the techniques that can be used to quantify the uncertainty of the system. Some of these techniques are explained in detail in this section, while others are mentioned and the basic concept is explained. This is by no means an exhaustive study; however, this section summarizes some of the commonly used techniques.

The major framework for UQ methods is the use of probability theory. This typically uses numerical distribution propagation techniques, such as MC or LHC. These sampling methods are explained in Section 1.3 and the implementation is summarized in [27]. Three of the most commonly used UQ methods are: Polynomial Chaos (PC), covariance propagation, and Bayesian inference. Some short descriptions of various other methods to quantify the uncertainty of the system are presented in Section 1.4.1. PC is described in Section 1.4.2. Covariance propagation is described in Section 1.4.3 and Bayesian inference is briefly explained in Section 1.4.4.

1.4.1 Brief Descriptions of Various Methods

One technique that is used to describe the model form uncertainty of the system is the use of fuzzy sets. This theory was originally proposed in [28] and is summarized in [26, 27]. One advantage of this theory is that it is effective near resonances whereas covariance propagation is invalid near these

resonances due to the nonlinearity. The main theory of fuzzy set is that an uncertain parameter is a member of a fuzzy set, which is a set that does not have distinct boundaries. Some non-engineering examples are describing the height of a person as tall or short, or a quantity as small or huge. The computations that use fuzzy sets are difficult to program and limits the use of this technique.

The uncertainty of a calibration, primarily the predictive error, can be quantified by using the information-gap method. Originally, this method is proposed by Ben-Haim in [29] for the use in model updating and further generalized for decision making in [30] then reviewed in [27]. This method characterizes the uncertainty of not having all the information of the system. There are five requirements for this method when applied to decision making: desired performance requirements, uncertainty model, system model, robustness function, and opportuneness function. The performance requirements are the decision making requirements such as cost or reliability information. Uncertainty model takes the uncertainty parameters and divides them into nested subsets, and the system model is the computational model. The robustness function is the requirements that the system must operate at, and the opportuneness function is the requirements that are desirable but not required to perform, such as noise levels in the cab of an automobile during off-road operation.

Another technique that is commonly used is interval analysis. This is a simple technique in theory however complicated in application. Interval analysis was introduced by Moore in [31] and utilized in [32]. This analysis is applied to finite elements in [33] and used to determine parameter sensitivity in [34]. Several reviews of the method are presented in [35, 36, 37]. In order to use this method, some information about the inputs of the system must be known. The input parameters must fall within a specified range, such as a machining tolerance requirement. This range is thought of as values that the input can take with equal probability. The interval range is then propagated through to the output data using either interval algebra or sampling methods. This algebra has some theoretical issues. One main issue comes from functions that require multiple evaluation of

the same interval. For example [35], if $x \in [1, 2]$ and $f(x) = x - x$, the expected output is zeros for all values. Applying the interval algebra overestimates the range of this output as $f(x) \in [-1, 1]$. This overestimation can be reduced if the output is analytically known as a function of the input parameters. In this type of analysis, the intervals can be applied to the closed form solution and an exact interval can be obtained.

Using interval analysis for multiple uncertain parameters can become very complex. Typically, the uncertainty parameters are not necessarily independent, and the sensitivity of the output to the input parameters is an important aspect of interval analysis. High dimensionality of the uncertain parameters quickly creates a large computational burden. The sample space becomes large and typically requires a sampling method to determine the output range. Two different methods to reduce the computational burden to determine the range are typically performed: reduced sampling and surrogate models. The reduced sampling method uses the physics model with more optimal sampling methods such as LHC. A surrogate modeling approach uses the physics model to generate a surrogate model or Parameterized ROM (PROM), such as response surface, and samples the surrogate a very large amount of times. The surrogate model is very fast to evaluate compared to the full physics model.

1.4.2 Polynomial Chaos

One method to reduce the computational burden of uncertainty propagation is to use surrogate models, such as PC. This technique was originally introduced by Weiner in [38]. Originally, PC was designed for random variables that are Gaussian distributed. This was later generalized to fit a larger variety of distributions but the methodology is the same [39]. Each distribution is distinguished by a different orthogonal polynomial set. The tools are expanded and summarized in [40] for the application of vehicle dynamics. In [41, 42], numerical examples, specifically the "quarter-

car" model, are presented for both linear and non-linear springs. This technique is typically done in the engineering field but not in the statistics field. In [43], O'Hagan describes this method from the standpoint of a statistician's view. The author explains a simplified methodology and application of PC along with some disadvantages from a statistical point of view.

In general, a system is modeled as

$$Y = f(X), \tag{1.15}$$

where Y is the output of the system, X is the input of the system, such as geometry, material properties, etc., and $f()$ is the function evaluation that maps $R^X \mapsto R^Y$. In general $f()$ can be the physics based model or a surrogate model to reduce the computational burden. In order to evaluate the uncertainty of the system, the input is assumed to have a simple distribution. The choice of this simple distribution defines the polynomials to be used in a PC analysis. For example, a uniform distribution uses Legendre polynomials and a Gaussian distribution uses Hermite polynomials [39]. This section shows an example of a situation where there is only one stochastic parameter, but the method is valid for multiple parameters. The implementation of these polynomials takes the form of

$$X = \sum_{i=0}^{\infty} x_i \psi_i(\Xi), \tag{1.16}$$

with Ξ is a standard random variable of the desired distribution, ψ_i is a polynomial in the appropriate set, and x_i are deterministic coefficients. For an exact solution, the summation is an infinite series but can be truncated based on the value of the coefficients.

The polynomials, ψ_i, have special characteristics. The first characteristic is the orthogonal condition, which can be expressed as

$$< \psi_i, \psi_j >= h_n^2 \delta_{ij}, \tag{1.17}$$

where δ_{ij} is the Kronecker delta where $\delta_{ij} = 1$ for $i = j$ and zero otherwise, and h_n is a constant. If h_n is unity, the polynomial is considered orthonormal. The notation $<,>$ is the inner product and can be expressed as

$$< g_1, g_2 >= \int_S g_1(\xi) g_2(\xi) p_\xi(\xi) d\xi, \tag{1.18}$$

with ξ being an element of Ξ, S is the support of Ξ, and p_ξ is the probability density function of Ξ. The same expansion can be applied to the output of the system and is written as

$$Y = \sum_{i=0}^{\infty} y_i \psi_i(\Xi), \tag{1.19}$$

and the deterministic coefficients can be calculated as

$$y_i = \frac{< f, \psi_i >}{< \psi_i, \psi_i >}. \tag{1.20}$$

The denominator can be computed simply based on the normalization of the polynomial. The numerator, however, is difficult to calculate since typically the function $f()$ does not have a simple form that is integrable. Usually, the numerator is computed using numerical integration. This numerical integration requires several functional evaluations. The number of functional evaluations is typically orders of magnitudes less than traditional MC sampling. The convergence of the mean and variance is studied in [39] for the number of polynomials to express the distribution and in [40] for the number of integration points.

1.4.3 Covariance Propagation

Many of these techniques discussed require the use of sampling methods, such as MC or LHC. Covariance propagation is a technique that does not require any sampling methods. However, there is a drawback that the covariance propagation assumes a linear perturbation and can only describe the mean and variance of the uncertainty of the system. This linear perturbation assumption becomes invalid near the resonance and anti-resonance frequencies of the frequency response function, which is very nonlinear. Covariance propagation is typically performed in the modal domain to reduce the computational cost. In [44], Kammer describes the limitation of this method and in [45] improves the usefulness of this techniques by the use of a series approximation to a matrix inversion. This method is also summarized and reviewed in [26].

The first step in this technique is to characterize the uncertainty in terms of the physical impedance matrix. This is done with a first order perturbation with N_p design variables and is written as

$$Z_R = Z + \sum_{r=1}^{N_p} Z'_r \Delta d_r, \tag{1.21}$$

with the nominal physical impedance given by

$$Z(\omega) = -\omega^2 M + i\omega C + K, \tag{1.22}$$

in which M, C, and K are the corresponding nominal mass, damping and stiffness matrices, respectively, ω is the driving frequency, and the normalized designed variable d_r. The normalized sensitivities Z'_r can be determined using the finite element (FE) code with a finite difference method or a more advanced method such as the HD step, which is explained in more detail in Chapter 2.

The next step is to transform into the modal domain. This is done by using the nominal mode

shapes of the system. The result can be expressed as

$$z_R = z + \sum_{r=1}^{N_p} z'_r \Delta d_r, \tag{1.23}$$

where $z = \phi^T Z \phi$ is the nominal modal impedance matrix, etc. The nominal displacement frequency response matrix, h, at a given frequency ω is determined via

$$hz = I. \tag{1.24}$$

Using a perturbation of the nominal system, the frequency response function for the system can be expressed as

$$(h + \Delta h)(z + \Delta z) = I. \tag{1.25}$$

This can be expanded and rearranged to give the relationship

$$\Delta h = -h \Delta z h_R, \tag{1.26}$$

where h_R is the true frequency response matrix after the perturbation. This gives an exact expression for the change in the frequency response for a given change in the modal impedance. In reality, the true frequency response is not known, so a first order approximation is given by

$$\Delta h = -h \Delta z h. \tag{1.27}$$

This approximation is accurate for small values of system uncertainty with a frequency that is not close to the resonance frequency. In the vicinity of a resonance, the change in modal impedance becomes very nonlinear, and the linear approximation becomes insufficient. As an alternative, as

developed in [45], the exact expression for the uncertainty in the frequency response is of the form

$$\Delta h = -h\Delta zh\left[I + \Delta zh\right]^{-1}. \tag{1.28}$$

The matrix inversion is difficult to perform numerically, but can be expressed as an infinite series expansion to give

$$\Delta h = -h\Delta zh\left[I - \Delta zh + \cdots + (-1)^{k-1}(\Delta zh)^{k-1} + \ldots\right]. \tag{1.29}$$

This series expansion holds true if the spectral radius of the matrix Δzh is less than 1.0, or equivalently, all the eigenvalues are within the unit circle.

To express the uncertainty of the physical system, a reverse transformation is required. This modal response can be transformed into the physical domain and vectorized as

$$p = vec(\Delta H) = vec(\phi_s \Delta h \phi_a^T), \tag{1.30}$$

where H is the physical frequency response matrix, ϕ_s is the mode shapes partitioned to the sensor locations, and ϕ_a is the mode shapes partitioned to the actuator or force locations. This vector p contains the information of the mean and variance of the uncertainty. The variance is calculated by the covariance and relation matrices of the vector p. The relation matrix is given as

$$S = E\left[(p - E[p])(p - E[p])^T\right], \tag{1.31}$$

where $E[]$ is the expected value; the correlation matrix is given by

$$C = E\left[(p - E[p])(p - E[p])^*\right], \tag{1.32}$$

with * being the complex conjugate transpose.

This technique has been implemented into finite elements with uncertain parameters. In [46], Falsone describes an implementation of this approach into static finite elements. He continues this implementation into dynamic finite elements in [47]. Each of these methods uses a linear perturbation. In [48], a perturbation is still used, but is not necessarily linear. This formulation requires the determination of polynomial coefficients that require knowledge of how the eigenvalues and mode shapes change with respect to the uncertain parameter.

This approach is able to give the mean and variance of the uncertainty of a system by using a linear perturbation. One major advantage of this technique is that there does not require any sampling methods such as MC. It does, however, require a linear perturbation that makes this approximations less accurate close to the resonance and for large changes in the system.

1.4.4 Bayesian Inference

All of the methods discussed so far are based off forward propagation methods. This assumes that knowledge of the input is fairly well known and the output is desired. Some UQ methods utilize known output data to determine these input values. These methods typically incorporates Bayesian statistics. This branch of statistics is based on Bayes' theory to express conditional probability and is written as

$$\Pr(A|B) = \frac{\Pr(B|A)\Pr(A)}{\Pr(B)}, \tag{1.33}$$

where A and B are events or quantities of interest, Pr() is the probability measure, and $\Pr(A|B)$ is the probability of event A given that event B is true. This is very powerful for situations where there are large amount of output data. There are several possible situations where this amount of data is available. One of the most common examples is situations where the system is inexpensive

to produce such as objects that are mass produced. This allows for relatively cheap physical testing compared to computational simulations. Another situation is when a product has a long operational life such as farm equipment or automobiles. This extended life provides a large amount of data that can be used to quantify the accuracy of the system and then be used in future design.

Bayesian statistics was introduced in the early 1700's and utilized for engineering in more recent years. Several books have been devoted to this method such as [49, 50]. This method is generalized in [51], and the study of the robustness of this method in [52]. There are two main uses for Bayesian analysis in engineering: model averaging and model updating/inference. Model averaging is explained in detail in [53, 54]. Essentially, the averaging technique takes multiple models and uses information from each of the models to produce the desired output. This assigns a probability to each model based on engineering judgment. Due to the dependencies on the type of model, traditional MC can become difficult so MCMC sampling techniques are typically used [55]. This sampling technique has dependencies based on the previous sample. The use of MCMC is not only used for the model averaging, but is also useful for model updating/identification. This has been studied in [56, 57]. The goal of model updating is to adjust parameters for the computational model to better represent the known output data. This is done by calculating the probability of the input parameter given that the output data is true. Statistically, this is the same as adding bias into the system to better match the collected data. Adding bias does not necessarily result in the true values of the system, but does better generate the expected data depending on the model. If the model is based on the physics, then the parameters correspond to physical quantities, while if the model is based on regression, the parameters do not have true values only optimal values.

1.5 Scope of Dissertation

The remainder of this dissertation is organized as follows. Chapter 2 gives a description of multiple methods used to calculate numerical derivatives. This chapter focuses on the use of HD numbers with the HD step as an exact method then implemented into FE for both material variation and geometric changes. Chapter 3 describes several methods of generating PROM. In particular, this describes the HDM and how this increases the accuracy and valid range as compared to the other methods.

In Chapter 4 the non-parametric maximum entropy approach (MEA) is discussed. This method is useful to describe variability from unknown sources. One additional use of this method is being able to describe the model form error when experimental truth data is available. Chapter 5 combines the PROMs, in particular the HDM, that is described in Chapter 3 into the MEA as described in Chapter 4. This is performed on a machined panel system. Finally, Chapter 6 gives a summary of the work presented and the major contributions that this work adds to the research field of uncertainty in structural dynamics. This chapter also describes some identified possible future work with both major and some minor works in scale.

2. PARAMETER SENSITIVITY AND HYPER-DUAL NUMBERS

2.1 Introduction

In the design process, an important analysis that must be performed is a model calibration or other various optimization processes. One of the most important considerations when performing a model updating or optimization analysis is determining the numerical derivative, also called the gradient, of a function. Most optimization techniques are gradient based and can require a large amount of computational resources to find an optimal solution. While there are non-gradient based optimization routines, using gradient based algorithms typically produce an optimal solution more efficiently and with less error compared to non-gradient based algorithms [58]. There are some issues with these algorithms such as determining a solution at a local extrema, and the computational time to find a solution. A large amount of the computational time is associated with the determination of the gradient at each location of the sample space. To decrease the number of solution locations, the addition of higher order derivatives can be implemented to create large step size within the sample space [59].

The determination on the gradient is typically determined via one of three different approaches, (1) finite difference, (2) complex step, and (3) dual step [59]. Each of these methods has its own advantages and disadvantages. This chapter describes each method in detail and compares each method to the others along with truth data generated analytically or with high-fidelity FE models. The finite difference approach is the simplest approach of the three and requires no special programming to perform. This, however, requires multiple code evaluations and increases the com-

putational burden significantly for multiple uncertain parameters [60]. The derivatives generated from the finite difference methods are subject to truncation and subtractive errors. Truncation error occurs when an infinite series is truncated to a finite series, such as the Taylor's series expansion of the function at the specific parameter values. Subtractive error occurs whenever two values are subtracted in the computer. This is typically important when the two numbers that are being subtracted are close or very far in value. The cause of this is the numerical precision of the computer. For double precision, this occurs on the order of 10^{-16}, so any two numbers that are within 10^{-16}, results in a difference of zero.

While the finite difference approach is simple, it also introduces errors that can become significant. The complex step is a method that involves evaluating the function with an imaginary step instead of a real step as in the finite difference approach. Doing this allows for the elimination of the subtractive error since the first derivative only requires a single function evaluation [61]. This method, however, requires the program to be able to perform complex arithmetic. Programs such as Matlab don't require many changes to perform complex calculations, but commercial programs such as Ansys are not as easy to program the solver to perform complex calculations. The complex step is still subject to truncation error due to the Taylor series still being an infinite series. To alleviate this error, the dual step can be used. This method uses a generalized complex number, the dual number [58]. The computations for dual numbers is not typically standard in programs like Matlab, but can be specially implemented. Using a dual step allows for determination of the gradient in a single function evaluation with no truncation or subtractive errors.

This chapter gives the mathematical formulation of the three main approaches to determine the gradient and then compares the error associated with each method. Section 2.2 describes the finite difference method for both a single uncertain parameter and multiple parameters. In Section 2.3, the mathematics behind the complex step is explained. The multi-dimensional expansions,

quaternions and multi-complex numbers, are also explained along with the downfalls of this method. Section 2.4 describes the generalized complex number, the dual number. The multi-dimensional expansion of the dual number, HD numbers, are explained in detail in Section 2.4.1. All of these methods are then compared for a simple case in Section 2.5. Due to the novelity of the HD numbers, an example of the implementation of HD numbers into a FE code is presented in Section 2.6.

2.2 Finite Difference

The simplest and most commonly used method for determining gradients is the finite difference approach. This is based on the Taylor series expansion about a design point. The Taylor series can be written as

$$f(x+h) = f(x) + hf'(x) + \frac{h^2 f''(x)}{2!} + \cdots + \frac{h^n f^{(n)}(x)}{n!} + \ldots, \tag{2.1}$$

where x is the design point, h is a perturbation from the design point, and $f^{(n)}()$ is the n^{th} derivative of the function. This infinite series can be truncated to give an approximation, but this introduces truncation error. The magnitude of this error varies based on the size of the perturbation and the order of the truncation.

The finite difference scheme uses this expansion at multiple perturbation points to estimate values of the derivatives. This assumes that the perturbation is small such that the series can be truncated. These multiple evaluations are then combined in a linear combination to eliminate the undesirable components of Equation 2.1. The linear combination of the evaluations introduces subtractive errors when the perturbation is small. Subtractive error is the error associated with the bit resolution of the computer. Since the computer can only store a set number of digits, for any two numbers that are very close in value, the computer interprets the numbers as the same and can result in a zero difference.

There are three main categories that finite difference methods can be categorized as: forward,

backwards, and central. The forward methods use perturbations where h is positive, while the backwards methods use perturbations where h is negative. Central difference approaches uses both positive and negative perturbation. The selection of which category to use involves engineering judgment of the function, number of function evaluations, and desired error. One important consideration is the continuity of the design space. If the design point is close to a discontinuity, then a directional finite difference method should be used. One possible example is a specified length that cannot physically have a negative distance, so if the distance is small, a directional derivative can be more efficient and accurate. For a set number of function evaluations, the central difference methods tend to have the best accuracy. The first derivative using two function evaluations can be determined by

$$f'(x) = \frac{f(x+h) - f(x-h)}{2h} + \mathcal{O}(h^2). \tag{2.2}$$

In Equation 2.2, the Taylor series is truncated to the second derivative. The notation of $\mathcal{O}(h^2)$ represents that the infinite series is truncated for terms that contain higher orders of the step size. Any term that contains h^3 or higher in Equation 2.1 is assumed to be small and is neglected. This determination only requires two function evaluations at $x = \{x + h, x - h\}$. If more function evaluations are used, the truncation error can decrease. Since the determination of the derivative requires taking the difference of two different function evaluations, subtractive error is introduced when the step size becomes small. There is a trade-off between decreasing the truncation error and the subtractive error. This trend can be seen later in the comparison section.

Higher order derivatives can also be found with similar methodology. By using higher order derivatives, larger steps in an optimization routine can be used and thus account for larger variability on the design parameters. A second order central difference for the second derivative can

be calculated as

$$f''(x) = \frac{f(x+h) - 2f(x) + f(x-h)}{h^2} + \mathcal{O}(h^2). \tag{2.3}$$

Using the HDM and optimization routines typically only uses up to the first two derivatives at each design point. Determining the coefficients for any arbitrary derivative and arbitrary order of truncation error can be calculated with the algorithm developed in [62]. This gives both the algorithm and the solution of the algorithm for the first four derivatives at several orders of truncation error for both central and directional difference.

2.2.1 Multiple Variables

The expansion of this technique into multiple dimensions is straight forward. The expansion of Equation 2.2 with two uncertain parameters can be written as

$$f_{,x}(x,y) = \frac{f(x+h,y) - f(x-h,y)}{2h} + \mathcal{O}(h^2) \tag{2.4}$$

$$f_{,y}(x,y) = \frac{f(x,y+k) - f(x,y-k)}{2k} + \mathcal{O}(k^2), \tag{2.5}$$

where $f_{,x}$ is the partial derivative of f with respect to the x input and $f_{,y}$ is the partial derivative of f with respect to the y input. The higher order partial derivatives of each direction follow the same equations as a single uncertain parameter with the other input variables held constant. Cross derivatives can also be determined using the finite difference method. This first cross derivative can be calculated as

$$f_{,xy}(x,y) = \frac{f(x+h,y+k) - f(x+h,y-k) - f(x-h,y+k) + f(x-h,y-k)}{4hk}, \tag{2.6}$$

with $f_{,xy}$ also written as $\frac{\partial^2 f}{\partial x \partial y}$. The determination of this derivative requires four function evaluations. If there are two uncertain parameters, performing a second order perturbation analysis would require a total of nine function evaluations.

This technique is straight forward and requires no special solver to determine the gradient of a functional. Current finite element codes, such as Ansys and Nastran, use this formulation to perform sensitivity analysis. While this method does not give the most accurate solution, it is a robust method that is simple to implement in current commercial FE code.

2.3 Complex Step

One way to eliminate the subtractive error that the finite difference approach introduces is to determine the gradient by using a single function evaluation. This can be accomplished by using a perturbation step in the non-real direction [61, 63]. By using an imaginary step, Equation 2.1 can be rewritten as

$$f(x+ih) = f(x) + ihf'(x) - \frac{h^2 f''(x)}{2!} + \cdots + \frac{(ih)^n f^n(x)}{n!} + \ldots, \tag{2.7}$$

where i is the imaginary number defined as $i^2 = -1$. The determination of the first derivative can be calculated with a single function evaluation thus eliminating the subtractive error. There is still an induced error due to the truncation of the Taylor series. The first derivative can be calculated as

$$f'(x) = \frac{Imag[f(x+ih)]}{h} + \mathcal{O}(h^2). \tag{2.8}$$

Compared to the finite difference approach, the same truncation error is introduced but the complex step does not contain the subtractive errors and thus produces a more accurate calculation of the first derivative particularly for a small step size.

The second derivative using the complex step introduces a subtractive error. This is due to the fact that the real component of the expansion contains both the nominal function value and the second derivative. In order to determine the second derivative without subtractive error, a more complicated expression is needed. With two function evaluations, the second derivative can be calculated as

$$f''(x) = \frac{2(f(x) - Real[f(x+ih)])}{h^2} + \mathcal{O}(h^3). \tag{2.9}$$

While this derivative requires two function evaluations, using the finite difference approach for the second derivative requires three function evaluations. The fewer function evaluations implies less subtractive errors and also contains less truncation error.

The complex step shown contains a step purely in the imaginary direction. However, there are methods that use a combination of the finite difference and the complex step. This is presented in [64] for cases of the step being a complex number. When the step is purely in the imaginary direction, this method reduces to the complex step method. The same can be said when the step is in the real direction, reducing to the finite difference method. This combination allows for a reduction in the induced errors relative to either method individually but requires more code evaluations.

2.3.1 Multiple Variables

The multi-dimensional expansion of this complex step requires the use of multiple non-real components. This multi-dimensional expansion logically uses imaginary numbers, called quaternions. These quaternions can be characterized by three imaginary numbers: i, j, k. The imaginary numbers are defined by $i^2 = j^2 = k^2 = ijk = -1$. One important consideration is the relationship between these imaginary numbers. These are defined by two independent directions and a third that is perpendicular to these imaginary directions and the real direction. The relationships be-

tween these are similar to unit vectors on a Cartesian coordinate system. These relationships can be written as

$$ij = k \quad ji = -k$$

$$jk = i \quad kj = -i$$

$$ki = j \quad ik = -j.$$

This is one of the major problems with the use of quaternions. The multiplication of the imaginary numbers is not commutative. One realization of this problem is in the calculation of the second derivative. Due to this non commutative property, the second derivative is contained in the real part similarly to the complex step. This derivative can be calculated as

$$f''(x) = \frac{2(f(x) - Real[f(x + h_1 i + h_2 j + 0k)])}{h_1^2 + h_2^2} + \mathcal{O}(h_1^2 + h_2^2). \tag{2.10}$$

This is essentially the same as Equation 2.9, but requires the program to be capable of quaternion arithmetic and is still subject to subtractive errors. The use of quaternions allows for two possible uncertain parameters. It is possible to expand this method to more independent imaginary coordinates, but requires a substantial amount of programming to determine the relationship between each of the imaginary coordinates.

Another method of determining the higher order derivatives with complex numbers is with the use of multi-complex numbers. These are slightly different than quaternions and are able to produce higher derivatives will less error. The methodology was first introduced in [65] explaining the mathematics. Millwater has introduced this mathematics into a complex step analysis in [66] and into a time integrator in [67]. These multi-complex numbers are similar to HD in several aspects. They introduce independent imaginary numbers. While this is the same as quaternions, these are

communicative such that $i_1 i_2 = i_2 i_1$. This simple difference allows for calculation of the second derivative to be calculated with a single code evaluation, which is impossible with quaternions. Using multi-complex numbers eliminates the subtractive error in the determination of the higher-order derivatives, but it still is subject to truncation error. Typically a step of 10^{-16} is used, but is still problem dependent and thus needs to be verified that truncation error is small. Using multi-complex numbers, it is simple to expand these into multiple dimension. The methodology is the same for HD and multi-complex, as further explained in the next section. It is possible to use quaternions for multiple unknown parameters, but is limited and introduces larger errors compared to multi-complex numbers and therefore not discussed.

The use of the complex step allows for evaluation of the first derivative with a single function evaluation. This method, however, requires multiple function evaluations for the second derivative. With the single evaluation, the model solver must be able to handle complex numbers and the arithmetic associated with this. This may be difficult with some commercial software but is fairly simple with programs such as Matlab. The complex step still introduces truncation error and sometimes subtractive error. In order to calculate higher order derivatives with a single code evaluations, multi-complex numbers can be used. Multi-complex numbers are very similar to HD in the implementation, but are less accurate due to the truncation error.

2.4 Dual Step

One of the major errors with the complex step is the truncation error. This error can be eliminated with the use of a generalized complex number, in particular, the dual number. The basic concept for a generalized complex number is similar to the ordinary complex number, with the difference being how the non-real number is defined. For the ordinary complex number, the non-real number is defined as $i^2 = -1$, while the dual number is defined as $\epsilon^2 = 0$. This allows for the Taylor series

to become a finite series and thus Equation 2.1 becomes

$$f(x + h\epsilon) = f(x) + h\epsilon f'(x). \tag{2.11}$$

Using Equation 2.11 allows the first derivative to be expressed as

$$f'(x) = \frac{\epsilon Part[f(x + h\epsilon)]}{h}. \tag{2.12}$$

This results in an exact derivative, not subject to the truncation or subtractive errors that the other methods described are subject to. One major drawback to this method is that the higher order derivatives cannot be determined. Since the Taylor series is truncated to the first derivative, the information about the higher order derivatives are not included in this expansion. In order to determine the higher order derivatives, the multi-dimensional technique, HD numbers, must be used.

2.4.1 Hyper-Dual

The study of HD numbers originated in 2011 [59]. It is used for optimization techniques in [58, 60] and further developed in [68]. The use in terms of FE along with substructuring is analyzed in [69]. HD numbers are not specified to a certain number of non-real parts, but it is discussed similarly to the quaternions with two independent directions and one dependent direction. There is a clear possibility for expanding the method to more independent direction, but the programming is not as straight forward.

With the use of HD numbers, the Taylor series in Equation 2.1 becomes

$$f(x + h_1\epsilon_1 + h_2\epsilon_2 + 0\epsilon_{12}) = f(x) + h_1 f'(x)\epsilon_1 + h_2 f'(x)\epsilon_2 + h_1 h_2 f''(x)\epsilon_{12}, \tag{2.13}$$

where ϵ_k is an independent dual number and ϵ_{kl} is the dependent dual number with $\epsilon_k^2 = \epsilon_{kl}^2 = 0$. One main advantage of using HD numbers is the commutative property of these numbers. This property can be expressed as $\epsilon_1\epsilon_2 = \epsilon_2\epsilon_1 = \epsilon_{12}$. Using HD numbers for a single uncertain parameter allows for the determination of higher order derivatives. The first two derivatives can be determined as

$$f'(x) = \frac{\epsilon_1 Part[f(x + h_1\epsilon_1 + h_2\epsilon_2 + 0\epsilon_{12})]}{h_1} \tag{2.14}$$

$$f''(x) = \frac{\epsilon_{12} Part[f(x + h_1\epsilon_1 + h_2\epsilon_2 + 0\epsilon_{12})]}{h_1 h_2}. \tag{2.15}$$

These derivatives are by definition exact. There is no truncation error of the Taylor series and is not subject to subtractive error. One interesting aspect is that the accuracy of the derivative is not dependent on the step size due to the lack of truncation and subtractive errors.

With multiple uncertain inputs, the mathematics does not change within the simulation but does change what each non-real component represents. For example, the ϵ_1 direction and ϵ_2 correspond to two different inputs and the ϵ_{12} direction corresponds to the correlation between the two inputs. The first derivatives of the two different inputs can be calculated with an input vector $\boldsymbol{x}$ as

$$\frac{\partial f(\boldsymbol{x})}{\partial x_i} = \frac{\epsilon_1 Part[f(\boldsymbol{x} + h_1\epsilon_1\boldsymbol{e_i} + h_2\epsilon_2\boldsymbol{e_j} + \mathbf{0}\epsilon_{12})]}{h_1} \tag{2.16}$$

$$\frac{\partial f(\boldsymbol{x})}{\partial x_j} = \frac{\epsilon_2 Part[f(\boldsymbol{x} + h_1\epsilon_1\boldsymbol{e_i} + h_2\epsilon_2\boldsymbol{e_j} + \mathbf{0}\epsilon_{12})]}{h_2}, \tag{2.17}$$

where $\boldsymbol{e_i}$ is a vector of zeros with unity at the i^{th} input. This calculation is also able to determine the cross derivative as

$$\frac{\partial^2 f(\boldsymbol{x})}{\partial x_i \partial x_j} = \frac{\epsilon_{12} Part[f(\boldsymbol{x} + h_1\epsilon_1\boldsymbol{e_i} + h_2\epsilon_2\boldsymbol{e_j} + \mathbf{0}\epsilon_{12})]}{h_1 h_2}. \tag{2.18}$$

In order to calculate the second derivative with respect to a single uncertain parameter, the unit vector is set as $i = j$. Doing this transforms the cross derivative into the second derivative with respect to the input parameter. Extending this concept to more dimensions is not theoretically complex. This would only involve including more non-real dimensions, such as ϵ_3. Including this also involves programming the cross directions, ϵ_{13},ϵ_{23}, and ϵ_{123}. These extra directions increase the computational time and storage requirements to perform the calculations. The current programming is classified as either two or three independent dual numbers. Current research is being conducted to program an arbitrary number of independent dual numbers.

For the most part, the algebra using HD numbers is similar to quaternions and almost identical to multi-complex numbers. This allows for relativity simple programming in Matlab. Some examples of the algebra and functions are given in [59]. All of the analysis done in this proposal uses Matlab with some validation and output from other commercial codes. More complicated functions require some extra considerations. Some of the functions that are used include but not limited to: square root, inverse, sort, logical arguments, and Eigen analysis. A couple of the required functions that are used were derived theoretically while others are reduced to the basic algorithm and let the elementary functions, such as add and multiply, perform the calculations. The extension of this method to more directions is simple for functions that use the original algorithm but is more complex for functions that are derived theoretically.

In Matlab, both the second and third order HD numbers are programmed. Along with the basic algebra, several functions are also programmed. The speed of running these functions is based heavily on the skill of the programmer and the platform. Most of the functions used in this work are programmed by engineers and not professional programmers. It is believed that some improvements to the programming can be made. Due to this fact, the main criterion that is used is the accuracy of the analysis. Another important criteria to consider is the time to perform the

analysis, but is subject to programming efficiency and thus is not always reported.

2.5 Comparison of Methods

Three different methods are explained in the chapter: finite difference, complex step, and HD step. Each of these methods has its own advantages and disadvantages. To compare these methods, the accuracy of the first and second derivatives is analyzed. One of the main considerations of using any of these methods is the step size. For two of the methods, the Taylor series is truncated based on step size. This implies that the accuracy of the truncation is highly dependent on the magnitude of the step size.

To examine the error on the derivatives, a polynomial function is used. This choice allows for quick calculations and a known value for validation. The polynomial is not a commonly used output function, but does show the trend and is able to show the trade-off between the truncation and subtractive errors along with the relative errors between the three methods. This trade-off is also examined in [59] for a more complicated analytical expression but shows the same trends. A normalized error is used, and the error of the first derivative can be seen in Figure 2.1. The range used in this figure is larger than typically used. This is done in order to show the subtractive errors in the first derivative.

The first trend is for step sizes of 10^{-4} or larger, the complex step and the central finite difference have the same errors. One important comparison is the accuracy of the HD step. The error is considered a numerical zero. Since the HD step is not subject to truncation error or subtractive error, the total error does not depend on step size. Another important trend noticed is for the central finite difference. For large step sizes, the main source of error is the truncation error, but as the step size decreases, the error is dominated by the subtractive error. If the step size is smaller than around 10^{-15}, the difference between the function evaluations are zero due to

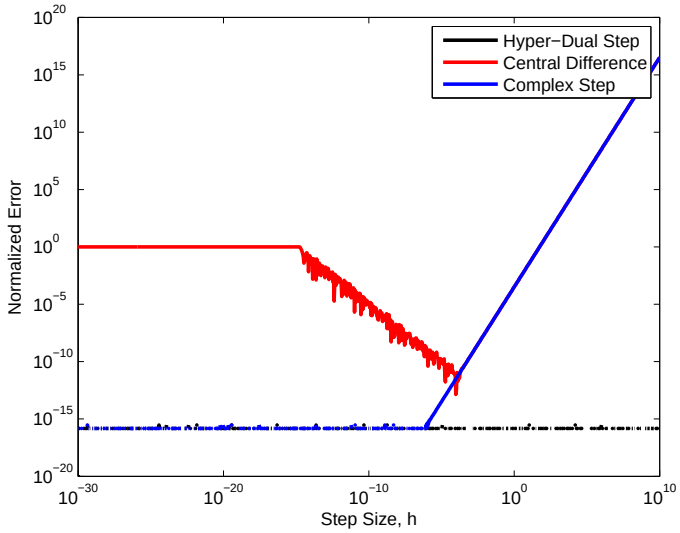

Figure 2.1: First Derivative Error as a Function of Step Size

the bit resolution. Some of the same trends can be found in Figure 2.2 for the second derivative.

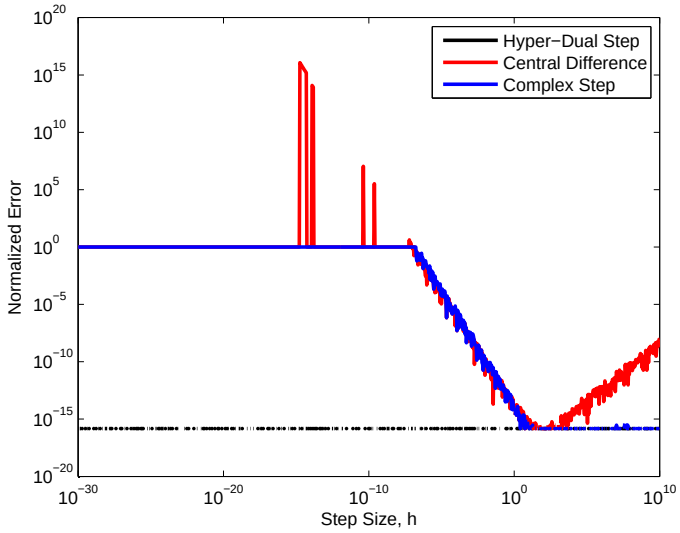

Figure 2.2: Second Derivative Error as a Function of Step Size

The first trend that is consistent between the first and second derivative is the HD step. This method has a numerical zero error and is independent of the step size. One important difference between the first and second derivatives is within the complex step method. As stated in Section 2.3, the second derivative requires multiple function evaluations and is thus subject to subtractive

error that can be seen with a small step size. Another interesting characteristic of the second derivative is that the truncation error is not prominent until a much larger step size compared to the first derivative.

2.6 Implementing Hyper-Dual Numbers into Finite Elements

The implementation of HD number into engineering problems is not a simple task. In order to test the implementation, PROMs using substructuring techniques is explored and is the results are originally presented in [69]. This example is a frame with an appendage that is constrained to planar motion, and is split into two substructures with repeated nodes that are identified by the red nodes in Figure 2.3 at $x = 0$. The frame has some unique characteristics that add a level of complexity to the system. One complexity is that the cross-sectional area of each substructure is different. The cross-section of the left substructure is a 1x1in^2 square while the substructure on the right has a cross-section of a 1x0.75in^2 rectangle.

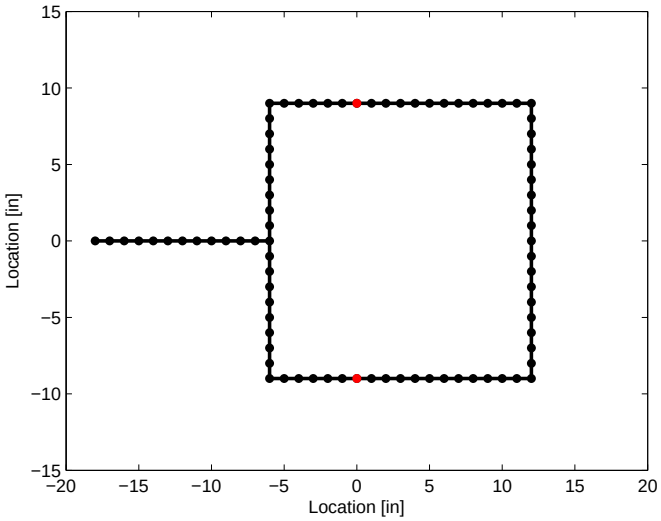

Figure 2.3: Example System Finite Element Model

For each substructure, the red nodes are defined as the interface nodes, each possessing two translations and one rotation, totaling six interface DOF due to the constrained planar motion. The

structure is modeled using Euler beam elements. Substructure fixed interface modes are retained up to 500 Hz. This results in nine modes for each sub-structure, including three rigid-body modes, producing a dramatic reduction from 129 to 15 DOF.

The mass and stiffness matrices for each substructure are generated with the HD step. In order to do this, uncertain model parameters must be defined. For this example, two different material parameters are used, (1) Young's modulus and (2) mass density along with one geometric value that is the length of the appendage. Due to the implementation within Matlab, a single evaluation of the FE code can only produce a single second derivative. This requires the code to be evaluated three times, once for each the Young's modulus, the mass density, and the change in appendage length. The second order perturbation analysis requires the second derivative, which can be determined based on the ϵ_{12} term of the HD number. For a first order perturbation analysis, only the ϵ_1 or the ϵ_2 value of the HD number are used. In order to do this, a non-real step is taken. For example, the Young's modulus is defined as

$$E = E_o + 1\epsilon_1 + 1\epsilon_2 + 0\epsilon_{12}, \tag{2.19}$$

where E_o is the nominal value of the Young's modulus. With this redefinition, the substructure system matrices are determined. By using the HD step, the stiffness matrix takes the form of

$$[K] = [K_o] + \frac{\partial [K_o]}{\partial E}\epsilon_1 + \frac{\partial [K_o]}{\partial E}\epsilon_2 + \frac{\partial^2 [K_o]}{\partial E^2}\epsilon_{12}, \tag{2.20}$$

where $[K_0]$ is the nominal stiffness matrix. Both the mass and stiffness matrices take the form of Equation 2.20. Since the non-real step is a value of 1, then no extra calculations are required to determine the sensitivities. These matrices are then transformed into a CB substructure representation and then synthesized together. This synthesized system is then compared to the high-fidelity

model.

2.6.1 Results

The first result for this system is a perturbation on the Young's modulus. The fundamental elastic natural frequency as a function of the change in the Young's modulus is shown in Figure 2.4a. This shows three different curves, the black curve is the truth data that is generated from the high-fidelity FE code, the red dotted curve is for a first order Taylor series expansion, and the blue dashed curve is for a second order Taylor series expansion. It is easy to see that the second order approximation is accurate for a larger region compared to the first order approximation. This region is clearer to visualize via the percentage error and is shown in Figure 2.4b with the same resolution as the rest of the figures. The resolution is consistent as a 0.1% change in the uncertain parameter and is swept on the range of $X \in \pm 75\%$

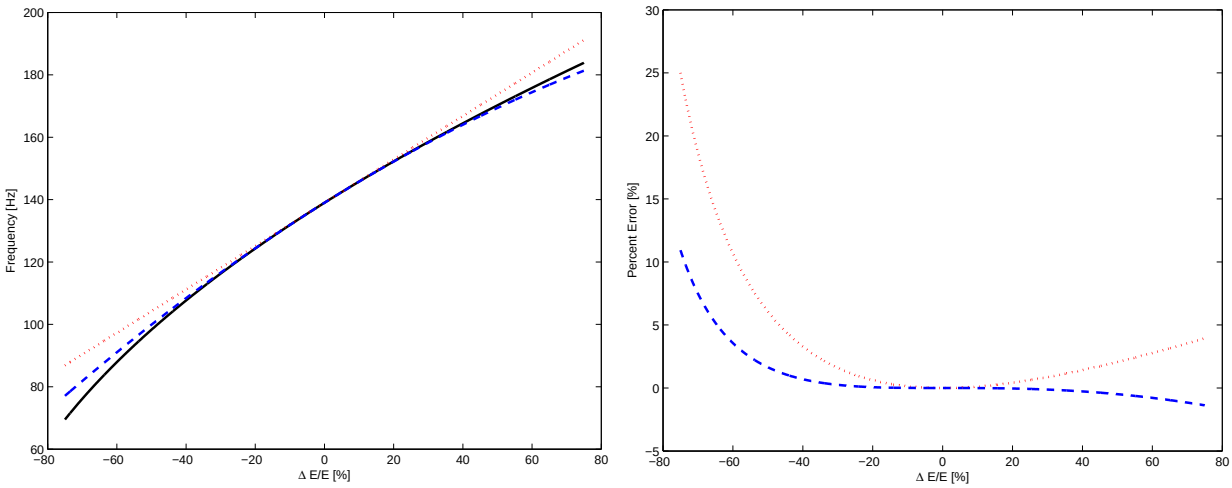

(a) Natural Frequency *(b)* Percentage Error

Figure 2.4: Change in Young's Modulus With: Black-Truth Data, Red-1st Order, Blue-2nd Order

The Young's modulus is not the only model parameter for the FE code, the mass density is also an important parameter. The mass density of a material can also change based on environmental factors such as humidity and temperature. For this reason, the same calculations are also performed

for a perturbation in the mass density. The first system elastic natural frequency is shown in Figure 2.5a with the same lines as in Figure 2.4a. Compared to the change in Young's modulus, the mass density is more nonlinear. This is emphasized in the percentage error that can be seen in Figure 2.5b.

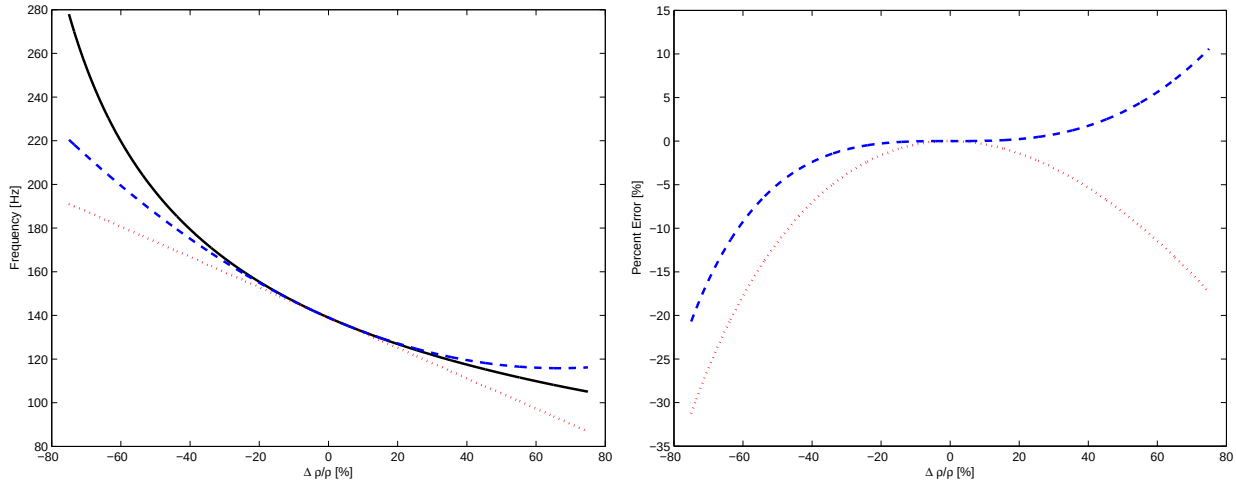

(a) Natural Frequency *(b)* Percentage Error

Figure 2.5: Change in Mass Density With: Black-Truth Data, Red-1st Order, Blue-2nd Order

For a 5% tolerance range, the first order approximation can be treated as accurate for a percentage change in mass density on the range of $\rho \in [-40\%, 40\%]$ and the second order approximation can be treated as accurate on the range of $\rho \in [-55\%, 60\%]$. The time required to perform this calculation was compared to assembling the entire system for each value of mass density or Young's modulus. This essentially represents the computational time to generate the plots, such as in Figure 2.4a. For this particular example, using the HD step was significantly faster. On the computer used, which is a fairly standard desktop, constructing the full system takes about 175 times more computational time than using the HD numbers at the nominal value and then using a perturbation. For the HD step, the time measured the construction of the substructures, synthesis of the full system, and then a matrix perturbation based on a Taylor expansion.

The last simulation consists of a change in geometry, which is much more difficult. This would

typically require re-meshing of the system at each iteration. With the use of HD numbers, this re-meshing is not required. The geometry affected is the length of the appendage. This length change has a large effect on the mass of the system. The change in stiffness is small since the appendage is only connected to one node of the rest of the system. Since this change is not as straight forward as the Young's modulus or the mass density, the steps required for this analysis are described in more details.

The non-real step is applied to the element length between the nodes. This is then propagated to the physical locations of the nodes. Doing the implementation this way is one possible method. Another common implementation is to apply the HD step to the physical location of the nodes after the mesh has been generated. The rest of the calculations are performed as before with one minor exception; In the generation of the transformation matrix of the elements from the local coordinate system to the global coordinate system was taken only to be real numbers. When the HD numbers are used for a geometric parameter, this transformation matrix leads to a correct nominal solution but has incorrect sensitives. To correct this, only the real part of the transformation matrix is used. The first natural frequency from this simulation is shown in Figure 2.6a. This shows a very nonlinear behavior since both the mass and stiffness are changing but at different rates. The calculated percentage error for the first and second order perturbations are shown in Figure 2.6b. A first order perturbation gives a 95% accuracy range of $L \in [-60\%, 30\%]$. The second order perturbation gives an accuracy range of $L \in [-60\%, 45\%]$.

The use of HD numbers for computing parameter sensitivities and UQ within structural dynamics applications is relatively new. This example is a novel assessment of the application of HD numbers to the sensitivity analysis of substructures within the framework of the component mode synthesis (CMS) formulation. The approach was applied to two CB substructure representations of a planar frame with an appendage. The accuracy of the method is compared to the full system

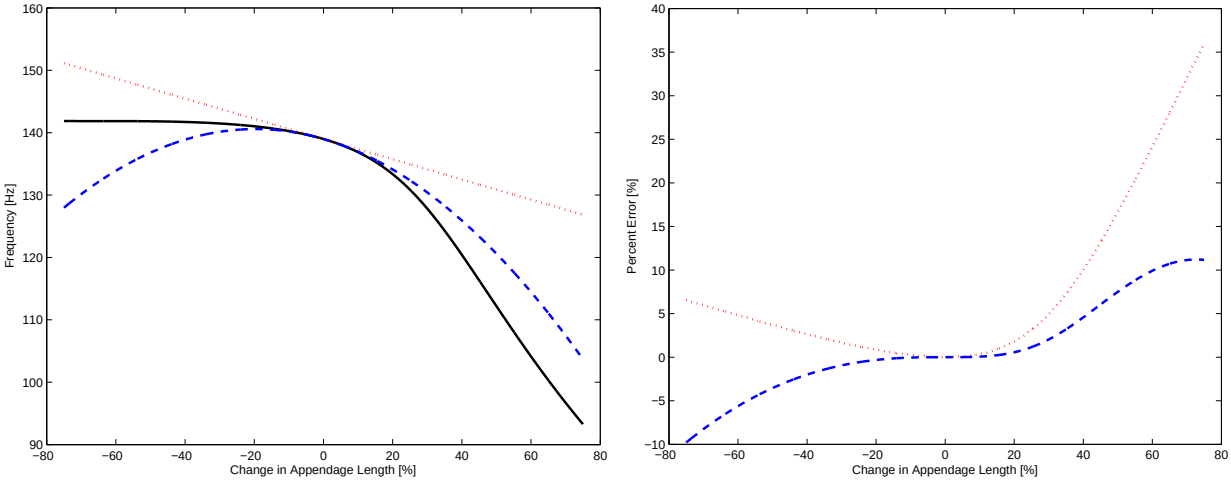

(a) Natural Frequency *(b)* Percentage Error

Figure 2.6: Change in Appendage Length With: Black-Truth Data, Red-1st Order, Blue-2nd Order

FE model that is constructed at each perturbed parameter value to determine the true solution.

2.7 Remarks

This chapter presents three different methods to determine the gradient of a functional: finite difference, complex step, and HD step. The finite difference method uses multiple code evaluations to determine the numerical derivative. One advantage of this is that it does not require any special programming and can easily be used with commercial engineering tools and programs. The major disadvantage is that the gradient is subject to both truncation and subtractive errors. Using the complex step method is one technique to reduce these errors. The complex step is not subject to subtractive errors for first derivatives but is for the second derivative. This step requires some minor solver manipulation to ensure that it is able to calculate complex math, which can easily be done in Matlab and is possible in select commercial programs. While the complex step is still subject to truncation error like the finite difference, using the HD step eliminates both the truncation and subtractive errors. This requires some complex programming but is able to produce exact gradients with a single functional evaluation.

These three methods are compared for a simple case of a polynomial function. While this is not a common engineering functional, this function shows the trends of the errors as function of step size. Large step size makes the truncation error become large while small step size makes the subtractive errors become large. The HD step is not subject to these errors and is thus not dependent on the step size.

The newest technique out of the three is the HD step. In order to further explore this technique, a more complicated example is investigated. This example is a substructuring problem with uncertain inputs. Two material properties, Young's modulus and mass density, and one geometric parameter, the length of appendage, is investigated for variations up to 75% from the nominal value. This study shows the results from the implementation in Matlab with a high-fidelity code used to verify the programming. It also shows that using a PROM to generate the first elastic natural frequency requires much less time to generate the true curve with the same resolution.

3. PARAMETERIZED REDUCED ORDER MODELS

3.1 Introduction

The implementation of high-fidelity models has recently become the engineering standard in order to produce more accurate results. This increase in model fidelity has emphasized the question of the accuracy of the computational models. In order to know this, the practice of UQ must be utilized and improved in order to tell the accuracy of the high-fidelity models. UQ, however, requires a statistical approach that typically includes distribution sampling, which requires multiple evaluations of the model [24]. This raises the problem of the computational resources since each high-fidelity model takes a large amount of computational power and man-hours to evaluate. To alleviate this computational burden, ROMs are typically used. One major drawback to using ROMs is that they do not give any information about how the system evolves with uncertain inputs. For each change in an uncertain parameter, a brand new ROM must be created, which is computationally restrictive. The goal of this chapter is the creation of a ROM for any value of an input parameter, a PROM.

This chapter discusses what information should be gathered from the high-fidelity calculations to generate the PROM in order to characterize the quantity of interest. The desired information generated from the PROM can include many types of information such as: natural frequencies, mode shapes, fatigue life, ultimate tensile strength, system matrices, etc. The desired outputs used in this chapter are the natural frequencies and an element of the system stiffness matrix. This is chosen for the relative simplicity of the calculation, and allows for the truth data to be calculated

in order to validate the various methods.

Once the PROM is generated and validated, an UQ analysis can be performed. A typical analysis used is a distribution propagation. One method to propagate a distribution is with sampling methods such as MC or SROM. The method used in this chapter for implementing the SROM method is not the usual use of this technique. Typically, the SROM technique is used to determine the input values of the high-fidelity model. Once the input is determined, then a Taylor series with a finite difference approach to determine sensitivities is used to create a surrogate for the high-fidelity model. With the mathematical model, a large scale MC sampling method is used to determine the output distribution. The methodology in this chapter has a fixed input of the high-fidelity model and then uses the SROM technique to sample the PROM distribution. This is performed to match the typical use of LHC in order to give a direct comparison with the traditional MC sampling method used as validation data.

3.2 Various Parameterization Models

The choice of what type of reduction model to use is very important. Each method has its own drawbacks and advantages; this research focuses on five different models. The methods that are used are, (1) A Taylor series expansion using finite difference methods to determine sensitivities, (2) A POD of the data, (3) Using a CB representation, (4) Implementing HD numbers in order to obtain the sensitivities, and (5) using a Meta-Model approach that fits a basis function to the data. All five of these models are applied to the Brake-Reu*ss* Beam (BRB) while a subset of these methods are applied to the frame and panel systems, primarily the HDM (5) and HD with Taylor series (4).

3.2.1 Taylor Series

The first method is the most straight forward and the most commonly used, the generic Taylor series expansion. This method uses the output data and a finite difference approach to determine the sensitives. The method for using the finite difference approach can be found in [62] and Chapter 2. This computes the sensitivities of different orders as a weighed sum of the functional output at different parameter values. For example, the first derivative for a scalar variable can be expressed as

$$f'(X_o) = \frac{f(X_o + \Delta) - f(X_o - \Delta)}{2\Delta} + \mathcal{O}(\Delta^2), \tag{3.1}$$

where $f : R^1 \mapsto R^{N_f}$, $f'()$ is the first derivative with respect to X, X_o is the nominal input parameter, and Δ is the small change in the input parameter. This equation assumes that the high-fidelity model was evaluated with three different input parameter values of X=$\{X_o - \Delta, X_o, X_o + \Delta\}$. The more data points that are available, the more accurate the numerical derivatives become along with the added benefit that higher order derivatives can also be determined.

Results shown for the BRB uses five data points to generate the sensitivities which can produce up to the fourth derivative of the functional. This model also assumes that the uncertain parameters are independent, which is an important assumption to consider and verify. Otherwise, this form of the finite difference approach can only determine conditional derivatives. Once the sensitivities are determined, they can be applied to a Taylor series expansion about the nominal value. This can be seen as

$$f(X_o + \delta) = f(X_o) + \frac{1}{1!}f'(X_o)\delta + \frac{1}{2!}f''(X_o)\delta^2 + \cdots + \frac{1}{n!}f^{(n)}(X_o)\delta^n + \cdots . \tag{3.2}$$

In Equation 3.2, δ refers to the difference from the nominal parameter value and the evaluation

value, and the superscript (n) is the n^{th} derivative of the function. This equation is an infinite series but is truncated at the highest order derivative available. This method is very straight forward; it does not require any change in the high-fidelity code and is accurate for small changes in the input parameters. One problem this method has is that the accuracy is directly related to the amount of times the code is evaluated. The accuracy of the PROM is also greatly depends on the accuracy of the derivatives. This is the most commonly used method of reduction since the analysis is very simple, but can be time consuming since multiple code evaluations must be used.

3.2.2 Proper Orthogonal Decomposition

The next method used is the POD. This method utilizes basis vectors in order to reduce the computational time of the analysis. This method is very similar to the Taylor series method, since it uses a finite difference approach to approximate the derivatives. The main difference comes in how the uncertainty parameterization is performed. Further explanation is given in [13] and in Section 1.2.3.

The diagonal matrix D can be truncated basis on its values. This can give a reduced order representation of the matrix which will require less computational time to compute and require less memory storage than the Taylor series method. The orthogonal vectors Σ and V are invariant with respect to the change in material properties for the BRB [14], so the only value that need to be parameterized is the diagonal matrix D. This invariance comes from the definition of Σ and V, which are direction vectors to the singular value space. The derivatives of D are found using the finite difference approach as discussed in the Section 2.2.

This method is advantageous because the matrix D is diagonal and is smaller in size than the raw data matrix. The disadvantage is that the data matrix must be decomposed, which takes more overhead to compute since three matrices are being evaluated instead of just one. This increase in

overhead time must be compared to the savings in the propagation step of UQ.

3.2.3 Craig-Bampton

While the previous two methods were numerical based, the CB method is a physical reduction model. This method takes the system matrices that are generated from the model and reduces the size by introducing a hybrid coordinate system that contains both physical interface DOF and fixed-interface modal DOF. This method is explained in [3, 70] and Chapter 1. This is useful because the modal DOF are by definition independent so they can be truncated based on the frequency. It is common to choose a truncation frequency based on twice the desired range of importance. As an example, if the highest frequency of interest is $100Hz$, all the modes that have a frequency less than $200Hz$ are typically kept. This is a rule-of-thumb in order to get acceptably accurate results. The more modes that are selected, the more accurate the solution, but that requires more DOF which diminishes the reduction effect.

This method is different from the rest of the methods because it is a model based on physical characteristics of the system. One major advantage is that the reduction doesn't require a full high-fidelity model code evaluation, just the extraction of the system matrices are required. The sensitivities are computed normally by finite difference, but if available, the derivatives can be computed using HD numbers, which is explained in Section 2.4.1. This would not the same as the HD reduction but the underlying math can be used in both methods. A major disadvantage of this reduction is that it requires an evaluation of the reduced system. The other methods so far only required a plug-into a formula but this method requires a full code evaluation, which takes longer to compute compared to the other methods but still less than the high-fidelity model. This method is useful for a physical interpretation of the system and can be used in multiple techniques such as CMS.

3.2.4 Hyper-Dual Reduction

The previous models consisted purely in the real domain where the HD reduction utilized the non-real domain. Using these generalized complex numbers allows for a determination of the numerical derivatives in a single code evaluation [59]. The generalized complex number is called a HD number. This is a multi-dimensional expansion of the dual number, similarly to the use of quaternions for the ordinary imaginary number. The math behind these HD numbers are explained in [60, 71, 72] and also in Section 2.4.1. This is used to generate the derivatives and then implemented into a Taylor series.

3.3 Hyper-Dual Meta-Model

The previous four methods are classical and well established. This explanation section is larger than the previous method due to the novelty of the HDM and fully describes all the engineering choices in order to utilize the HDM. The main motivation for this technique is to create an accurate and inexpensive representation for the response of a system that undergoes a large change in the input parameters to be further used in sampling techniques such as MC or LHC. One of the main uncertain input of interest that causes a very large change in the response is a geometric variation, in particular for values that are small in nominal value, such as in aerospace components. Typically, each change in geometric variation would require a re-computation of the FE mesh. This can require a large amount of man-hours and computational power for each simulation run. Due to this, a numerical sampling method becomes computationally prohibitive.

The HDM uses the FE code at a few selected values of the input variable. Along with the desired output, the information about the sensitivity of the output to the varied input is also needed. This sensitivity can be generated via many different methods. An in-depth discussion of the numerical derivatives is presented in Chapter 2. The main development is based on methods

that determine the output and the sensitivities with a single code evaluation, such as the HD step [71]. For the analytical example that is presented in this section, the analytical derivatives are known via beam theory.

Once the output and the sensitivities are known, the HDM characterizes this data with the use of basis functions. These functions can be any function that matches the output and derivatives at all of the code evaluations. Some of the possible basis functions are discussed in Section 3.3.2. This selection can be based on a known relationship or as a simple mathematical function such as a polynomial. For the analytical example, a simple matrix polynomial is used.

Another important engineering decision is where to parameterize the model within the simulation. This is an important decision and is based on how the simulations are performed. If the geometry is complex and the analysis is simple, this parameterization is more effective at the system level, such as the mass and stiffness matrices. One important check when performing the parameterization at the system level, particularly for geometric variations, is to ensure that the DOF are the same for each evaluation. This introduces a requirement that any geometric change does not change the number of nodes in the system and to enforce the same ordering of DOF within the matrix. The analytical example is parameterized at the stiffness matrix level. Another possible level of parameterization is at the output level. One major advantage of this parameterization is that the mesh for each simulation run can contain different number of DOFs depending on the output. This is particularly important for geometric changes. One example of this importance is for a system that contains a hole that grows larger than the previous mesh size, removing elements from the mesh. A disadvantage of this is that the solver must be able to calculate the derivative. All solvers are able to calculate derivatives with a finite difference approach, but if a more accurate result is required, the solver must be able to perform in either multi-complex math or HD math. This parameterization is expected to be more accurate, but typically requires special solvers.

3.3.1 Analytical Example

In order to show the core concept of this method, a simple analytical example of a cantilever beam is presented. This system can be seen in Figure 3.1. The variability expressed in this system is the total length of the beam and the desired result is the tip deflection/rotation due to a constant load P applied at the tip.

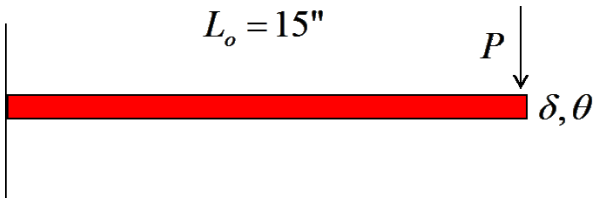

Figure 3.1: Example Cantilever System

Due to the simplicity of this system, an analytical expression for the tip displacement and rotation for a linear isotropic material is used. These outputs can be determined via

$$EI_x \begin{bmatrix} 12/L^3 & 6/L^2 \\ 6/L^2 & 4/L \end{bmatrix} \begin{pmatrix} \delta \\ \theta \end{pmatrix} = \begin{pmatrix} P \\ 0 \end{pmatrix}, \tag{3.3}$$

where E is the Young's modulus, I_x is the area moment of inertia, L is the length of the beam, δ is the tip deflection, and θ is the rotation of the tip. This is thought of as a classic linear system of $KX = F$. Since the tip deflection is known analytically, the derivative with respect to the changing length is also known analytically.

This system contains an uncertain length of the beam. For this example, the beam length is described by the interval of $L \in [10, 20] in.$ Due to the relationship between the output and the length of the beam, using a traditional Taylor series expansion requires higher order derivatives to be accurate. This leads to the implementation of the HDM. For this example, the stiffness matrix is evaluated at three different lengths, $L = \{10, 15, 20\}\ in.$, and the first derivatives are also calculated

at each of those lengths. This information is used to generate the HDM using a polynomial fit that matches the stiffness matrix and the derivative at each value of length. The stiffness matrix is expressed as

$$K(\gamma) = K_0 + K_1\gamma + K_2\gamma^2 + K_3\gamma^3 + K_4\gamma^4 + K_5\gamma^5, \tag{3.4}$$

where K_i are deterministic matrix coefficients and γ is a non-dimensional length. This is defined as $\gamma = \frac{L-L_0}{5}\left[\frac{in}{in}\right]$ for this specific system, such that the maximum and minimum have values of unity and negative unity respectively. The reason for this is for numerical conditioning in order to determine the matrix coefficients. These are determined by solving the linear equations of

$$\begin{bmatrix} I & -I & I & -I & I & -I \\ I & 0 & 0 & 0 & 0 & 0 \\ I & I & I & I & I & I \\ 0 & I & -2I & 3I & -4I & 5I \\ 0 & I & 0 & 0 & 0 & 0 \\ 0 & I & 2I & 3I & 4I & 5I \end{bmatrix} \begin{bmatrix} K_0 \\ K_1 \\ K_2 \\ K_3 \\ K_4 \\ K_5 \end{bmatrix} = \begin{bmatrix} K(L_{-1}) \\ K(L_0) \\ K(L_1) \\ K'(L_{-1}) \\ K'(L_0) \\ K'(L_1) \end{bmatrix}, \tag{3.5}$$

with I being the identity matrix, K' being the derivative of the stiffness matrix with respect to the non-dimensional length γ, and L_γ is the length associated with the non-dimensional length γ.

The linear system in Equation 3.5 can then be solved for the unknown matrix coefficients. Those coefficients are used in Equation 3.4 for the stiffness matrix then used to determine the tip deflection and rotation at any given length. This method is compared to a traditional Taylor series with the first two derivatives used at the nominal length, calculated via the HD step. The results are shown in Figure 3.2. This shows that the HDM very closely matches the truth data while the Taylor series is accurate close to the nominal length but becomes very inaccurate for large changes

in length.

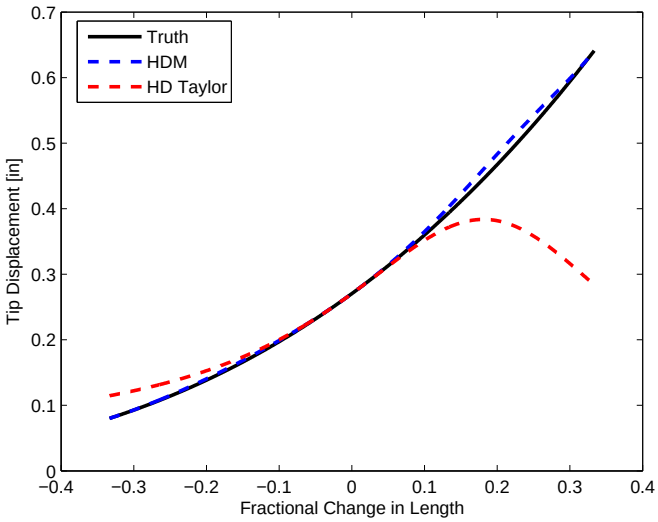

Figure 3.2: Tip Deflection as a Function of Length

3.3.2 Selection of Basis Function

One of major decision in the use of the HDM is what basis function(s) to use in the model. While there are many candidate functions, some are discussed here and two are implemented. The first basis is the use of a polynomial function. This is a classic function that is simple to generate and evaluate. The current use of this polynomial is to match the data from the full simulation runs exactly. This forces the surrogate model to match both the nominal value and derivatives at each data point. Using this type of formulation increases the accuracy of the surrogate, but can require many unknown matrix coefficients. One simple example of how to use this polynomial is shown in Section 3.3.1 within the analytical example. Another interesting aspect of this example is the use of a dimensionless parameter γ. The main reason for this is the numerical conditioning of the equations used to determine the matrix coefficients. If the uncertain parameter has a nominal value that is small, some numerical issues arise during the matrix inversion in the determination of the coefficients.

The HDM presented in this dissertation uses the information from the high-fidelity model to generated a determined system, where the number of unknown coefficients and collected data is the same. This was performed to incorporate the information and be able to reproduce the results from the high-fidelity model exactly. One alternative to this approach is to utilize the higher order derivatives in a least squares sense, thus creating an overdetermined system. While this is possible, it is not currently implemented in this work. One advantage by using an overdetermined system is that it provides a much greater history of methods to determine the accuracy of the meta-model, such as regression metrics and maximum residuals [73].

While this formulation of a polynomial is simple, there are other possible basis functions to use. Another possible basis function is the use of orthogonal polynomials. There are many possible orthogonal polynomials, such as Legrange, Hermite, or Jacobi. This is similar to the formulation of PC [38] and presented in Section 1.4.2. These would utilize a matrix coefficient for each polynomial to generate the HDM. Computationally, this would require more time for a single evaluation compared to previous use of polynomials, but can be more accurate depending on the desired analysis. This formulation has not previously been implemented.

The previous basis functions are candidate functions that do not consider any information about the physics of the system. These can be used for any variable on any system. If some information about how the response changes with the uncertain input, this can be used to increase the accuracy of the system. One example of how this can be used is the interpolation function used by Epureanu in [74] for the stiffness matrix. This basis function can be used on the stiffness matrix for the case of geometric variation. The function used is based on a 8-node brick finite element, but the procedure can be used for other element types with a slightly different function. This function

can be expressed as

$$K(p_0 + \delta p) = \frac{K_0 + K_1\delta p + K_2\delta p^2 + K_3\delta p^3 + K_4\delta p^4}{D(\delta p)}, \tag{3.6}$$

where K_i are unknown matrix coefficients, p is the unknown parameter, and $D(\delta p)$ can be expressed as

$$D(\delta p) = (1 + \frac{\delta p}{p_0})(1 + \frac{\delta p}{2p_0})(1 + \frac{\delta p}{3p_0}). \tag{3.7}$$

This implementation uses five unknown matrix coefficients and requires at least five data points. The work done in [74] only applies this basis function for the stiffness matrix and a classic polynomial for the mass matrix. Useful insight into the physics of the system is able to give a much more accurate surrogate model. Even at a possible increase in computational requirement, the computational time is significantly less than that of the full system due to the possible re-meshing and new models to be generated at each desired thickness.

The functions discussed in this section are only a selected few candidate functions that are simple to use. These are by no means an exhaustive survey of functions, but show a couple examples of polynomial type of basis functions. Other possible classes of functions can be used. One example of this would be similar to a Fourier transform, where the response is described with the use of sine functions. Another class of functions would be that of splines or exponentials. These different classes of functions are not implemented but are feasible.

3.4 Brake-Reuß Beam Example

In order to evaluate these methods, the example is chosen to be the BRB. This system is chosen due to the relative simplicity and the ability to complicate the system due to the joint mechanics [75, 76]. The material is assumed to be an uncertain temper of aluminum. This uncertain temper

leads to an uncertainty in the Young's modulus. This physical beam is constructed with two identical specimens and screwed together through a lap joint. The assembly can be seen in Figure 3.3.

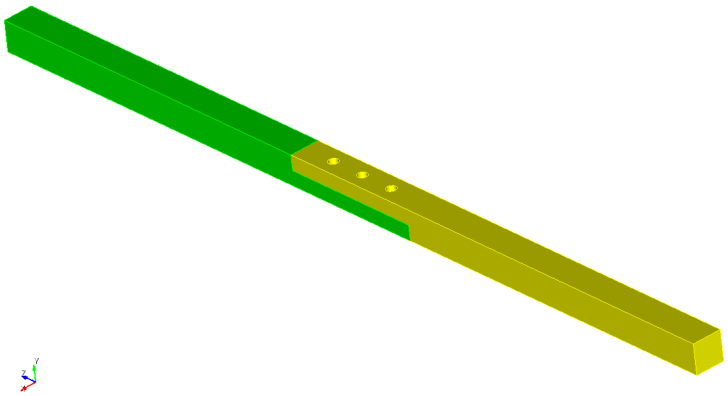

Figure 3.3: The Brake-Reuß Beam Geometry

For the purpose of these calculations, no interface dynamics are considered. The model is assumed linear and with a rigid connection between the two specimens. This model is created using hex elements and has a total of approximately 63,000 translational DOF. The rotational DOF are statically reduced out of the model to reduce the overall size of the model.

The comparison between the models will consist of the first fourteen elastic free-free modes. Selecting the first fourteen is based on determining the effect of this uncertainty in the low and mid-frequency ranges. This range of frequencies contains bending, torsional, and axial mode shape. Another important aspect to consider is the interface for the CB representation. For this model, one end of the beam is determined to be the interface. This is chosen for the relative small amount of node, 81 nodes on each end. One important note is that the screws are not physically modeled in this analysis. Since this report considers the interface as rigid, the addition of the screws is not considered.

This system can become a very useful example for both model reduction and mechanical joint

analysis. When used for model reduction, the system becomes a linear-elastic beam with constant cross-section. Investigating the mechanical joints are a very interesting aspect to this example. Since the specimens are manufactured, each can contain slightly different surface finishes at the lap joint that can lead to different dynamics experimentally. While the investigation into this is interesting, this is not presented here but the preliminary investigation is documented in [77].

3.4.1 Small Variability

The first simulation presented is for the case where some information is known about the uncertain parameter. This is interpreted as a small variability in the uncertain parameter. The first result is a parameter sweep that gives an idea on how accurate the reduction methods are compared to the true solution. All modes were computed individually and the first and fourteenth natural frequencies are presented. The results are presented in Figures 3.4a-b. These figures show the first order models, which is the least accurate models generated.

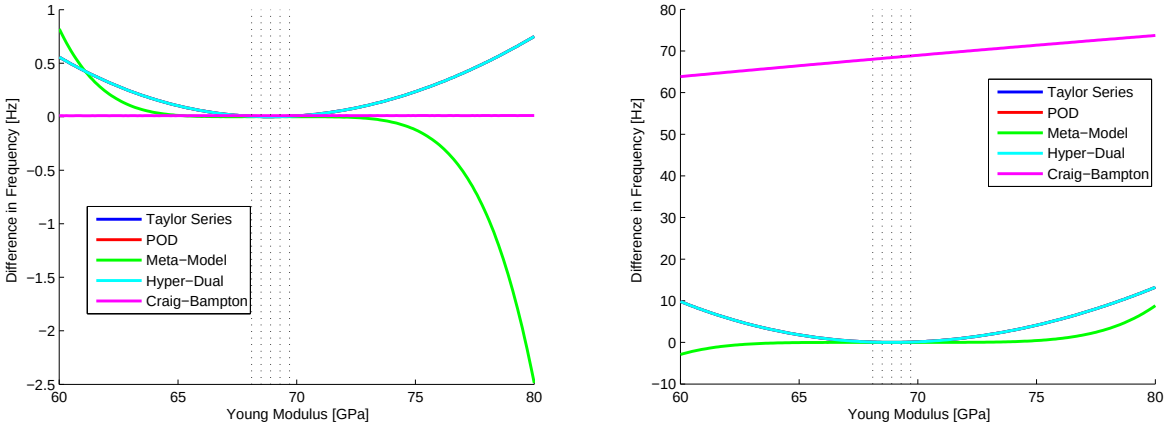

(a) Fundamental Natural Frequency *(b)* 14^{th} Natural Frequency

Figure 3.4: Difference in Natural Frequency with Small Variability Parameter Sweep

In Figures 3.4a-b, the vertical black dotted lines correspond to the data points that the models were generated at. The Taylor series, POD, and CB used the data from all five data points. The HDM used the middle and the outer points so that only three points were used in the derivation,

and the HD method only used the nominal value, which is the middle vertical line. It can be seen that for the first natural frequency, all the methods do very well for the majority of the range but start to lose accuracy closer to the extremes of the parameter sweep. For these figures, the POD, HD, and Taylor series have lines that overlay. This can be seen as the HD curve. The fourteenth natural frequency however shows more inaccuracy. One thing that can be seen is that the CB model has a frequency offset from the truth data. This is not unexpected since the CB is a matrix level reduction method and the higher frequency modes typically require more information, which is reduced out. This error however can be acceptable depending on the accuracy requirement or decreased by including more DOF during the reduction process.

One of the major motivations for this research is to compare both accuracy and time requirements to use these PROMs. The first quantitative comparison is the required time to compute these parameter sweep curves. This utilizes 201 model evaluations to get the desired resolution. The time required to produce the parameter sweep curve is presented in Table 3.1. Each method uses less than 6 high-fidelity code evaluations while the truth data requires 201 high-fidelity code evaluations.

Table 3.1: Computation Time to Generate Parameter Sweep [s]

Order	Taylor	POD	HD	HDM	CB
1	28.78	6.61	16.20	0.21	88.14
2	29.86	6.65	17.48	0.19	85.01
3	30.75	6.64	18.90	0.18	86.07
4	32.08	6.55	N/A	N/A	86.07

In Table 3.1, the order refers to the number of derivatives that are used in the parameterization. The CB representation takes the longest to compute by a factor of almost three to the next slowest method. This is a major drawback, but this is due to the parameterization. For the CB representation, the system is parameterized at the system matrix level while the others are parameterized at the natural frequency level. The HDM requires the least amount of time to

compute the curve. This is due to the basis function that is simpler to evaluate than a Taylor series. The HDM however takes more time to determine the unknown coefficients compared to the Taylor series, but this increase in time is not considered in Table 3.1 as it only records the time to generate the parameter sweep and not the generation of the model. One other possible reason for this difference is due to the storage of the model. For the HDM, only the natural frequency model is stored, while the other four models contain both the natural frequencies and the mode shapes. The HDM was unable to be generated for the collection of mode shapes. This is due to the large matrix inversions that are required. When the mode shapes are removed for the HD model, the evaluation times are comparable.

The next result to report is the root mean square (RMS) error of the parameter sweep. Model reduction error can be quantitatively measured using this value. The model reduction error measure takes the RMS of the percent difference for each value of the Young's modulus for each natural frequency. This produces a singular value that can be used for comparison. The first and fourteenth natural frequencies are presented in Table 3.2.

Table 3.2: RMS Frequency Error for Small Variability [%]

Order	Taylor	POD	HD	HDM	CB
Fundamental Frequency					
1	0.119	0.119	0.119	0.225	0.004
2	0.008	0.008	0.008	41.96	0.004
3	0.001	0.001	0.001	Large	0.004
4	0.000	0.000	N/A	N/A	0.004
14^{th} Frequency					
1	0.119	0.119	0.119	0.045	1.556
2	0.008	0.008	0.008	8.422	1.556
3	0.001	0.001	0.001	Large	1.556
4	0.000	0.000	N/A	N/A	1.556

One trend to note is that the Taylor series, POD, and HD methods have the same accuracy for all frequencies and each order. The POD and Taylor series are expected to have the same accuracy but the HD gives the same accuracy because the points used for the finite difference

are very closely spaced that approximates the same derivative as the HD. The CB model is the only one that is expected to have different accuracies for different natural frequencies since it is system parameterized while the other methods are purely output based parameterized. This system level parameterization is also able to determine other possible outputs, such as frequency response functions or higher frequency modes, without needing to be regenerated.

Another important trend of note is for the HDM. The first order model matches the value and the first derivative at each of the three data points. This provides a very accurate representation for the range enclosed by the data. When the extra derivatives are also matched, the error increases over the extrapolation range of the sweep. This is believed to occur due to added powers on the polynomial curve. Using these extra powers is an over fitting of the data. This is similar to fitting a cubic curve on a quadratic function. Over fitting of the data greatly increases the predictive error as the input extends from the range enclosed by the data used for the model generation. This can easily be seen in Figure 3.5 that shows the second order approximation for the fundamental frequency where all the models are overlay-ed on each other except the HDM curve. The results show that near the extremes of the range, the HDM creates a very large error.

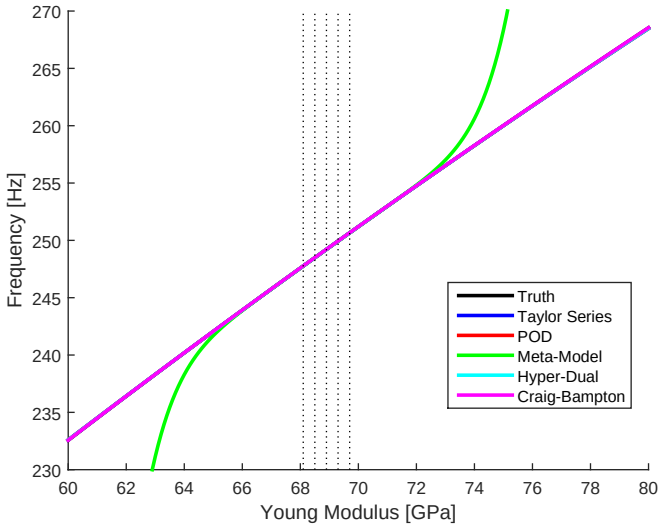

Figure 3.5: Fundamental Frequency using Second Order Models with Small Variability

3.4.2 Large Parameter Sweep

The simulations that only contained small variations are unable to differentiate between the Taylor series, POD, and HD methods. There is a difference in computation time but the computations resulted in the exact same numerical values. In order to determine if there is a difference, the variation of the Young's modulus is increased. The previous sweep ran between $E \in [60, 80]$ GPa, while this sweep is between $E \in [50, 300]$ GPa. Each model is reconstructed at different specified values. The results of the sweep are shown in Figures 3.6a-b.

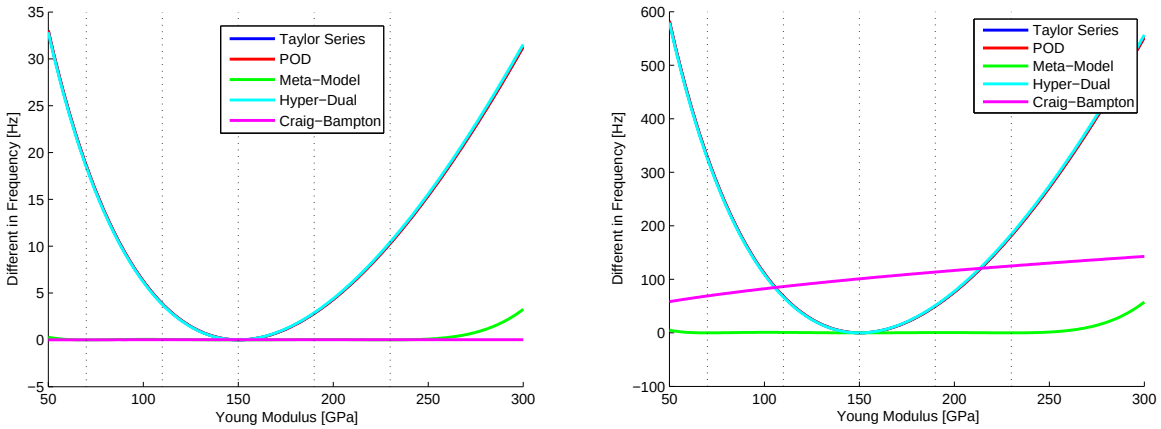

(a) Fundamental Natural Frequency

(b) 14^{th} Natural Frequency

Figure 3.6: Difference in Natural Frequency with Large Variability Parameter Sweep

It is easy to see that the overall accuracy has decreased due to the large variability range. The first natural frequency illustrates this decrease in accuracy, which can be seen for the first order analysis in Figure 3.6a. A majority of the methods are linear with the change in the Young's modulus due to the Taylor series truncation. There are only two nonlinear methods at this order, the CB and HDM that follow the truth data almost perfectly. The fourteenth natural frequency shows more differences between the nonlinear methods.

The accuracy of the models depends on how the output changes with a varied input. That implies that the more linear the relationship, the more accurate these reductions are. The Young's

modulus is fairly linear with respect to the natural frequencies. Other types of variability, such as Poisson ratio or a geometric length, decrease the accuracy of these reduction techniques. These other possible variabilities are currently being researched with some results for other systems also reported in this dissertation. The first quantitative measurable difference between the methods is the computational time to compute the parameter sweep curves. These computational times are shown in Table 3.3 and shows the same trends as in Table 3.1. The HDM is the fastest by a substantial amount and the CB model takes the most time.

Table 3.3: Computation Time to Generate Parameter Sweep [s]

Order	Taylor	POD	HD	HDM	CB
1	33.75	8.00	20.56	0.24	107.75
2	35.11	8.36	21.40	0.23	107.84
3	35.41	8.16	22.75	0.23	109.87
4	37.04	8.06	N/A	N/A	109.87

The next result is the RMS error. This measure is the same as in Section 3.4.1, and the results are presented in Table 3.4. One important trend is that the Taylor series and POD gives the exactly same solution. This is a good comparison because the time required to evaluate the POD model is significantly less than Taylor but gives the same accuracy measurement. Another important trend is the comparison between the Taylor series and the HD representation. The HD only takes data from a single data point and it provides a more accurate solution than the Taylor series method which uses five data points. This shows the advantage of using the HD method.

Another interesting trend is between the HDM and HD methods. The HDM provides better accuracy than the HD method at about 1% of the computational time. While the determination of the model takes more time, this method can overall be a cost savings in the long run. The last trend of interest is the CB model. This model produced the same accuracy for both the scenarios of small and large variability, as seen in Tables 3.2 & 3.4.

Table 3.4: RMS Frequency Error for Large Variability [%]

Order	Taylor	POD	HD	HDM	CB
Fundamental Frequency					
1	4.311	4.311	4.304	0.127	0.004
2	1.519	1.519	1.488	0.052	0.004
3	0.808	0.808	0.671	0.269	0.004
4	0.221	0.221	N/A	N/A	0.004
14^{th} Frequency					
1	4.311	4.311	4.304	0.127	1.556
2	1.519	1.519	1.488	0.053	1.556
3	0.808	0.808	0.671	0.270	1.556
4	0.221	0.221	N/A	N/A	1.556

3.4.3 Distribution Comparison

The accuracy of the reduction models is not purely based on a point-by-point comparison from a parameter sweep; It is also dependent on how the model correctly generates the output distribution. This is important information when using a ROM, particularly for UQ analysis. Using this information allows for statistical correlations and reliability calculations to be performed. In order to generate this distribution, a MC sampling analysis is typically performed. This is a traditional MC analysis that takes random samples from the input parameter distribution and propagates it to determine the output distribution. The first important determination is the distribution of the input parameter. For some parameters, this is a simple determination based on a large amount of data while some others are dependent on engineering judgment. One major consideration is that the bounds of the distribution must remain physical, the mass density must remain positive for example. For the Young's modulus, a log-normal distribution was selected. This was chosen based on the support of $E \in (0, \infty)$. The distribution never reaches zero but is always positive.

It is chosen that this distribution has a mean of 150 GPa and a coefficient of variation of 14%. This was chosen to fully test the range of the parameter sweep, with only the mean based on experimental data. The input probability density distribution can be seen in Figure 3.7 with $100,000$ samples. This distribution is generated from both a histogram and with a Gaussian

kernel estimator. For sample sets with a large number of samples, both methods yield the same distribution. The use of the kernel estimator is very useful for a small amount of samples, such as in the reduced sampling methods. All of the distributions shown for this system are generated with this Gaussian kernel estimator with the Matlab function "ksdensity.m".

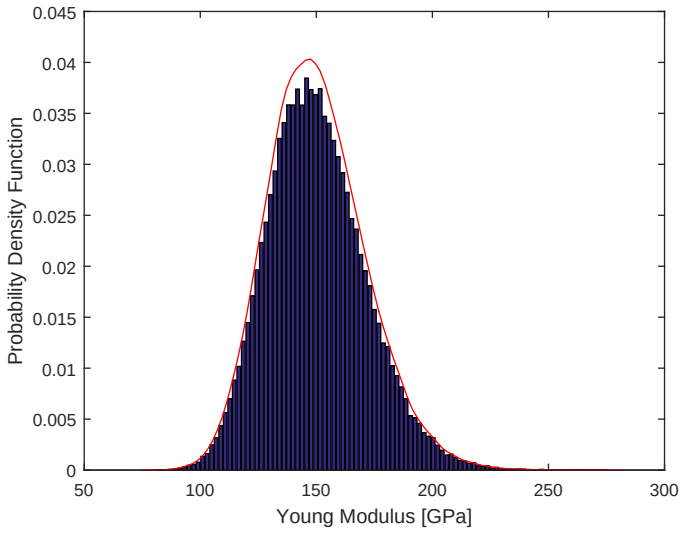

Figure 3.7: Histogram of 100,000 Samples of Young's Modulus in Monte-Carlo analysis

The next major consideration is how to compare the distributions. There are several ways to compare distributions: visually, box-plot, statistical moments, etc. Statistical moments were chosen to be the comparative value, in particular, the first four statistical moments and the lower fractile were chosen for the quantitative reporting. The probability distributions are also presented visually to compare qualitatively. This comparison between statistical moments requires some truth data to be compared to. The output distribution is not analytically known so an approximation must be used. In order to approximate the high-fidelity distribution, the truth data from the parameter sweep is utilized. For each value of the Young's modulus, the tabular data of the high-fidelity model is used as the truth data in the MC analysis. If the value is between two data points in the tabular data, a linear interpolation is used to determine the truth data.

The first result presented is a qualitative analysis of the distributions. Figure 3.8a shows the

distributions for each type of model reduction and the truth data. The truth data in Figure 3.8a is difficult to see but it is overlay-ed with the HDM. By a visual examination, the distributions look very similar. The first trend is that the CB method is shifted to the right of the other curves. The rest of the curves are very close to the truth data. A point-by-point difference of the distribution is shown in Figure 3.8b. One of the main things to see in Figure 3.8b is that the HDM has very little difference in probability, practically zero. The other trend to note is that the Taylor series, POD, and HD methods are similar in error as seen by the overlay of the lines.

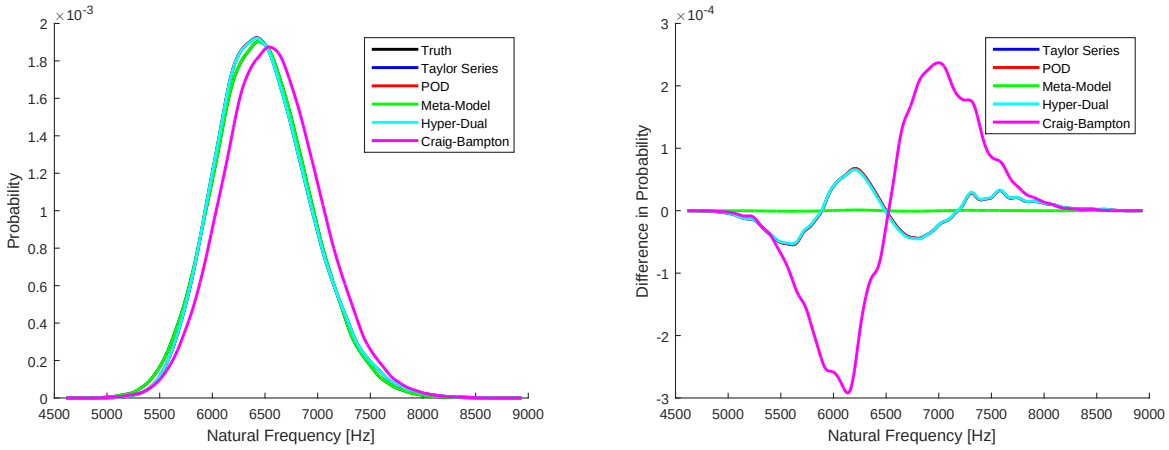

(a) Distributions *(b)* Difference in Distributions

Figure 3.8: 14^{th} Natural Frequency with 100,000 MC Samples Distribution

Qualitative results do not show many differences between the distributions besides the CB and HDM, requiring a quantitative analysis. The first analysis presented is the time requirement to compute the distribution. These times follow the same trend as the parameter sweep as shown in Table 3.3. For $100,000$ samples, the HDM takes 5 seconds and the CB takes 9 minutes on 128 cores with the help of parallel processing. The actual values are repetitive and therefor not reported. The next quantitative analysis is the difference of the statistical moments. For this analysis the first four statistical moments are compared, which are related to the mean, variance, skewness, and kurtosis of the distribution. This error is taken as the percent difference from the statistical

moments of the truth distribution. Table 3.5 shows the RMS error for the first four statistical moments combined for the first fourteen natural frequencies.

Table 3.5: RMS Error for the Statistical Moments for all Natural Frequencies [%]

Order	Taylor	POD	HD	HDM	CB
1	0.685	0.685	0.690	0.009	1.909
2	0.032	0.032	0.030	0.000	1.933
3	0.021	0.021	0.014	0.000	1.944
4	0.001	0.001	NA	NA	2.037

The results in Table 3.5 show that every method used has relatively small error. CB representation had the largest error of 2%, which can be acceptable. POD and Taylor again result in the exact same results but the time difference between the two methods is significant. The HD and Taylor series produce very similar results, except that the HD only required one high-fidelity code evaluations. Similarly, the HDM gives the best results out of all the methods and gives the results in the least amount of time.

While the distributions are a good measure of accuracy, the lower fractile is a more useful quantity for reliability engineers. In this analysis, the lower fractile is defined as

$$x \ni Pr(X \leq x) = 0.1\%, \tag{3.8}$$

where x is the location of the lower fractile. The probability is calculated based on the kernel generated distribution of the sampled data. These value for the fundamental frequency is presented in Table 3.6.

Table 3.6: Fundamental Frequency Value of the Lower Fractile Location

	Frequency [Hz]	% Difference
True Data	295.24	-
Taylor Series	302.47	2.45
POD	302.47	2.45
HD	302.38	2.42
HDM	295.29	0.02
CB	295.24	0.00

The data in Table 3.6 shows a very similar trend as the parameter sweep, where the HDM gives very high accuracy and the Taylor series proves a decent accuracy. The trend also follows that the CB model is the most accurate for the fundamental frequency. This accuracy decreases for higher frequencies but is still more accurate than Taylor series, POD, and HD. The results for the other frequencies are not reported but show the same trend.

3.4.4 Distribution Determination using Reduced Sampling

The previous section utilized $100,000$ sample in a traditional MC analysis. That large of a sample space is not usually available for more difficult or complex systems even with the use of ROMs and parallel processing. Some ROMs can still take a large amount of time depending on what type of ROM is used. In practice, a reduced sample size is required due to time and computation restrictions. These methods are discussed in more detail in Chapter 1. Two methods are examined in order to test the accuracy of each method compared to the full MC analysis, (1) SROM and (2) LHC. The SROM technique is presented in [78] and Section 1.3.3. This method takes a subset of the large sampling that best matches the statistical moments by using different probability values at each data point. The LHC sampling technique is presented in [79] and Section 1.3.2. LHC sampling is essentially dividing the distribution into equal probable sections then selecting a random point within each section to use for the sampling, and treated with equal probability. For each sampling technique, two different number of reduction points are used: 50 and 100 data points. This is a dramatic reduction from $100,000$ but shows the effectiveness of these different sampling techniques.

Latin Hypercube Sampling

The LHC sampling technique splits the input domains into equally probable sections and uses one sample from each section. LHC is implemented in Matlab for a normal distribution, but not a log-

normal distribution. A custom function is created to use this sampling technique for a log-normal distribution. LHC sampling can become more complicated to implement in multiple dimensions, while this system uses only a univariate distribution of the Young's modulus. Using this method requires more memory to store the samples compared to the traditional MC analysis, which selects each data point randomly at each iteration. This memory increase is typically acceptable since the required number of samples is much smaller.

The first case of this sampling technique is the results for 50 samples. Qualitative results are shown in Figures 3.9a-b. This shows that the HDM and the truth distribution are almost identical. Figure 3.9a shows the distribution of the fourteenth natural frequency with the use of a Gaussian kernel, and the point-by-point difference between the distributions shown in Figure 3.9b.

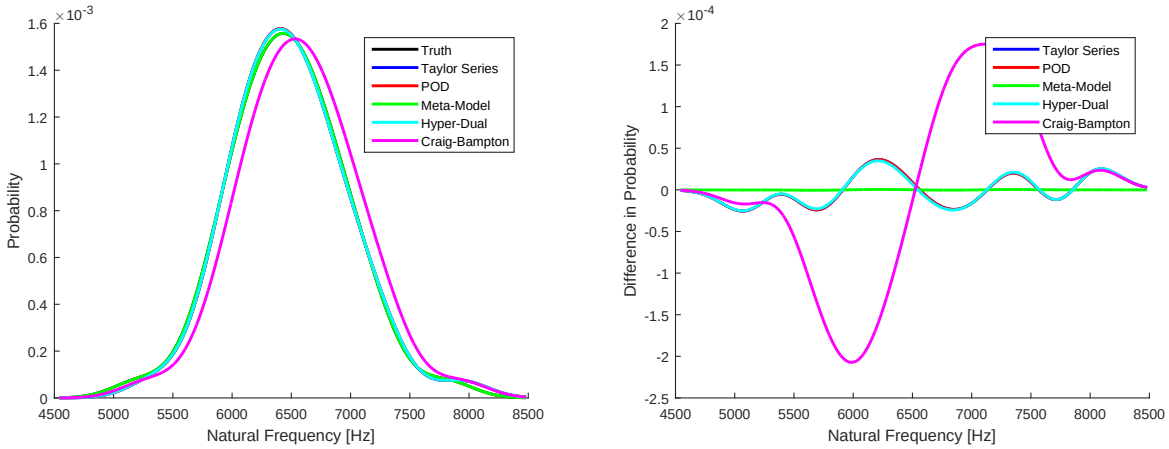

(a) Distributions *(b)* Difference in Distribution

Figure 3.9: 14^{th} Natural Frequency with 50 Sample LHC Distributions

One important comparison is between the reduced sampling and the full MC analysis. The error of the statistical moments are shown in Table 3.7. This shows the percentage error compared to the moments from the full MC analysis statistical moments using the truth distribution for the first fourteen natural frequencies. The first interesting trend is that the HDM gives very accurate results even in the first order approximation. Secondly, the CB performed worse than the

other reduction methods. This is partially due to the inaccuracy of the CB on an individual code evaluation. The inaccuracy is also noted in Figure 3.8a for the large MC analysis with the shift in the peak, and this inaccuracy is further increased due to the use of the reduced sampling methods.

Table 3.7: LHC RMS Error for the Statistical Moments for First Fourteen Frequencies [%]

Order	Taylor	POD	HD	HDM	CB
50 Samples					
1	0.739	0.739	0.744	0.009	1.821
2	0.038	0.038	0.036	0.000	1.821
3	0.028	0.028	0.019	0.000	1.821
4	0.001	0.001	NA	NA	1.821
100 Samples					
1	0.685	0.685	0.690	0.009	10.029
2	0.034	0.034	0.032	0.000	1.821
3	0.022	0.022	0.014	0.000	1.821
4	0.002	0.002	NA	NA	1.821

While the accuracy of using 50 samples is decent, an increase in the number of samples can increase the accuracy; thusly, the accuracy of using 100 samples is also desired. These distributions can be seen in Figures 3.10a-b. They show the same general trends as the 50 sample results.

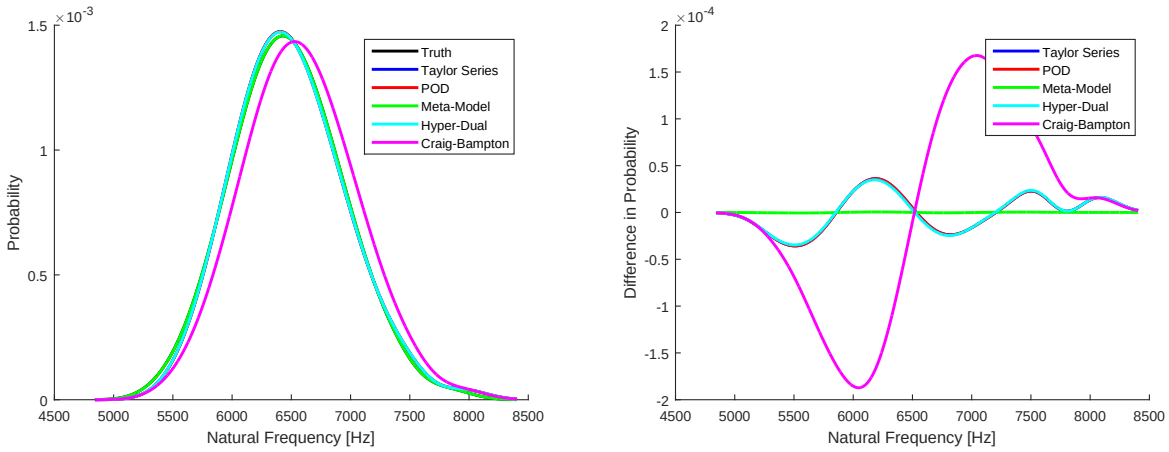

(a) Distributions *(b)* Difference in Distribution

Figure 3.10: 14^{th} Natural Frequency with 100 Sample LHC Distributions

The more interesting aspect is the accuracy increase for 100 samples. These results are also presented in Table 3.7. The first comment is the error for almost all the methods decrease at most

orders. An exception is the HDM that has no change in the RMS error. For the CB model, the first order approximation has an increase in error while the other orders have the same error as with 50 samples. Reasons for this increased error is not known, but is being investigated. The next trend of note is that the double in samples does not correspond to a halving of the error. The Taylor series, POD, and HD methods only have a small change in the error with zero change for the HDM and CB methods.

SROM Sampling

Another technique of reducing the required number of samples is the SROM technique. This method selects the optimal subset to match the first six statistical moments of the input distribution. One of the main aspects of this method is the use of non-equal probabilities to better represent the distribution curve. Another interesting aspect is the flexibility of the method. The selection of the samples and probabilities is defined by minimizing an objective function that the user defines based on the important information for the system, such as statistical moments.

The first results are for 50 samples in the distribution. The distributions are shown in Figures 3.11a-b. These distributions follow the same trend as the LHC method, where the HDM is almost perfect while the Taylor series, POD, and HD methods all are close to the true value but with noticeable error. The CB method also has a very large error.

The error on the statistical moments are presented in Table 3.8. One of the most interesting comparisons between the LHC and the SROM sampling is the difference for the Taylor, POD, and HD methods. For the SROM sampling technique, the error is less than for the LHC sampling. The 50 sample SROM has similar error to the 100 sample LHC. Another interesting comparison is the HDM and CB methods that has the same error, independent of sampling method.

The next analysis is to increase the number of samples to 100. The distributions are presented

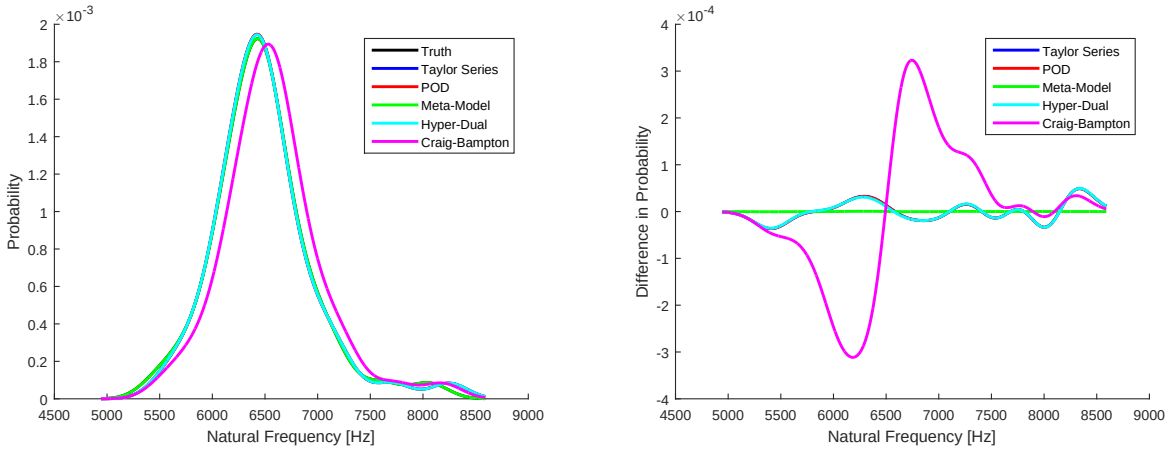

(a) Distributions *(b)* Difference in Distribution

Figure 3.11: 14^{th} Natural Frequency with 50 Sample SROM Distributions

Table 3.8: SROM RMS Error for the Statistical Moments for First Fourteen Frequencies [%]

Order	Taylor	POD	HD	HDM	CB
50 Samples					
1	0.678	0.678	0.682	0.009	1.821
2	0.033	0.033	0.032	0.000	1.821
3	0.022	0.022	0.014	0.000	1.821
4	0.002	0.002	NA	NA	1.821
100 Samples					
1	0.677	0.677	0.681	0.009	1.821
2	0.033	0.033	0.031	0.000	1.821
3	0.022	0.022	0.014	0.000	1.821
4	0.001	0.001	NA	NA	1.821

in Figures 3.12a-b. These figures show the same trend as the LHC. The only noticeable difference in these distribution is the difference from the truth data around 7500 Hz, which is near the extreme of the distribution range.

The comparison between these distributions and the true distribution in terms of RMS error is presented in Table 3.8. One of the interesting characteristics of this data is that it is very close in error to the 50 sample case of SROM. The overall error decreases with the increase in samples but not by as large amount as the LHC sampling. For the HDM and CB methods, the error is the same for both sampling methods at all the orders except for the singular case of LHC with 100 samples for the first order model.

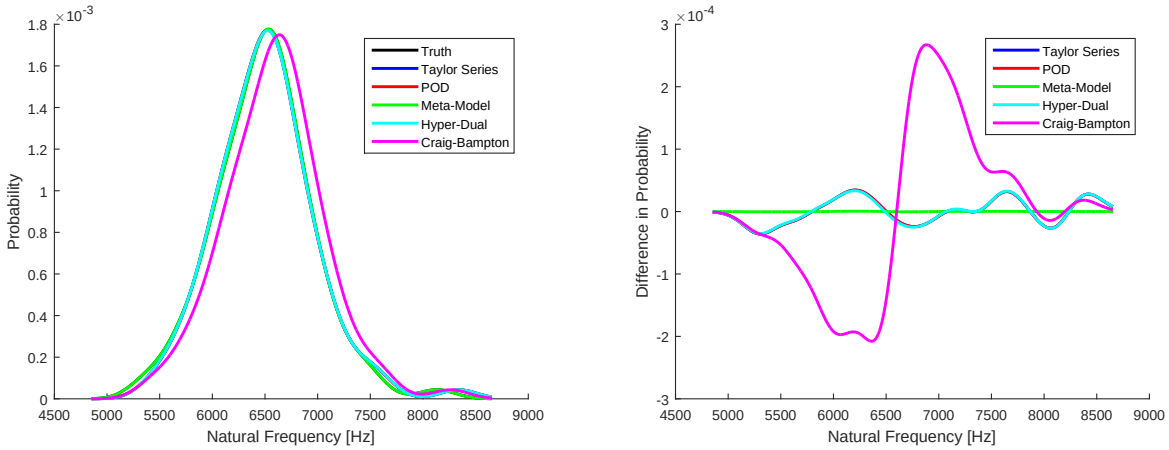

(a) Distributions *(b)* Difference in Distribution

Figure 3.12: 14^{th} Natural Frequency with 100 Sample SROM Distributions

Both the LHC and SROM methods are able to produce reasonably accurate results with much fewer samples than a traditional MC sampling approach. The SROM technique is very useful for situations where very little number of samples are required. One downside to this technique is that an increase in the number of samples does not reduce the error by a substantial amount. The LHC technique is still able to produce accurate results but requires more samples than the SROM technique. One advantage of the LHC technique is the computational time to generate the sample points. This technique is also more straight foreword compared to the SROM technique, which is relatively new and requires an optimization algorithm.

3.5 Frame Example

In a more realistic system, geometric parameters are often uncertain. This uncertainty can come from an uncertain design or physical issues such as manufacturing tolerances. The relationship between the output and the geometric change is much more difficult to determine. In order to explore this relationship, a simplified system with a geometric change is presented. The system that is explored is presented in Figure 3.13. The geometric variation for this system is the length

of the appendage on the left side of the system. This nominal length is 12 inches and is varied by a substantial amount.

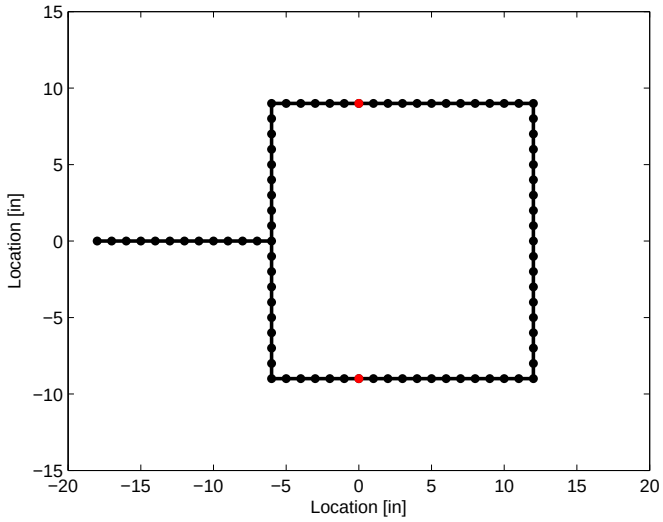

Figure 3.13: Nominal Frame Geometry

This system is the same as analyzed in Chapter 2. In [69], this system explores the use of HD numbers compared to the finite difference method to determine sensitivities. This analysis is an expansion of that research by applying the HDM to the system. In [80], this system is treated as two substructures and the model form error is calculated using the MEA. The system in Figure 3.13 is generated using a custom-made Matlab FE code. This allows for the generation of the system matrices in HD numbers and provides up to the first three derivatives of the mass and stiffness. The HDM is applied to this system at two different parameterization levels and at two different variability ranges, representing different possible uses.

Firstly, the HDM can be applied at any level in the analysis. In this analysis, the HDM is applied at the matrix level and the output level. This is done to show the possibilities of the HDM and how it can be used based on the software available. Applying the HDM at the output level is the simplest implementation as long as solver can use HD numbers. For the system used, the Eigen analysis is programmed in HD numbers, so this output can be done fully in HD numbers, which

is typically much smaller in size than the matrix parameterization. The other parameterization is applied at the system matrix level. This applies the basis functions to the mass and stiffness matrix. As one can expect, the matrix coefficients are much larger in size compared to output coefficients. This shows that if the solver is not programmed in HD numbers, the HDM can still be applied and can give reasonable results. For example, if the time history is desired, current programming does not allow for time integration. But if the basis function is applied before the integration, the system can be reduced to the real domain then sent through the required solver. This provides the possibility of using advanced codes and solvers without a complete reprogramming of the algorithms. As a side note, if the algorithm is expressed simply, a redefinition of the elementary functions, such as plus and multiply, can be implemented to allow for easy conversion of the complicated solver to a HD solver.

This analysis is also applied for two different ranges of variation, small and large. The small variation is a representative analysis for a production variation analysis. This would be representative of manufacturing tolerances and thus be able to determine reliability information such as failure probability. The other range is representative of the design stage. If the design engineer desires to vary geometric components to best match requirements, such as nuclear qualification or compartment size requirements, then the HDM can be used as a surrogate model to decrease the design time and thus reduce design costs.

3.5.1 Reliability Analysis

This type of analysis is based on a completed design process to quantify the effect of tolerances and defects on the final output. The range of variability is representative of a tolerance build-up or a small defect due to physical handling. Mathematically, this is defined as a length variation of $\pm 10\%$. The HDM uses three data points at $L = \{10.8, 12.0, 13.2\}$in. At each of the data points,

the first two derivatives are computed. This allows for up to the second order HDM generation. The main output investigated is the fundamental frequency along with the second elastic natural frequency to investigate the scalability of the method. The results show two versions of the HDM: one where the parameterization is performed at the system level, and one parameterized at the eigenvalue level. One of the metric of comparison for the HDM is the computational time for both parameterization levels. The difference in the computational time is due to the re-evaluation of the eigenvalue analysis for the matrix parameterization. The first result presented is the fundamental frequency of the system as a function of the length of the appendage using the first derivative information and can be seen in Figure 3.14a. First thing to note is the limits on the length of the appendage. The length is varied from $L \in [8, 15] in.$, which indicates a 33.3% range.

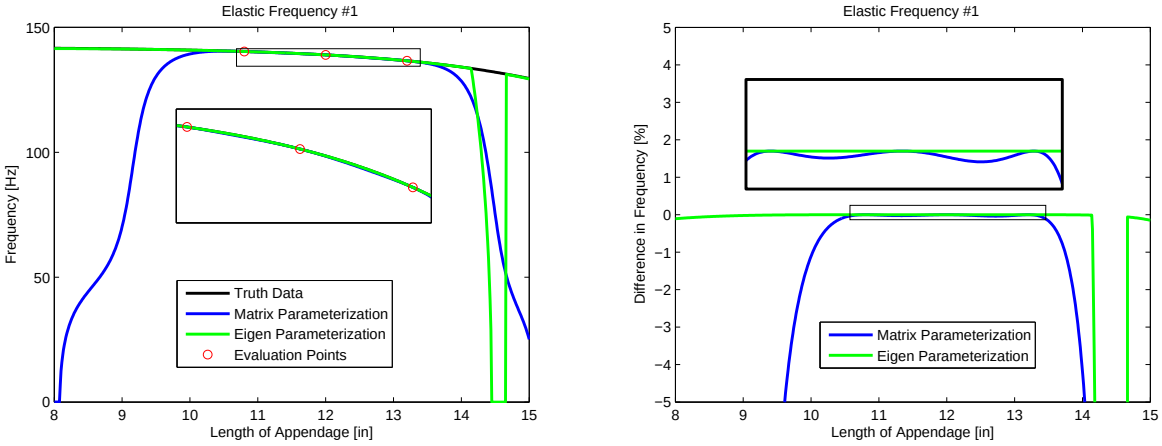

(a) Frequency *(b)* Difference in Frequency

Figure 3.14: Fundamental Frequency with 10% Variation

In Figure 3.14a, a zoomed in region shows the range enclosed by the data used in the HDM generation. The difference between the parameterizations and the truth data is small. This shows that either type of parameterization is accurate for this type of range enclosed by the generation point with this level of variability. Once the model is extrapolated, the differences between the parameterizations becomes more apparent. This is better displayed as the a point-by-point difference

in the fundamental frequency as shown in Figure 3.14b.

This curve also shows a zoomed region to show the small differences within the model evaluations. The difference is very small, but does show that the Eigen parameterization is more accurate. It can also be seen is that the Eigen parameterization is valid for a much larger range than the system matrix parameterization. For a 95% accurate model, the matrix parameterization is valid from $L \in [9.6, 14]in$ and the Eigen parameterization is valid from $L \in (< 8, 14.1]in$. Around $14.5in$, there is some numerical issues that occurred within the Eigen parameterization model. The reason for this is being investigated, but is primarily believed to be due to ill-conditioning or mode switching.

Along with the fundamental frequency, the second elastic natural frequency is also evaluated. This was done to evaluate higher natural frequencies and to see if the more physics based matrix parameterization if more effective in the higher natural frequencies. The second natural frequency is presented in Figure 3.15.

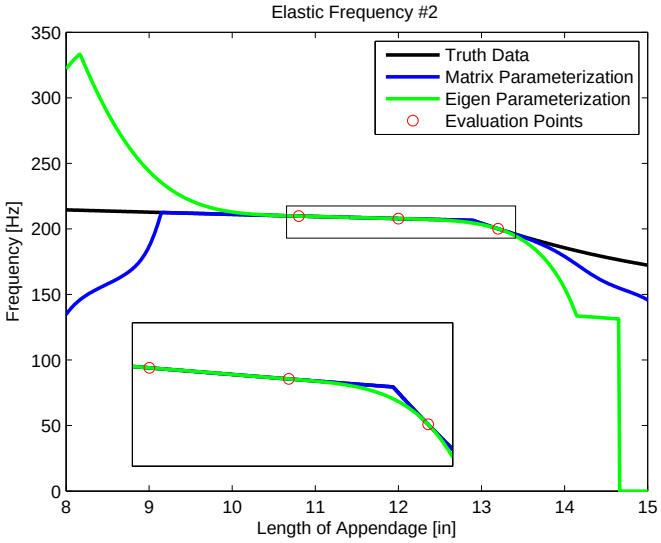

Figure 3.15: 2^{nd} Elastic Natural Frequency with 10% Variation

One of the most interesting aspect of Figure 3.15 is that the matrix parameterization produces accurate results for a larger range than the Eigen parameterization. For the matrix parameteri-

zation, the 95% accuracy range is $L \in [9, 14.1] in$ and the range for the Eigen parameterization is $L \in [9.5, 13.7] in$. Another interesting aspect of the matrix parameterization is that the predicted natural frequency is lower than the true value. This is not true for the Eigen parameterization as easily seen in Figure 3.15.

The results shown are for only taking the nominal values and the first derivative at each data-point, called the first order HDM. This is the most expected version of the HDM since this can be done for a single uncertain variable with the use of a simple complex step. Higher order models and multi-dimensional systems require the use of HD or multi-complex numbers to produce accurate derivatives. Using this extra information produces a more accurate model within the evaluation points. This accuracy can be seen in Figure 3.16. One interesting aspect of this higher order model is that there is more numerical errors with the Eigen parameterization. This does not affect the matrix parameterization. One issue with the use of the higher order HDM is the possibility of over fitting the data. This can be seen at the extremes of the range for the matrix parameterization. Over fitting is thought of as applying higher order polynomial than required. This is primarily seen when extrapolating outside of the evaluation points. The values within the evaluation points tend to get more accurate with more information at these points since the information is implicitly contained via the derivatives.

Overall, for this type of analysis, the HDM performs excellent over the desired range. One interesting aspect found is that the extrapolation past the evaluation points is still reasonably accurate. For this amount of variation, 10% of the nominal length, both type of parameterization produce accurate results for length values change of at least 15%. This range is not uncommon for manufacturing tolerances, particularly for small nominal values. The accuracy of the model does depends on what parameterization is used, but for this range of values, there is only a small difference between the parameterizations. This selection depends heavily on the computational

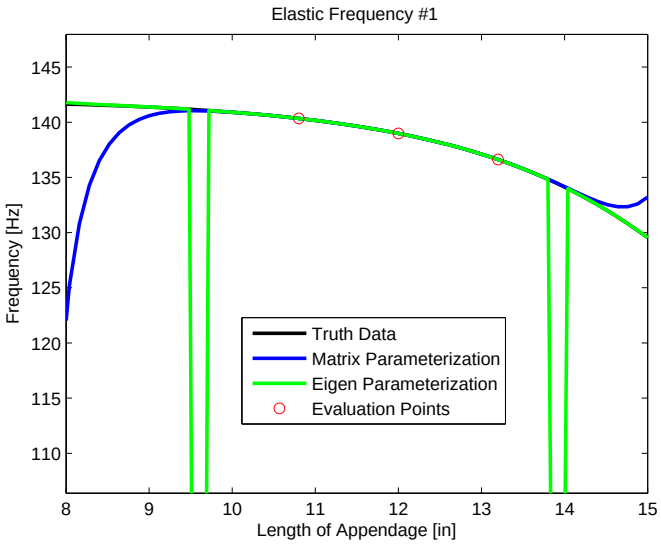

Figure 3.16: Fundamental Frequency Using 2^{nd} Order HDM with 10% Variation

capabilities available, in particular if the solver is capable of evaluating the solution in HD or multi-complex math.

3.5.2 Design Analysis

For this design analysis, an assumption is made that the length of the appendage is unknown and therefor a large variation must be tested. The main difference between the two sections is the location of the evaluation points on the sample space. For this analysis, the variation is performed at $\pm 20\%$. This value was selected to explore a much larger sample space to reflect that a final design is not finalized. The first result for this analysis is the fundamental frequency as a function of the appendage length, as seen in Figure 3.17a. A point-by-point difference can be seen in Figure 3.17b.

One of the main difference between the design analysis and the reliability analysis is the comparison between the two parameterizations. In the reliability analysis, both parameterizations yielded very accurate results within the evaluation points, while a difference between the two parameterizations appear in the design analysis. The first difference between Figure 3.14b and

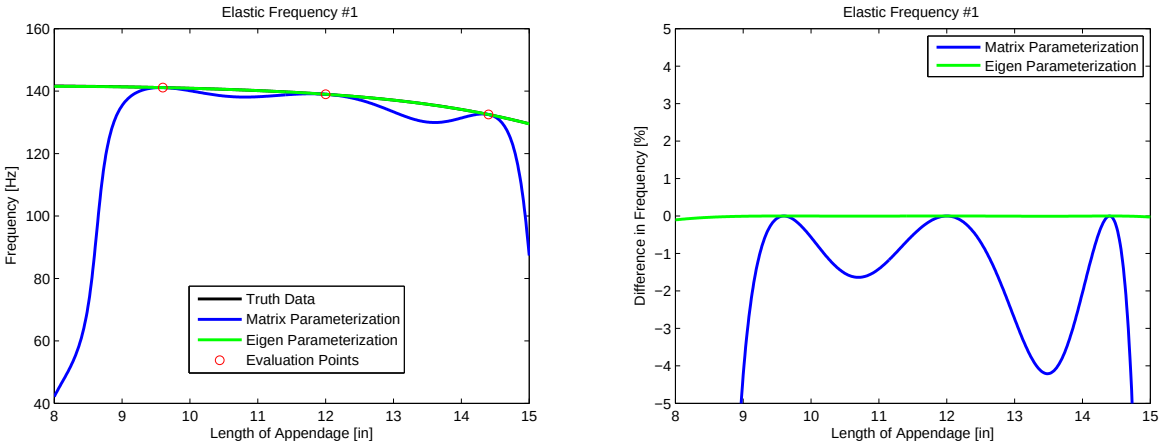

(a) Frequency *(b)* Difference in Frequency

Figure 3.17: Fundamental Frequency with 20% Variation

Figure 3.17b is that the Eigen parameterization does not have a numerical issue around $14.5in$ for the length. This is believed to because there is an evaluation point in the vicinity of that length value. One noticeable aspect in Figure 3.17b is that the matrix and Eigen parameterization show different trends. The matrix parameterization still has a 95% accuracy range within the evaluation points. This range is the reason that 20% variation was selected for this design analysis. When the range is increased to 25%, the accuracy drops below 95% within the evaluation points.

The second order model improves the model compared to the first order model. This can be seen in Figure 3.18. Using the second order model greatly increases the accuracy for the matrix parameterization and slightly increases the accuracy for the eigenvalue parameterization. The Eigen parameterization suffers from some numerical issues around lengths of $8.25in$.

For this design analysis, a large variation of the sample space is explored. Among the two parameterization, the Eigen level parameterization is the most accurate as long as the solution is available with HD or multi-complex numbers, but is not always available depending on the analysis. Using a higher order HDM improves the matrix parameterization greatly and allows a large possible range of variability for a given accuracy.

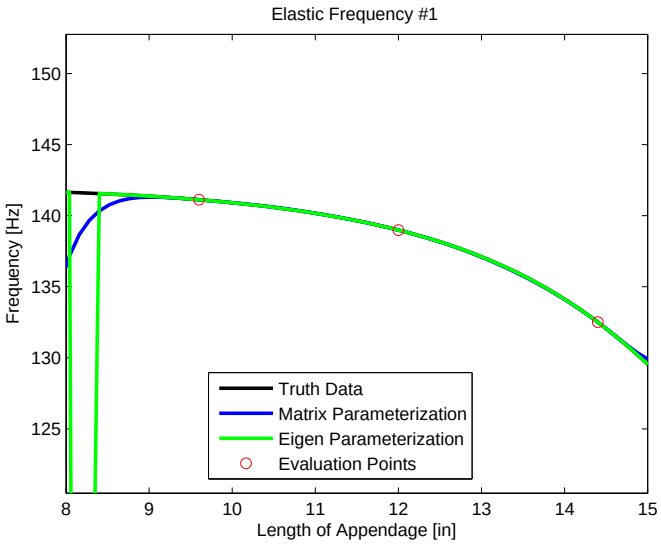

Figure 3.18: Fundamental Frequency Using 2^{nd} Order HDM with 20% Variation

3.6 Paneling Example

The second system that uses a geometric variation is slightly more complicated, but represents a more realistic system. Figure 3.19 shows the panel system with Figure 3.19a showing geometry of the plate for one of the used meshes. The height of the "bumps" is the uncertain parameter in this system. Due to known applications of similar panels, the height of this bump is bounded by the range of $h \in [0, 6]mm$, but is not expected to experience this large of range in typical use. Due to the geometric variations, some special considerations must be taken into account within the mesh. With the increase in volume, two possible options are available: increase element size, or increase the number of elements. Since the stiffness elements for all possible heights are compared directly, the size of the elements at the bump is chosen to increase. The thickness of the panel is comprised of two brick elements. For the bump, one of those elements is fixed then the other is increased in size by the moving of the top set of nodes as shown in Figure 3.19b.

In this system, the sensitivities of the output to the height of the bump is computed with a HD step. Since the uncertain parameter is a geometric variable, the implementation of the HD step is

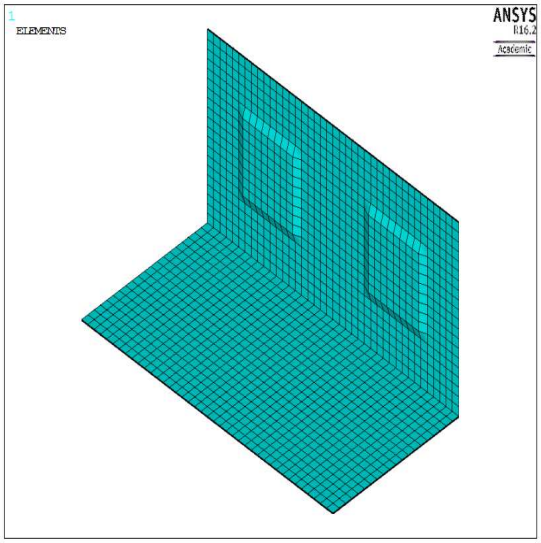

(a) Schematic

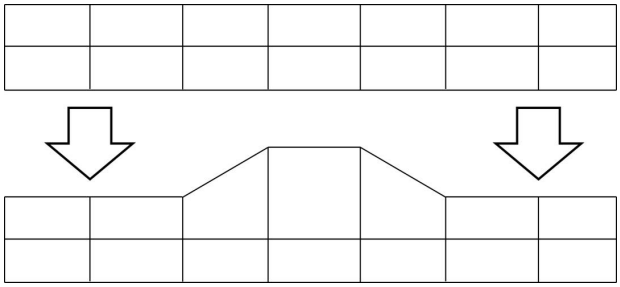

(b) Cross-Section Change for Bump

Figure 3.19: Paneling System

not straight foreword. One method would be to write a program to recreate the geometry and mesh for each value of the geometric parameter as was done for the frame system. For most systems, this is impracticable since the geometry generation is not typically simple. The current implementation generates the geometric location of the node points, then the HD step is implemented into the XYZ location of the changing nodes.

The bump is thought of as an extra deposit of material, such as from additive manufacturing or casting. This change on element height affects both the stiffness and mass of the system. The implementation of the HDM is tested with two different basis functions, (1) a simple polynomial and (2) the interpolation function described in Section 3.3.2, which is denoted in this chapter as 'NX'. Along with the two basis functions, the HDM is also implemented at both the system matrix and the eigenvalue parameterization level. Since the NX basis function is designed for the stiffness matrix, it is only used for the system matrix level implementation.

In order to test out the design choices of using the HDM, two different evaluation sets are discussed, (1) far point selection and (2) close point selection. These sets are based on the assump-

tion that the nominal value of the height of the bump is $3mm$. For the far point selection, three data points are used at $h = \{0, 3, 6\}\, mm$. The close point selection uses data points at heights of $h = \{1.5, 3, 4.5\}\, mm$.

When using the NX basis function, five pieces of data are required in order to determine the matrix coefficients. Since this is a physics based function, the data used should not affect the basis function. This was tested out using multiple combinations of data points and derivatives. While the results are not shown, all the combinations give the same results for the NX HDM. The stiffness matrix uses the NX basis function while the mass matrix uses a simple polynomial.

In order to show the accuracy, two main outputs are selected to be reported. The first output is one element of the stiffness matrix. This is selected as a diagonal element that is affected by the change in the bump. To measure this accuracy, the system matrices are generated at many different values for the height of the bump to be used as truth data. These are clustered around a small value in height since that has the most nonlinear behavior. This output is primarily used to show the accuracy of the polynomial fit along with the NX basis function. The second output is the fundamental frequency of the system. This frequency in around 175 Hz and is a bending mode of the system. Since this system is fixed along one edge, no extra treatment is needed for rigid body motion. This output primarily is used to visualize the difference between the parameterization levels. Looking at this data will show that, if applicable, the HDM should be applied as late in the analysis as possible. This is however not always possible since the desired solvers must be able to evaluate HD numbers. Simple solvers, such as eigenvalue/eigenvector, can easily be programmed with HD numbers, but this is more difficult for nonlinear vibration and dynamic stress analysis.

3.6.1 Far Point Selection

The first analysis to report is the far point selection showing a diagonal term of the stiffness matrix. This result can be seen in Figure 3.20. The first thing to note is that using a polynomial fit for the stiffness matrix does not give a very accurate answer for this large of variability/distance between evaluation points. Along with this inaccuracy, the higher order polynomial also shows an over fitting of the data.

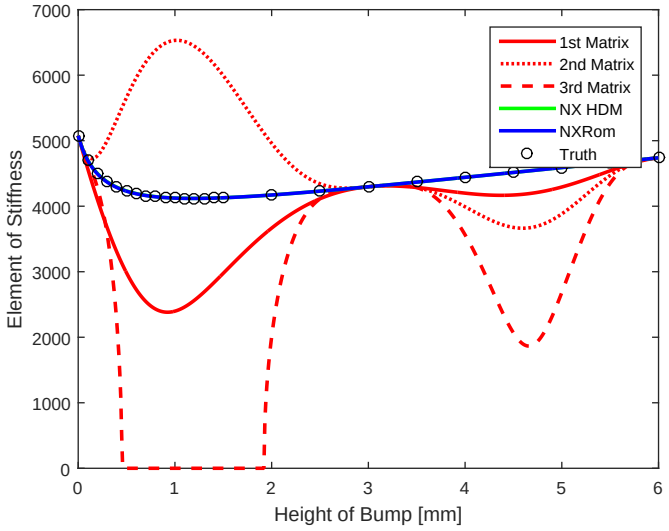

Figure 3.20: Diagonal Term of Stiffness Matrix

There are five different plots in Figure 3.20. The red lines represent a simple polynomial basis function and the different dashing on it represent how many derivatives are used at each evaluation point. A solid line represents using the nominal value and the first derivative at each data point, the dotted line represents using the nominal value and the first two derivatives, and the dashed line represents using the nominal value and the first three derivatives at each point. This shows an over fitting of the data with the higher order polynomials, since the third order HDM has the largest error with height values that are far away from the evaluation points.

The other two lines represents when using the NX interpolation function. The green line

represents when it is applied to the HDM, thus using three nominal values and two derivatives requiring only three simulation evaluations. Theoretically, the same information can be generated by a single code evaluation with the first four derivatives calculated, but not tested. Not shown here is a study of the selection of evaluation points for the generation of the NX interpolation function. This study showed that the selection of the evaluation points produced nearly identical matrix coefficients for the stiffness matrix. The blue line represents when you use five nominal value simulations. This requires more time since a total of five code evaluations are required where the green line only requires three. On this plot, there is no difference between these two models, but future plots will show some slight differences. The black circles represent the truth data generated from the full FE model. Each of these simulations required several man-hours to remake the node locations at the variable heights while maintaining the same number of DOF and indexing of the node numbers.

The main desired output is how the fundamental frequency changes with the geometric variation. For the first result, the Eigen level parameterization is shown in Figure 3.21a. This shows a similar analysis as performed on the BRB in Section 3.4. The HDM is applied using the information at the output level since the Eigen analysis has theoretical derivatives that can be calculated using HD numbers. The result of the HDM gives almost exact results for the entire range. The dotted line represents using the first two derivatives at each evaluation point and gives a more accurate result than using just the first derivative.

If parameterization is possible at the final result level, the HDM shows to have very accurate results, but this is not always feasible. When parameterization must happen earlier in the analysis, the accuracy can decrease, and this result is shown in Figure 3.21b. The first thing to notice is that using the matrix parameterization does not produce as accurate result as the Eigen parameterization. This can easily be seen by the difference between the red and black curves. One interesting

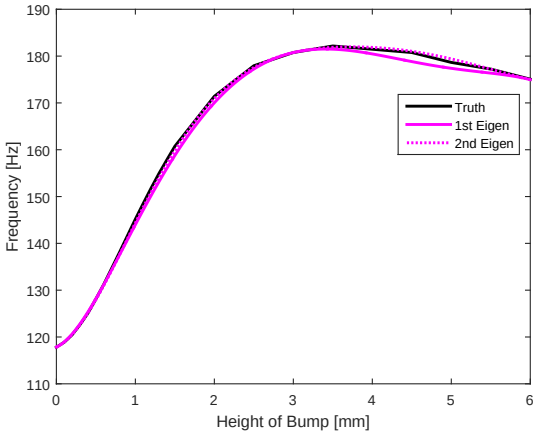

(a) Eigen Parameterization

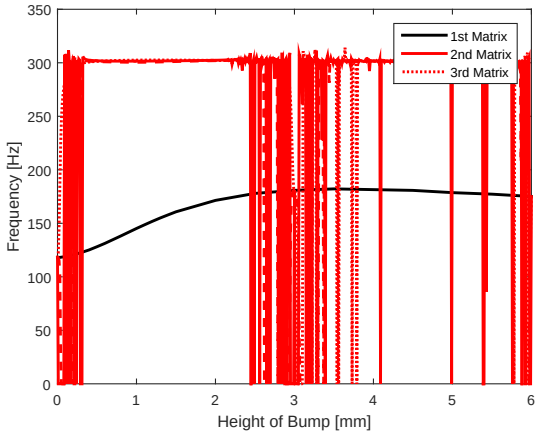

(b) Matrix Parameterization

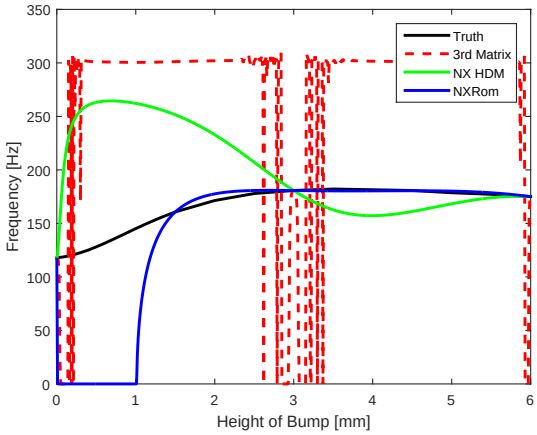

(c) NX Parameterization

Figure 3.21: Fundamental Frequency with Far Point Selection

aspect is that the fundamental frequency is exact for the evaluation points. This is due to how the HDM is derived, the stiffness and mass matrix are exact at each of those evaluation points. Due to this, the frequencies must also be exact. When the height of the bump is not near an evaluation point however, the accuracy is very poor. This is believed to be caused by the distance between the evaluation points being too large for accurate results. Due to this realization, the close point evaluation is used to test this belief.

Along with the polynomial, the NX interpolation function is shown in Figure 3.21c. This also shows the 3^{rd} order polynomial fit, the NX interpolation function in the HDM, and using the

NX-PROM as it is originally derived. One of the most interesting aspects is that the NX-PROM and the NX HDM show different results. This is unique since the interpolation function is the same for both PROMs. Another interesting aspect is the comparison between the polynomial fit and the NX HDM. While the NX HDM is not perfectly accurate, it is much more accurate compared to the polynomial fit. This leads to the thought that using a more realistic basis function allows for a larger variability compared to a generic polynomial fit.

For a large variability of a system, any selection of a PROM is a difficult choice. The most accurate solution for this large variability is to parameterize at the result level. This analysis shows that the HDM is very accurate for the output parameterization. When the parameterization is performed at the system matrix level, the accuracy decreases due to the large variability. Using a more physics based basis function can greatly increase the accuracy of these matrices for a given large range. The variability of $h \in [0, 6]mm$ is very large and is greater than the expected acceptable range. In order to more accurately test the expected range, the variability of the evaluation points used to generate the HDM is reduced.

3.6.2 Near Point Selection

For the variability of $h \in [0, 6]mm$, the Eigen parameterization is accurate while the matrix parameterization is less accurate. Using a more physics based basis function gives a more accurate results as compared to a simple polynomial. In order to test the limit of variability when using a matrix parameterization, the variability is reduced to $h \in [1.5, 4.5]mm$. This range also assumes that there is an expected bump in the design.

For the far point selection, the design space was fully enclosed within the evaluation data points. When the variability is reduced, the simulations are evaluated for the full range of $h \in [0, 6]mm$ to test the accuracy of an extrapolation of the HDM. In Figure 3.22a, the Eigen pa-

rameterization is shown. The accuracy within the evaluation points is almost perfect and the extrapolation is accurate when the second derivatives are used, and slightly less accurate when only using the first derivative.

The far point selection showed that the Eigen parameterization is accurate for large variability. When the parameterization is performed at the system matrix level, the accuracy decreases for large variability. Figure 3.22b shows the parameterization for the reduced variability at the matrix level. When using only the first derivatives, the HDM is not very accurate. However at this variability level, when the higher order derivatives are used, the accuracy becomes reasonable. This can especially be seen when the first three derivatives are used. For almost every point within the evaluation data points, the 3^{rd} order HDM produces very accurate results. The extrapolation however is not very accurate. This is due to the higher order polynomial used in the basis functions.

While the third order HDM is accurate, it requires a large amount of data collection, mainly the determination of 24 matrix coefficients (12 for stiffness and 12 for mass). One method to reduce the number of matrix coefficients is with a more accurate basis function. The accuracy comparison between the polynomial basis and NX basis is shown in Figure 3.22c along with the same NX-PROM as presented in the previous section. When looking within the evaluation data points, the NX HDM and the third order HDM have nearly identical accuracy with the NX HDM only using 8 matrix coefficients (5 for stiffness and 3 for mass). Another major advantage of the NX HDM is the larger accuracy range compared to the polynomial basis function. This is especially true for larger bumps since the NX basis function is more accurate for larger deviations.

The variability shown in this section is approximately the accuracy limit of the matrix parameterization. Using a simple polynomial required the use of the first three derivatives at each evaluation point while the NX basis function only required the three nominal values and two first derivatives with both giving approximately the same accuracy. It is expected that a smaller range

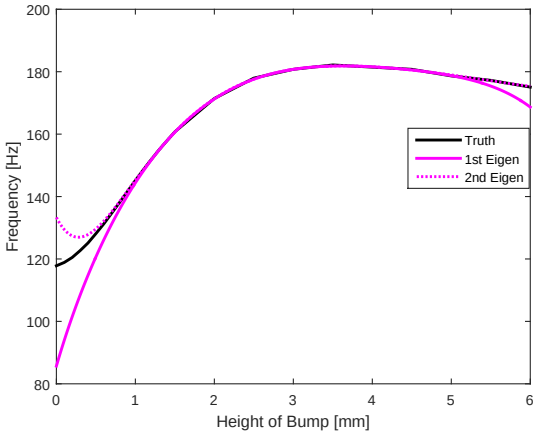

(a) Eigen Parameterization

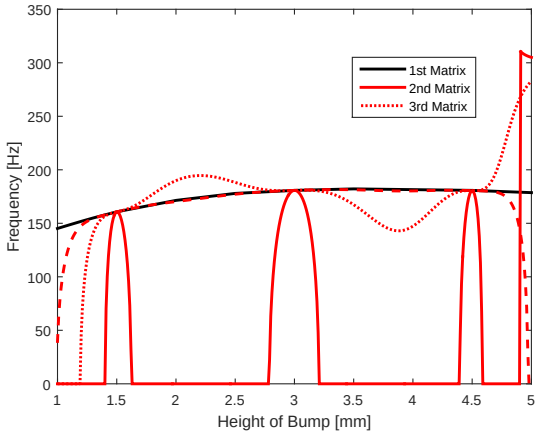

(b) Matrix Parameterization

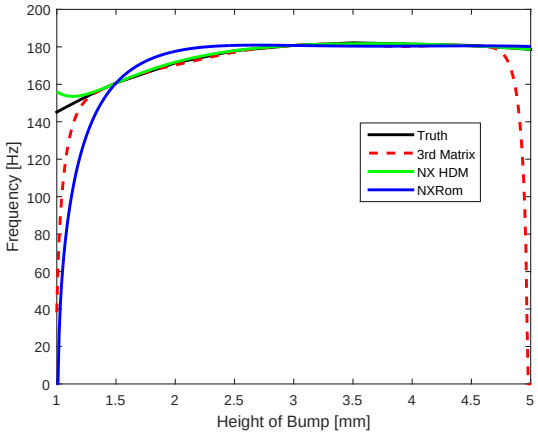

(c) NX Parameterization

Figure 3.22: Fundamental Frequency with Near Point Selection

would require less information to be accurate for the polynomial basis function. Further investigation is needed to find a general rule-of-thumb for the variability range for a given accuracy requirement.

3.7 Remarks

This chapter explores multiple types of PROMs, both well established methods and the newly developed method, HDM. To evaluate these methods, three systems are evaluated, (1) the BRB, (2) a planar frame, and (3) a paneling system. The methods used on the BRB are, (1) Taylor

series with finite difference, (2) POD, (3) CB reduction, (4) HD formulation, and (5) the HDM method. Each method discussed has specific advantages and disadvantages. The Taylor series is straight forward but can be computationally expensive. POD reduces the size of the Taylor series but requires singular value decomposition of the output data and still uses a finite difference to generate the derivatives. CB representation is a physical reduction model but still requires a code evaluation since the parameterization is at the system matrices level. HD method provides the same or greater accuracy as the Taylor series with only a single high-fidelity code evaluation but requires special programming in order to extract the extra information. The HDM method uses a basis function to characterize the output of multiple HD calculations but the determination of the unknown coefficients can become computationally expensive. This method is parameterized at the natural frequency level, but the technique can also be applied to any parameterization, such as the system matrices level.

For the BRB system, the CB reduction provided the least accurate results and required the most computation time to evaluate since the parameterization is performed at the system matrices level. This method, however, is the most feasible if the expected output is not completely known. The CB reduction doesn't require any high-fidelity code evaluations; it simply reduces the size of the model. CB is also very accurate at predicting the lower fractile of the distribution for all frequencies, although it is most accurate at low frequencies modes. The rest of the models were based purely on a numerical approximation and contains no physical information while the CB contains some physical information. Each model is able to accurately predict, (1) the parametric sweep curve, (2) the output distribution by using the statistical moments, and (3) the lower fractile as an error measurement.

The selection of the reduction model is predominantly dependent on the available computational ability. If only a single code evaluation is possible, the HD method provides very accurate

results as long as the code if able to evaluate HD numbers. If only a few evaluations are available and the code is able to evaluate HD numbers, the HDM method is very good since it can provide accurate results and requires very low computational cost once the unknown coefficients are determined. It is important to select points near the extremes of the input parameters to not over fit the output data. If no high-fidelity code evaluations are possible, a CB reduction is very useful. This method does not require a full high-fidelity code evaluation and provides a reasonable error measure. If many code evaluations are available, POD or Taylor series can be used. Both of these require multiple high-fidelity code evaluations in order to provide high accuracy results. The POD method is preferred if the output data is manageable in a matrix since it requires less computational power to produce the distribution and uses less parameterized values.

The determination of the output distribution using a large MC analysis can become very computationally expensive. Two techniques for reducing the number of required samples are evaluated and compared: LHC and SROM sampling. Both techniques are able to represent the output distribution accurately while using a small fraction of the number of samples. As a general trend, the SROM sampling produced less error in the calculations compared to LHC but requires more computational effort to determine the sample points.

The planar frame system utilized a more complex uncertain variable, a geometric length. In order to further expand the HDM, the other PROMs are not used. The main goal of this system is to test two things, (1) selection of evaluation points and effective range, and (2) the parameterization level. One of the major results from this analysis is the effect of the parameterization level. This is dependent on the desired analysis since the HDM utilized HD numbers up to the level of parameterization. If the solver is able to process HD numbers, the parameterization at the output level produces very accurate results for a large range. Should this solver not be able to evaluate HD numbers, then parameterization at the system level can still produce accurate results. The

accuracy range decreases with this parameterization, but still within reason. Inclusion of higher order derivatives into the HDM at the system parameterization greatly increases the accuracy for this system at large variations.

For the HDM, the previous systems have used a simple polynomial basis function. With a more complicated system, the selection of basis function can greatly increase the accuracy with a reduction of time. This was tested on the panel system that also contains a geometric variation. The addition of the NX basis function for this geometric uncertainty increases the applicable range of the model. This was tested against both a polynomial basis function at the same parameterization level and an output based HDM. While the accuracy is less than the output parameterized HDM, it has a greatly increased accuracy compared to the polynomial basis function. This system also shows a realistic system with large variations that test the range of applicability.

This chapter shows a comparison of multiple PROMs for parameter sweeps, distribution propagation, and reliability criteria determination. The main focus of the work presented in this chapter is the introduction of the HDM and the engineering judgments that are required for an accurate model. This tested the parameterization level, evaluation point, and basis function determination. The work shows that the HDM is a promising novel PROM methodology that can increase the accuracy of the analysis and decrease the computational time compared to traditional methods.

4. MODEL FORM ERROR DETERMINATION USING NON-PARAMETRIC MAXIMUM ENTROPY APPROACH

4.1 Introduction

Model form uncertainty is a very important research topic in the study of computational mechanics, and is important to keep track of during the design process. Depending on how the analyst choses to represent the material or structure, the results from the simulations may differ. One major cause of this difference is model reduction; high-fidelity models can give high accuracy results but require a very large computational cost. To reduce the cost of this computational requirement, a model reduction is typically used. This reduction induces some model form error, which can be difficult to quantify and raises the question of the validity of the presented results.

The method used in this chapter to describe the uncertainty in the system matrices is the MEA [81, 82, 83, 84, 85]. This method, primarily developed by Soize, incorporates the use of random matrix theory to generate a stochastic model that can be calibrated to describe the model form error. The MEA is able to characterize the uncertainty of the physical matrices in terms of a scalar value for each system matrix. This scalar value is used to characterize the statistical variability of the system matrix, which is simple to propagate to a desired result using sampling methods such as MC. In the MEA, the mean is assumed to be the nominal or updated model.

4.2 Theory

The MEA is originally derived in [85] with the simplified methodology describes in this section and in [84]. For the first system of interest, the frame system, the equations of motion are based on linear mass and stiffness. The mass matrix is positive definite while the stiffness matrix can be either positive definite or positive semi-definite, depending on if the system is constrained or contains rigid body motion. Due to the definiteness of the matrices, these can be decomposed using a Cholesky decomposition similar to

$$[M] = [L_M]^T [L_M], \tag{4.1}$$

with $[L_M]$ is an upper triangular matrix that is the Cholesky decomposition of the mass matrix $[M]$. For a non-singular matrix, $[L_M]$ is a square, upper triangular matrix, while for a singular matrix, $[L_M]$ is a rectangular matrix obtained by using a Cholesky-like decomposition using the covariance of the matrix. The Cholesky decomposition is a function of the input parameters to the FE model.

In order to incorporate model form error, a random germ, a unit-less random matrix, is added. This germ is defined to be positive definite such that the resulting matrix is still either positive definite or positive semi-definite, and is incorporated using the relation

$$[\boldsymbol{M}] = [L_M]^T [\boldsymbol{G}(\boldsymbol{\delta_M})][L_M], \tag{4.2}$$

where $[G]$ is a random germ with an expected value of I, the identity matrix, and δ_M is the dispersion parameter for the mass matrix. The variance of the random germ is a function of δ scaled by the size of the matrix. More detail of how to formulate this germ is given in [81, 84, 85, 86]. This germ belongs to the ensemble SE^+ of random matrices and also called the positive-definite ensemble [82].

These matrices are symmetric, real, and second-order random variables.

There are two predominant methods of generating this germ. The first method to generate this germ, the method used in this dissertation, is to construct the Cholesky decomposition of the germ on a term-by-term basis. By examination of the probability density function, the diagonal terms are related to a gamma distributions while the off-diagonal terms are related to zero mean normal distributions. An alternative approach is to use an augmentation of Wishart matrices [85, 87, 88]. One downfall for the alternative approach is that number of Wishart matrices increases for small dispersion parameters. In order to reduce the analyst's input, the term-by-term generation is used.

The value of δ is bounded by the size of the system. This range is given as $\delta \in [0, \sqrt{\frac{n+1}{n+5}})$, where n is the size of the matrix. As the system becomes very large, this range approaches $\delta \in [0, 1)$, although, performing this analysis for such a large system becomes computationally infeasible. The range on the dispersion parameter leads to the presentation of this value as a percentage.

In order to use the dispersion parameter as an estimation of the model form error, the dispersion parameter is chosen to give a maximum likelihood estimate of the variance for the distribution. Truth data can be given as many things such as the frequency response function, mode shapes, natural frequencies, or even static properties such as residual stress. For the frame system, the first 11 natural frequencies are used to compare to the truth data, and the glass-to-metal seal (GTMS) system uses the residual stress on the surface due to a cool down during assembly. The probability is best given as the likelihood function, which is the objective function for determining the dispersion parameter. This likelihood value is defined as the joint probability that the truth data exists within the model with a given value of the dispersion parameter, and is shown as

$$L(\delta) = \Pr(TruthData|\delta), \tag{4.3}$$

where $L(\delta)$ is the likelihood value and $Pr()$ is the probability value that the truth data exists in the

model. In the frame system, each natural frequency is treated as independent, and in the GTMS system, some conditioning is used to generate independent second order variables, Z_i. Due to the independence, the joint probability can be rewritten as

$$\Pr(TruthData|\delta) = \Pi_i \Pr(\omega_i|\delta) \; or \; \Pi_i \Pr(Z_i|\delta). \tag{4.4}$$

This calculation yields a value on the range of $[0, 1]$. The optimal dispersion value is defined as the argument maximum of the likelihood function. Since this calculation has a very small range, the differences between each dispersion value can be small and may be subject to resolution errors. In order to reduce this error, the log-likelihood function is used. For these calculations, the negative log-likelihood function is used in order for future expansion of this method for the use of an optimization technique. The negative log-likelihood is calculated by computing $\ell = \sum_i -log(\Pr(X_i|\delta))$. The reason this is a valid operation is because $-log()$ is a monotonically decreasing function, which means that the argument minimum of the negative log-likelihood is the same as the argument maximum of the likelihood function.

The calculation of the likelihood is based on the probability measure. There are two ways to compute this probability: analytically or numerically. In order to calculate the probability analytically, the distribution of the truth data must be known, which is very hard to generate. These simulations calculate the probability numerically based on a MC simulation. In order to calculate the probability, two methods can be used: a histogram and a non-parametric calculation. An investigation of the differences between these is presented in [80] with some results reported in this chapter.

The argument minimum of this negative log-likelihood function is the statistical estimate of the dispersion parameter. In this research, the likelihood is calculated multiple times to show the randomness of the likelihood. This permits the calculation of the empirical negative log-likelihood

(EL) using the expression

$$EL(\delta) = \sup_i \ell_i(\delta), \tag{4.5}$$

in which, i is the independent evaluation of the negative log-likelihood, ℓ_i. This empirical formulation reduces the randomness caused by the MC sampling technique. In addition to reducing the randomness, using the EL is also able to give an estimate on the errors associated by the minimization procedure. Some previous work has investigated assigning a beta distribution on the probability measure in order to calculate bounds on the EL. This work is not presented and requires more investigation in order to make the practice viable. The optimal dispersion parameter is then chosen based on

$$\delta^{optimal} = \arg min\ EL(\delta). \tag{4.6}$$

The optimal dispersion parameter can be used in a forward propagation of the matrices to determine the distribution of the desired output, such as reliability measures or dynamic characteristics.

This same procedure is used for the GTMS. One change made is that the equations of motion is based on a linear static model. The other main difference is the truth data used is the stress profile. This vector is not directly used to compute the likelihood function, instead a second order random variable is used. This Z variable is used to represent the vector but not in terms of measured units but in terms of a decomposition. This decomposition is a statistical reduced representations, similar to a Karhunen-Loève expansion (KLE) [83].

In order to use this reduced representation, several new variables are created. The first vector that is created is the random observed vector $\mathbb{Y}$, which is a $n_{obs} \times n_{DOF}$ vector where n_{obs} is the number of MC samples used and n_{DOF} is the number of DOF used in the stress profile. For each

value of the dispersion parameter, this random matrix is constructed. The mean and covariance of each of these vectors were created via

$$\mathbb{M}_{\mathbb{Y}}(\delta_G) = E[\mathbb{Y}] \quad [C_{\mathbb{Y}}(\delta_G)] = E[(\mathbb{Y} - \mathbb{M}_{\mathbb{Y}}(\delta_G))(\mathbb{Y} - \mathbb{M}_{\mathbb{Y}}(\delta_G))^T], \tag{4.7}$$

where $\mathbb{M}_{\mathbb{Y}}(\delta_G)$ is the mean vector, $[C_{\mathbb{Y}}(\delta_G)]$ is the covariance matrix, and $E[]$ is the expected value function.

Once these variables are calculated, the covariance matrix is then decomposed by performing an eigenvalue decomposition where $\lambda_j(\delta_G)$ is the j^{th} eigenvalue and $\mathbb{H}^j(\delta_G)$ is the j^{th} eigenvector sorted in descending order. After these variables are calculated, then the Z variable is defined. The j^{th} value of Z is calculated via

$$Z_j = \frac{1}{\sqrt{\lambda_j(\delta_G)}} < \mathbb{Y} - \mathbb{M}_{\mathbb{Y}}(\delta_G), \mathbb{H}^j(\delta_G) >, \tag{4.8}$$

where $<,>$ is the inner product operator.

Not every value of Z_j is computed, a given number of the values can be compared. A subset of these values can be used to decrease computation time since these vectors can be very large. The same transformation as in Equation 4.8 can be done for the truth data. These Z parameters are used to calculate the EL function with the same procedure as the natural frequencies.

4.3 Frame System

The study of model reduction uncertainty due to truncation has typically been done by calculating a percent difference in the natural frequencies individually. This gives first order uncertainty information that cannot be propagated into an assembled system if substructuring techniques are used. In order to perform uncertainty propagation, stochastic information about the model itself is

required on a physical level, such as mass and stiffness matrices. MEA uses the optimal dispersion parameter determined from the MC analysis instead of a percentage difference of deterministic frequencies to characterize the reduction error. This technique is used on both CB [2] and CC [8] ROMs. Multiple variations of the CC technique are commonly used such as the dual CB, which uses the same substructure reduction but uses a Lagrange multiplier method to synthesize the system. This method does not ensure the positive definiteness of the system matrices, which is required for the MEA.

The first system used to illustrate these techniques is a planar fame with an appendage. This system is shown in Figure 4.1, and contains two subsystems that are combined to form the full system separated at the red nodes at $x = 0$. The subsystem to the right is called system "B" and the subsystem to the left with the appendage is called system "D". This is the same example system that is presented in Section 2.6 and 3.5. These subsystems are reduced using the desired ROM technique, then are combined using CMS. The red connection nodes are shared between the two subsystems and are defined as the interface. In this system, the nodes are connected using Euler beam elements. Each of the two subsystems has 129 DOF. This system is relatively small but large enough to show the complexity of the techniques and how they can be applied to more complicated systems.

The simulations for the CB reductions are based on matching the system frequencies for the first 11 elastic free-free modes. For subsystem B, the 11^{th} natural frequency is 4656.4 Hz and subsystem D has an eleventh natural frequency at 5511.5 Hz. This selection of the first 11 elastic free-free modes was chosen based on the idea that the higher frequency modes are more subject to model form error. For the CC simulations, the use of free-free modes for the substructure truth data is redundant since that information is used in the reduction. So in order to test the CC reduction, the fixed-interface modes are used for the truth data. These simulations still use the

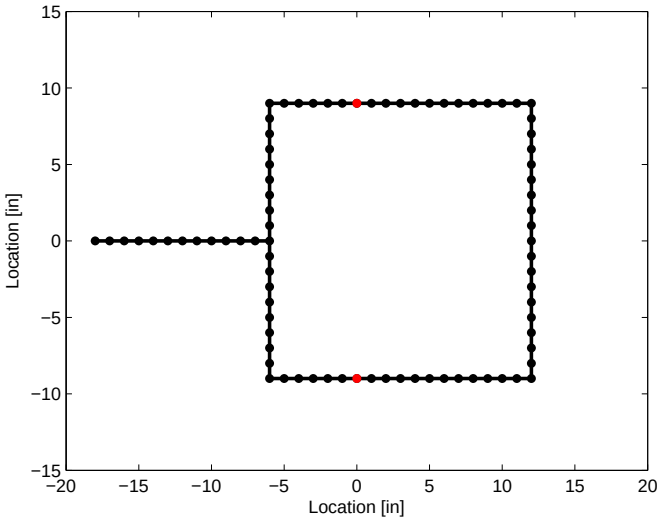

Figure 4.1: Planar Frame Example System

first 11 elastic modes.

4.3.1 Fixed-interface results

The first result for this system are when the fixed-interface/CB reductions are used for each sub-structure. One consideration in using this MEA is the selection of the truth data. For both of the model reduction techniques, the truth data is determined from the non-reduced system. Another important piece of information is the true optimal dispersion parameter. Since the true probability density function is not known, an approximation needs to be performed. For this approximation, a very large scale MC sampling is used. This MC analysis uses $100,000$ samples and is performed 30 times for the empirical likelihood. In addition to the large number of samples, the Gaussian kernel estimator is also used to generate the probability measure. This decision is based on the available time and computational resources.

There are four different analysis compared in this section: two different sampling and two different methods of determining probability. For the MC sampling method, $10,000$ samples are used, and for the LHC sampling method, 200 samples are used. All of analyses are performed with

30 evaluations for the empirical likelihood. These numbers of samples are chosen based on the computational time to perform the analysis.

The main accuracy criteria to report is the optimal dispersion parameter. This was determined based on the mass matrix, while treating the stiffness as deterministic. One of the main reasons for this judgment is the topology of the stiffness matrix. When the stiffness matrix is converted into the CB reduction, the reduced matrix is block-diagonal while the mass matrix is a full matrix. In order to maintain this block diagonal form, the stiffness is chosen to be deterministic and the mass to be stochastic.

The first system to be analysis is subsystem B. Results for the optimal dispersion parameter for the mass matrix is shown in Figure 4.2a. In both Figures 4.2a and 4.2b, the blue colored lines represent using the Gaussian kernel to calculate the probability and the red colored lines represent using a histogram with 0.1% bands. Solid lines represent using a traditional MC sampling method and the dashed line represents using the LHC reduced sampling method.

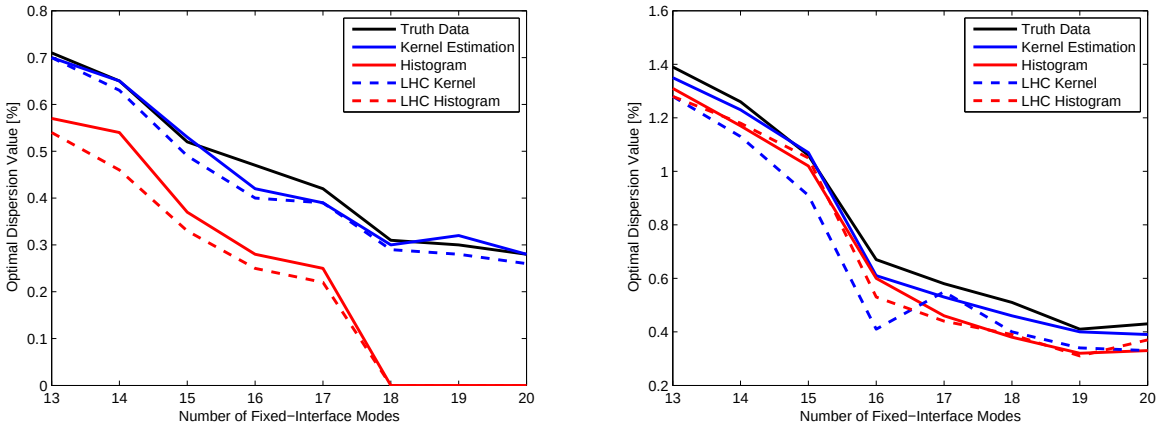

(a) System B *(b)* System D

Figure 4.2: Fixed-Interface Reduction

There are a couple trends in Figure 4.2a of interest. The first trend is the difference between using a histogram and the kernel estimator. Using the kernel estimator gives a larger dispersion

parameter that corresponds to a more conservative analysis. The second trend is that using the LHC compared to the MC produced smaller optimal dispersion parameters. This leads to the trend that the MC analysis is more conservative than the LHC sampling techniques. The final trend is the accuracy of each analysis compared to the truth data. As can be seen in Figure 4.2a, the kernel estimated data produces more accurate results. One possible reason for this trend is that the truth data is generated using the kernel estimator. The truth data using a histogram is not calculated due to computational and time restrictions. Taking the difference between the truth data and the kernel estimator data does not yield a trend. At some values, the truth data is more conservative while some other points have the kernel estimator as a more conservative value. The same analysis is also performed on system D. This analysis can be seen in Figure 4.2b.

There are several differences between the two systems. For system D, all four analyses have very similar values. Figure 4.2b shows that visually, the methods are difficult to differentiate. The only visual trend is for the LHC sampling always produced an optimal dispersion parameter smaller than the truth data. This inability to differentiate between the analysis leads to the necessity of a quantitative difference between the analyses. The quantitative result used is the RMS of the percent difference between the analysis and the truth data at each data point and is shown in Table 4.1.

Table 4.1: RMS Error of Optimal Dispersion Parameter for Fixed-Interface Reduction

Analysis	System B Error [%]	System D Error [%]
Kernel	5.30	6.69
Histogram	65.94	16.99
LHC Kernel	7.54	20.00
LHC Histogram	68.21	17.56

Table 4.1 also gives the same quantitative results for system B. The first note about Table 4.1 is that the MC analysis gives a more accurate result than the LHC for both the kernel estimator and the histogram. Both systems have similar trends. In general, the kernel estimator gives more

accurate results compared to the histogram with 0.1% tolerance bands. This value for the tolerance band is chosen as a singular value to work for both systems over the entire range of interest. For systems with a smaller optimal dispersion parameter, a smaller tolerance band should be able to get more accurate results, but the determination of this value is highly based on engineering judgment and the system of interest. Using a kernel estimator eliminates the engineering choice of this tolerance band and is more accurate.

4.3.2 Free-interface results

The same analysis that is performed on the fixed-interface/CB reduction is also performed on the free-interface reduction. This analysis results in some similar trends and some new trends as well. The first result for system B and is presented in Figure 4.3a.

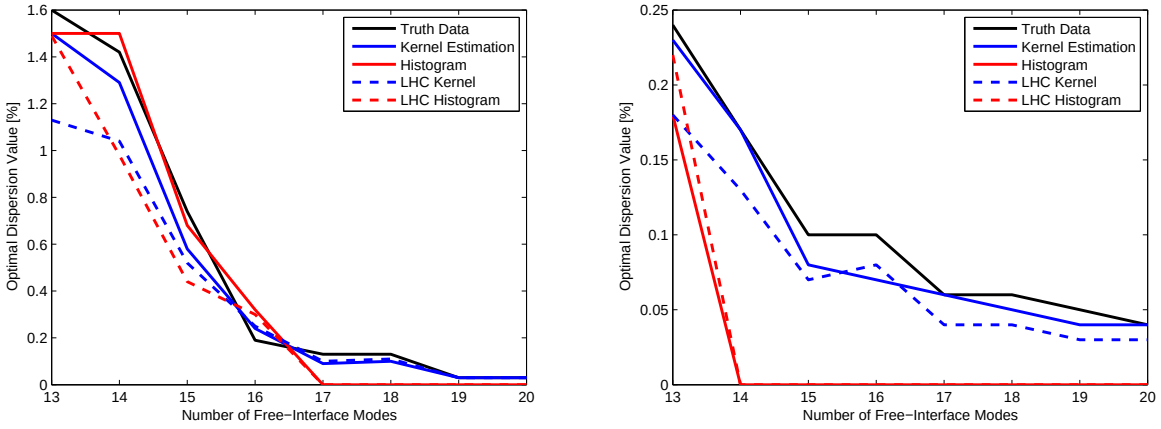

(a) System B *(b)* System D

Figure 4.3: Free-Interface Reduction

One new trend by using the free-interface reduction is that the conservative trend is no longer followed. At some data points, the LHC sampling is more conservative while at other points, the MC sampling is more conservative. This occurs when the optimal dispersion parameter is less than 0.3%. One reason for this change in trend is believed to be due to the resolution of the sweep relative to the number of MC samples. The dispersion parameter is swept up from zero with a

resolution of 0.01% to a value larger than the optimal value. As the optimal dispersion parameter becomes a small number, the differences between the probability measures at each value of the dispersion parameter becomes small and is more subject to the natural randomness of the sampling method. This trend is more apparent for system D that is shown in Figure 4.3b.

One important aspect to notice in Figure 4.3b is the expected value of the optimal dispersion parameter. The largest optimal dispersion parameter is 0.24% and thus is more subject to the randomness of the distribution sampling. Future work will look into a finer resolution in a sweep and an investigation into using an optimization technique that would eliminate the need for a sweep resolution. Another interesting trend is the histogram produced a zero optimal dispersion parameter. This is due to the tolerance band being too large for the optimal dispersion values that are small. Essentially, this tolerance band encompasses the entire distribution.

4.3.3 Craig-Bampton Synthesized System

The combination of the components into one system is a very typical utilization of these ROMs. This use of CMS produces system mass and stiffness matrices that can be used in any type of analysis. The results from performing the MEA on the full system to determine the optimal dispersion parameter is shown in Figure 4.4 for variable number of kept fixed-interface modes. Since the synthesized system is dependent on two independent systems, the effect of model reduction is a 2D surface as compared to a line. Due to time and computational limitations, the true optimal dispersion parameter is not shown for the synthesized system.

As more modes are added, the optimal dispersion parameter tends to decrease. This trend is followed for most cases with some discrepancies among them. The cause of these is believed to be due to the induced errors from the MC sampling. This is due to $10,000$ samples being used to calculate probabilities. It appears to be that the larger the system, the more samples are required

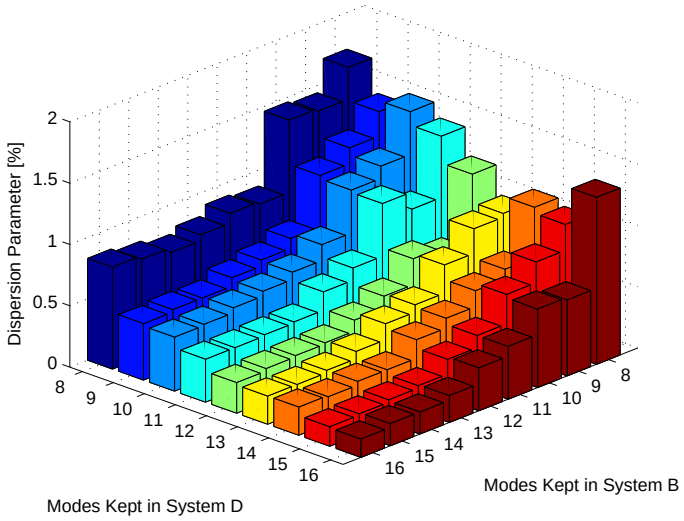

Figure 4.4: CB Synthesized System Dispersion Parameters

to get an accurate representation of the dispersion parameter.

One interesting aspect in this analysis is when 11 fixed-interface modes are kept for both of the substructures. The synthesized system has a dispersion parameter less than the dispersion parameter of either substructure. System B has a dispersion parameter of 0.82%, system D has a dispersion parameter of 1.58%, and the synthesized system E has a dispersion parameter of 0.62%. One possible reason for this decrease due to the fact that the truth data is different for each system. While the first 11 elastic frequencies are used for all systems, the frequencies represent different physical modes.

The number of modes shown in Figure 4.4 is not entirely typical for a substructuring analysis. As mentioned, typical rule-of-thumb uses one and a half or two times the highest frequency of the full system. System E has a highest frequency of interest of 1864.3 Hz so each substructure typically keeps modes with frequencies up to 2800 or 3700 Hz. For the case of one and a half times, substructure B keeps 8 fixed-interface modes and substructure D keeps 6 fixed-interface modes. Using these modes, system E has a dispersion parameter of 1.96%. If twice the highest frequency is kept, substructure B keeps 9 modes and substructure D keeps 7 modes. Using these substructures,

this results in a dispersion parameter of 1.69% for system E. This shows that increasing the amount of modes by one for each substructure creates a decrease in the optimal dispersion parameter by 14%.

One desired result from the combined system is to find a relationship between the dispersion parameter of the components and the dispersion parameter of the combined system. This is not a simple determination. One major difficulty is the theoretical issue that the truth data for the substructure and the full system are different. The fact that the first eleven modes are used to quantify the reduction error for both the substructure and combined system does not represent the same physical information.

In order to test the difference between using the stochastic components and optimal random system, distributions of the multiple frequencies are used. Four natural frequencies are presented in Figure 4.5 with 11 kept modes for both substructures. This shows frequencies $1, 4, 6$, and 10.

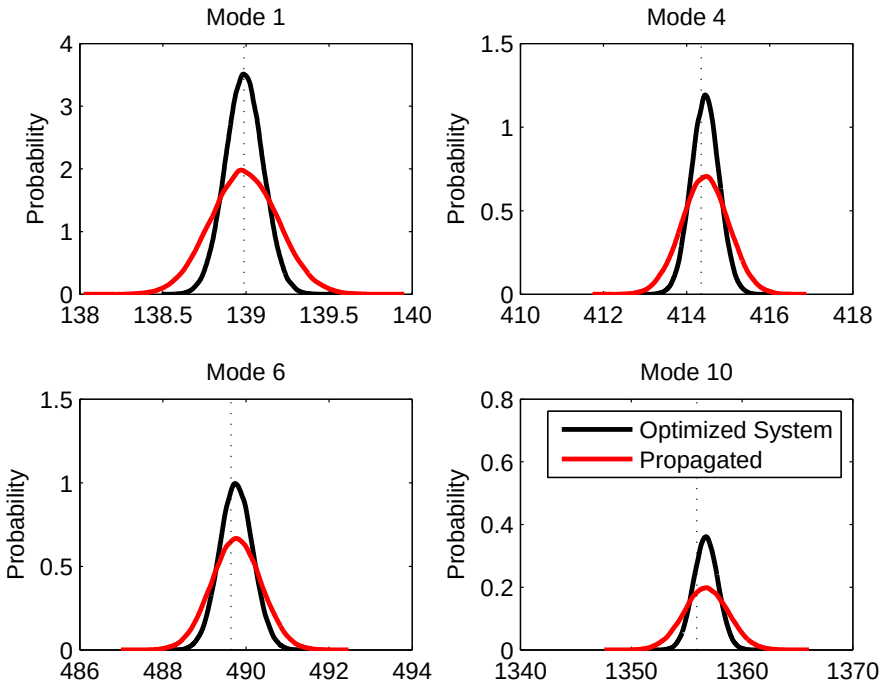

Figure 4.5: Comparison Between Propagated Distributions and Optimal

The goal of the MEA is to have the largest probability occur at the truth data. This can be seen by looking at the intersection of the truth/vertical line and the distribution in Figure 4.5. The optimized system has the largest probability value at the intersection of the truth data, with the propagated system containing a smaller probability value. This is also represented by the statistical moments of the distribution. The mean of each distribution is similar, but the standard deviation is about twice as much for the propagated system compared to the optimal system. This trend is not consistent for each natural frequency.

In order to get a singular value estimation for the propagated system, a sweep of the dispersion value was performed on the full system. The goal of this sweep is to get an approximate dispersion value that matches the distributions generated by the stochastic CMS. For this case of 11 modes kept for both components, system B uses a dispersion of 0.82% and system D uses a dispersion of 1.58%. The equivalent dispersion of the propagated system is 1.10%. This value is larger than the optimal dispersion value, 0.62, by a factor of 1.77. While this is not a conclusive study to determine a rule-of-thumb or trend, it does show a simple example where the use of substructuring gives a conservative estimate on the distribution by containing a larger spread of possible values.

4.3.4 Craig-Chang Synthesized System

For the synthesized system E, the free-free modes are used for the truth data for both the CB and CC synthesized systems. One major difference between the two reductions is the range of values for the dispersion parameters. When 8 fixed-interface modes are kept by each component, the optimal dispersion parameter is 1.70%. Comparatively, when 8 free-interface modes are kept for each component, the optimal dispersion parameter is 0.11%. Due to the magnitude difference between these methods, the number of kept modes are changed to $N_{modes} \in [6, 11]$ for each component. These results can be seen in Figure 4.6.

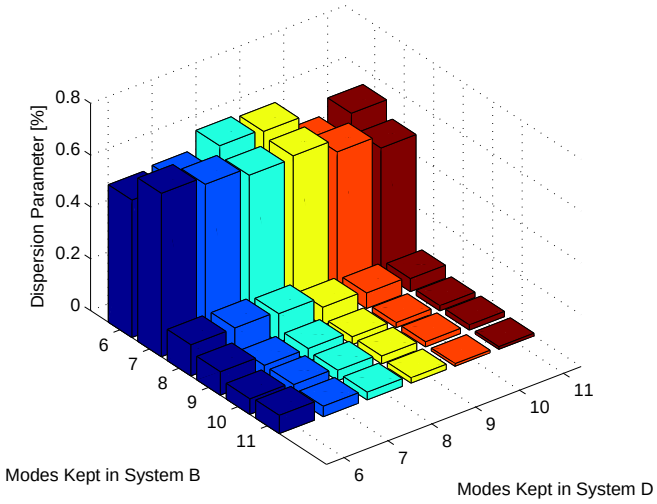

Figure 4.6: CC Synthesized System Dispersion Parameters

One interesting comparison is the case when the traditional rule of thumb for the substructure reduction is used. For both the one and a half and twice the highest natural frequency, the system keeps 9 modes from component B and 7 modes from component D. As can be seen in Figure 4.6, the optimal dispersion parameter is 0.05%. This is near the resolution of the sweep performed. Further investigation would require a more refined sweep. Another interesting aspect of the CC synthesized system is the relatively large drop in the optimal dispersion parameter when 8 or more modes are kept in system B. It is believed to be due to the completeness of the model and the sensitivity of the synthesized system to component B. The eighth mode for system B contain a mode shape very similar to the mode shapes in system E.

The magnitude difference of the optimal dispersion parameter suggests that the free-interface modes of the substructure better represent the free-free modes of the synthesized system. A couple of the mode shapes of the synthesized system can be seen in Figures 4.7a-b. One important thing to note in these figures is the motion of the interface at $x = 0$. This large motion is very difficult to describe by using the fixed-interface modes.

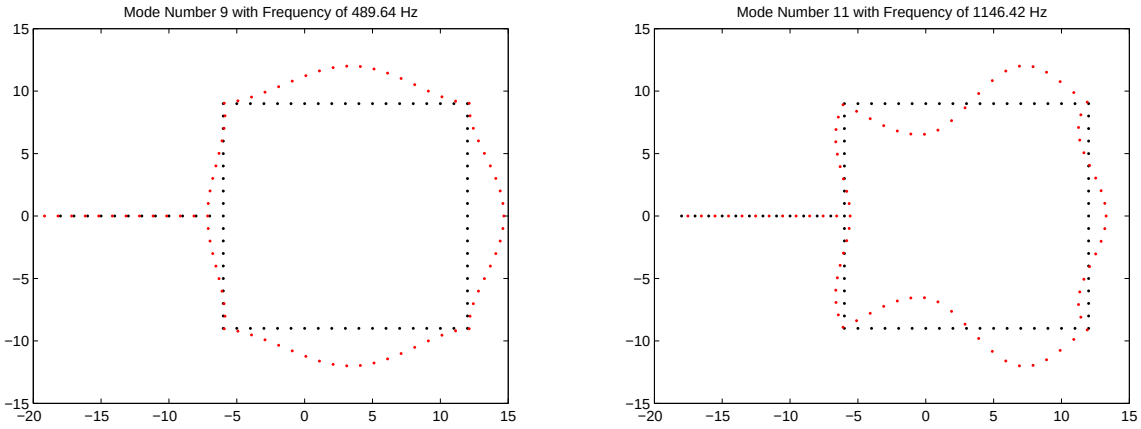

(a) Breathing Mode *(b)* Guitar Mode

Figure 4.7: Two Mode Shapes of the Synthesized System

4.4 Glass-To-Metal Seal

GTMS are commonly used to allow electrical signals to pass through a hermetic volume. Hermetic means the volume must not allow air to pass through. There are two methods traditionally used to create a hermetic seal: chemical and physical [89]. A chemical, or matched, seal relies on chemical bonding between glass and metal oxide. Secondly, a physical, or compression, seal relies on the mismatch between coefficient of thermal expansion between the metal and glass to ensure that the glass is under compression throughout the entire volume. The compression is created when the GTMS is cooled from a high temperature to room temperature, and residual compression stresses are retained in the glass. In the physical process, in addition to the desirable compressive stresses, there are also often undesirable residual stress components, which can only be quantified by solve the, potentially nonlinear, boundary value problem.

GTMS can vary in geometry, size, and materials. For this work, the seal used is a simple concentric seal made of a disk of Schott 8061 glass surrounded by 304L stainless steel shell. An image of the concentric seal is shown in Figure 4.8. In the image, the blue is the glass and the grey ring around the glass is the stainless steel shell.

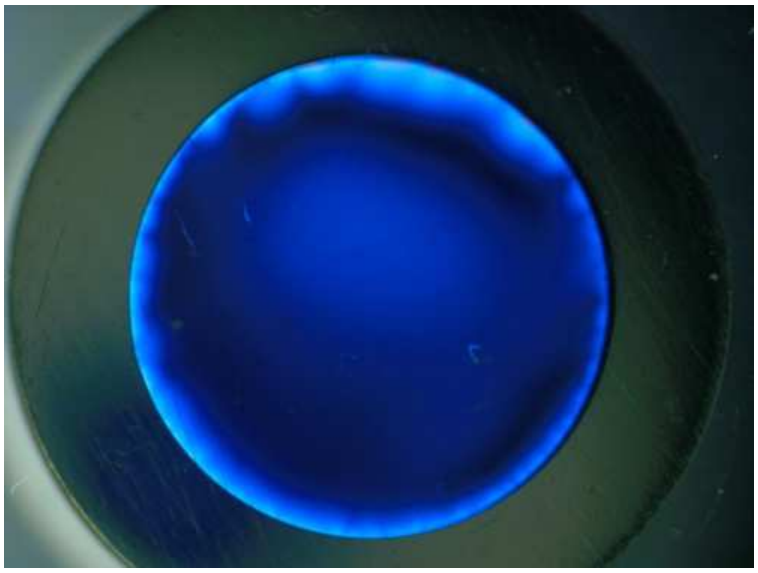

Figure 4.8: Photo of the GTMS Considered

A finite element simulation to determine the residual stress in a complex GTMS can take hours to complete. This is due to the time integration and nonlinear rate dependency of the materials. One method to reduce the computational time is to create a ROM. The ROM used for the majority of this report is a linear-elastic, static, axisymmetric model that uses temperature dependent material properties. This reduces the time of computation from several hours to a couple minutes. The linear model uses simplified physics and, thus, introduces model form error due to the linear and static assumptions.

4.4.1 Nonlinear Finite Element Model

A FE model of the simple concentric seal was created to determine the residual stress in the glass after the sealing cycle. The outer diameter of the stainless steel shell is 16.1 mm and the inner diameter of the shell is 10.8 mm. The thickness of the concentric seal is 3.1 mm. Since the geometry of the concentric seal is symmetric, the finite element model is axisymmetric as well as symmetric through the thickness. An image of the FE model is shown in Figure 4.9. In the image, the blue represents the glass and the gray represents the stainless steel shell. There is a plane of symmetry

in the horizontal direction on the bottom of the seal.

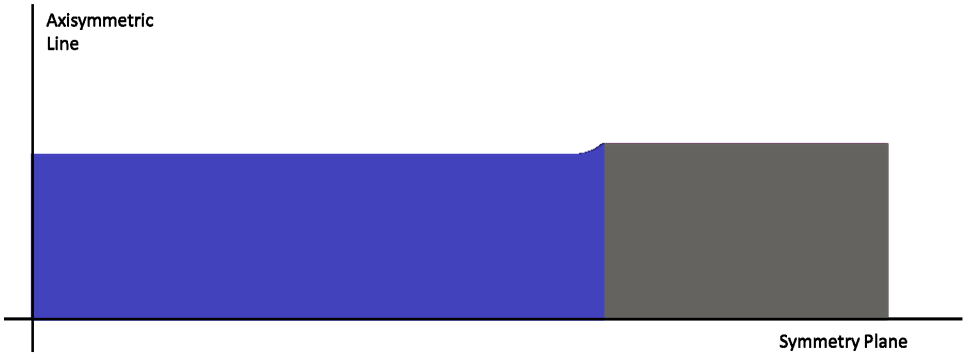

Figure 4.9: Axisymmetric FE Model of the Simple Concentric Seal

A uniform temperature boundary condition is applied to the entire model. The seal is cooled from 600°C to 20°C at a rate of 3°C/min. At 20°C, the free surface of the glass and the metal are polished. This is simulated in the model by deleting a layer of elements on the free surface of the model.

Schott 8061 is an inorganic, amorphous alkali-barium-silicate glass manufactured by Schott. The material model used to represent the glass is the nonlinear viscoelastic simplified potential energy clock model [90].This model is rate dependent and allows for structural relaxation as well as accurate representation of glass transition behavior. The 304L stainless steel shell is modeled with a rate-dependent elasto-viscoplastic constitutive model calibrated to small strain temperature data over a large temperature range [91]. In the finite element model, the interface between these two materials is assumed to be perfectly bonded.

4.4.2 Stochastic Linear Model

To test out the theory of the MEA, two main things must be chosen: a model and truth data. The model used in this chapter is an axisymmetric, static, linear-elastic model with dependency on temperature. This is a known simplification compared to the more realistic nonlinear model system which was shown in Section 4.4.1. The linear model assumes a rate independent cooling

from 460°C to 0°C. These temperatures are not the same for both this model and for the nonlinear model. This is due to the effective material properties are only available for temperatures from $T \in [0, 500]$°C.

This linear model solves the equations of motion by constructing the mechanical stiffness matrix and a forcing vector due to the change in temperature. For the MEA, a symmetric, semi-positive definite matrix must be randomized. In this analysis, the mechanical stiffness matrix is treated as stochastic. One important aspect to recognize is the size of this matrix. Since the matrix is large, the computational power and time is large; but with the help of supercomputer access and multiple meshes, this system is still feasible. There are two meshes that are investigated during the process of this analysis: a linear spacing, and a logarithmic spacing mesh. The linear mesh has the same size elements and contains 506 nodes in total. For the logarithmic mesh, the element size is not equal and is clustered around the interface between the glass and the metal and contains $3,171$ nodes. The majority of the analysis is performed on the linear mesh to accommodate time requirements. Once the calibration is performed on the linear mesh, the same parameters are input into the logarithmic mesh to get a more useful confidence interval and to investigate the robustness of the model/analysis due to the mesh.

The other important piece of information in the MEA is the truth data. There are generally two difference ways to get this truth data: experimentally or from a higher-fidelity model. Experimental results for the residual stress is typically done with strain gages. This only provides singular point information. In order to use the information for the entire surface, output from the nonlinear model described in Section 4.4.1 is used as the truth data. This can be thought of in two ways: the mean output, or an instance of the distribution. If the data is thought of as the mean, then the ROM should fairly accurately represent the full model. This is not the case for this system. A large discrepancy is found between the nominal output of the linear model and the truth data.

This can be seen in Figure 4.10. In this system, the maximum stress occurs close to the interface within the glass.

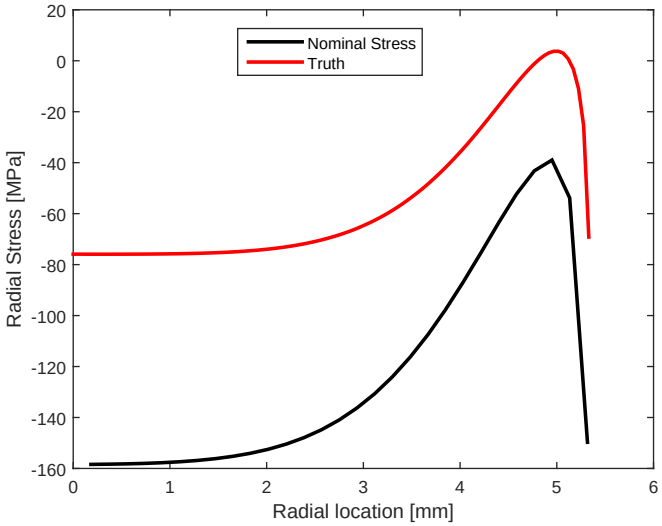

Figure 4.10: Radial Stress in the Glass

By looking at the discrepancy between the linear model and truth data, additional steps are required in order to validate the assumption that the nominal model is a good approximation of the true system. In addition to these steps, the explanation of this stochastic model represents also changes. For this system, the truth data is thought of as one instance from the underlying distribution.

Nominal Model Calibration

Within the linear model, there are two material properties that need to be measured for the glass: Young's modulus and Poisson's ratio. These can be difficult to measure for the glass due to the fracture properties and part-to-part variability. A linear-elastic material model for the glass is not the most physically accurate, but it provides a starting point in the analysis if further analysis is performed. This is also considered a source of model form error. One way to characterize this model form error would be to perform the same analysis with another material model and compare

the dispersion parameters.

Since the material properties for the glass are more difficult to quantify compared to the metal, these values are then calibrated to a truth data set. This calibration only affects the nominal values of each parameter and does not affect how each variable changes with temperature, a.k.a. the adjustment factors remain constant. These factors are applied based on the tempurature that the model is currently at. For the Young's modulus, these are applied via $E(T) = E_0\alpha(T)$. To calibrate the nominal values, the maximum stress was chosen as the truth data. This ensures that the maximum stress from the nonlinear model and the linear model match. There are two forms of this calibration, matching the maximum stress at any location, and finding the location of the maximum stress in the truth model and matching the corresponding stresses. Both of these yielded nearly identical calibration. The response surface for a sweep of the Young's modulus and Poisson's ratio can be found in Figure 4.11.

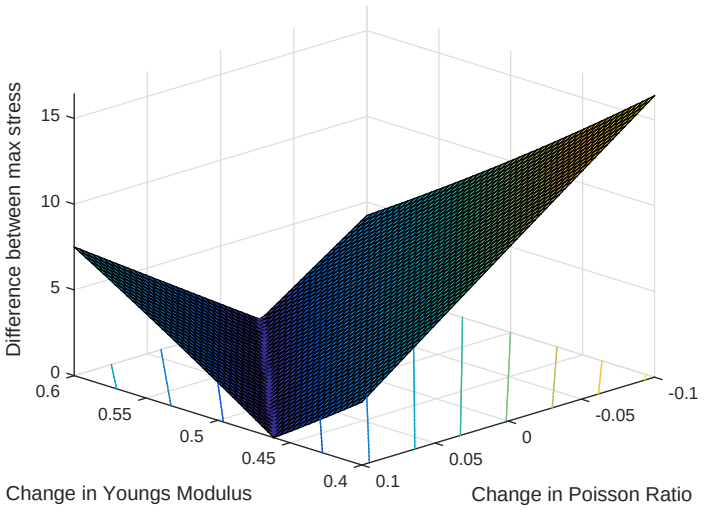

Figure 4.11: Response Surface for Calibration

One important aspect of Figure 4.11 is that there is a line of zero difference. This is due to the fact that a scalar value is being used for calibration and there are two variables that are varied; this leads to an underspecified system. To account for this, only the Young's modulus is varied.

This leads to an increased value of about 57%.

Since the stress profile, not just maximum stress, is desired, the calibrated model is plotted against the truth model. This can be seen in Figure 4.12. Both versions of the calibration are shown, and can easily be seen that both calibrations are very nearly identical.

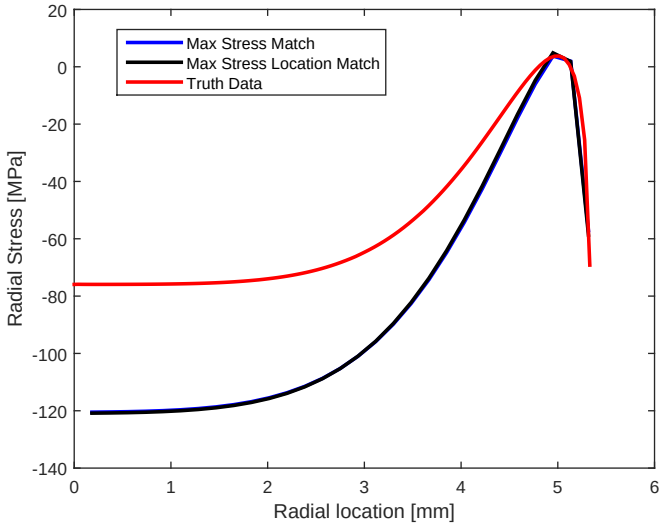

Figure 4.12: Calibrated Model

Determining Optimal Dispersion Parameter

Now that the input parameters are calibrated to match the maximum stress, the rest of the stress profile needs to be examined. This is done by applying the MEA and creating a stochastic model of the seal. The theory of this stochastic model is presented in Section 4.2 and the steps performed is presented in this section. First thing to note is how the probability measure is calculated. The MEA uses the maximum likelihood criteria for determining the optimal dispersion parameter. This maximum likelihood uses the probability of the joint distribution as the measure. In general, the stress profile is a complex system that cannot be treated as independent. To create this independence, the KLE is used on the collection of instances of the residual stress. The KLE is used to produce second order independent variables, as shown in Equation 4.8. This is useful to

reduce the probability of the joint distribution to the product of the independent probabilities. The individual probabilities are calculated based off a Gaussian kernel estimator built in Matlab, ksdensity.m. This is able to calculate the probability non-parametrically and does not require an input from the analyst to define a bin size that would be required for a histogram approach.

The first step in determining the optimal dispersion parameter is to perform a sweep of dispersion values with a given number of MC samples used to generate the probability. Results from this sweep can be seen in Figure 4.13. This sweep is performed at an increment of 0.01 on the dispersion parameter, $10,000$ MC samples at each value of the parameter, and is swept from $\delta_k \in [0, 0.60]$ and took about a hour on 128 cores with the use of parallel processing.

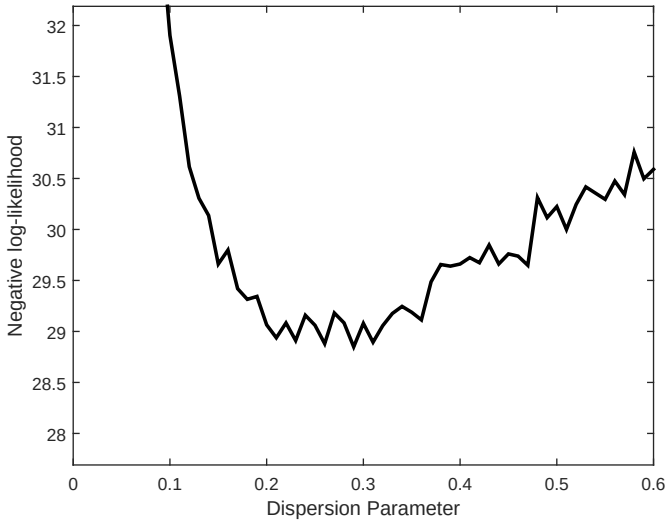

Figure 4.13: Sweep Results with 10,000 MC Samples

One important aspect of Figure 4.13 is the jaggedness of the curve. The true negative log-likelihood function is a smooth function, and the jaggedness does not lead to much confidence in the results it produces. Previous analysis has shown that if the curve is regenerated with the same inputs, then the optimal dispersion parameter would vary by a substantial amount when the curve is this jagged. To reduce this variability, a statistics tool called the EL is used. These increased number of runs require more computational time for the analysis, but is able to reduce

the variability by a substantial amount. By performing the analysis ten times at each dispersion parameter, Figure 4.13 becomes Figure 4.14.

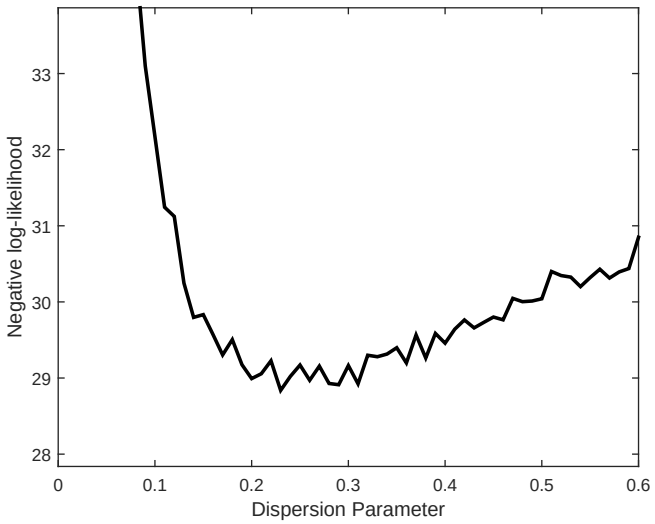

Figure 4.14: Sweep Results with 10,000 MC Samples and 10 EL Evaluations

While there is still some jaggedness in Figure 4.14, there is less than compared to Figure 4.13. The computational time increases by around nine times. Some information is able to be gleamed from Figure 4.14. The next sweep is performed on the range of $\delta_k \in [0.20, 0.32]$ with an increment of 0.001. This gives a more refined result, but is still subject to the variability as before. To alleviate this, two things are adjusted. First, more MC samples are used resulting in $20,000$ MC samples being used. Secondly, more EL evaluations are used resulting in 20 EL evaluations being used. This increase in the required computational power is only possible with the use of the supercomputer available. In order to reduce this computational burden, this sweep is only performed on the linear mesh, which contains about $1/6^{th}$ the number of nodes compared to the logarithmic mesh. The results from this refined sweep is shown in Figure 4.15. This evaluation used 256 cores and required close to four computational days.

One important trend found is that the optimal dispersion parameter is between 0.25 and 0.30. If time permitted, another sweep with more MC samples would be performed on this reduced range

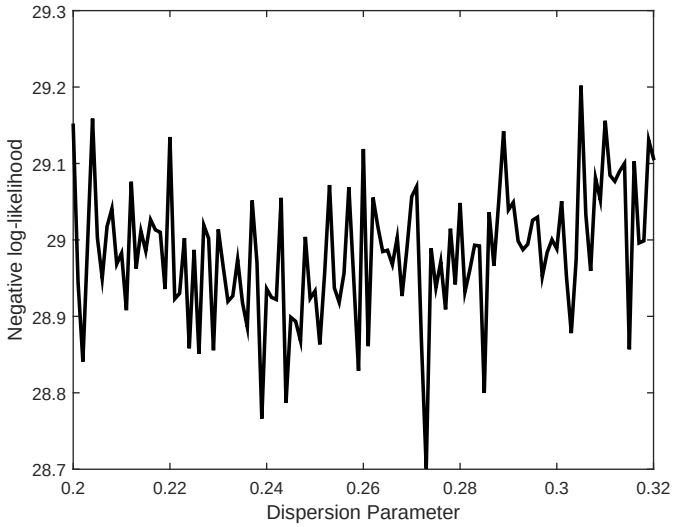

Figure 4.15: Refined Sweep with 20,000 MC Samples and 20 EL Evaluations

to decrease the randomness of the negative log-likelihood. Due to time constrains, this was not performed. From the results in Figure 4.15, the optimal dispersion parameter is determined to be $\delta_k^{opt} = 0.273$.

Stochastic Propagation

With the stochastic model calibrated, further reliability information can be calculated. This section will show that the MEA is not poised well for a static stress analysis using simplified physics. The quantity of interest is the confidence interval on the stress profile. This interval is calculated by performing a large MC analysis, $200,000$ samples, to determine the mean and error. Since the confidence interval is a measure on the mean model, a normal or student-t distribution can be used. The interval for the linear mesh can be seen in Figure 4.16a.

One important aspect to see is that the confidence interval is very large, ranging almost 1,000 MPa near the center. A large portion of this interval is within the positive stress range. This implies that there is a possibility of tension in the glass, which can cause cracking. One possible reason for this large spread is due to a mesh convergence issue. In order to get a more accurate model,

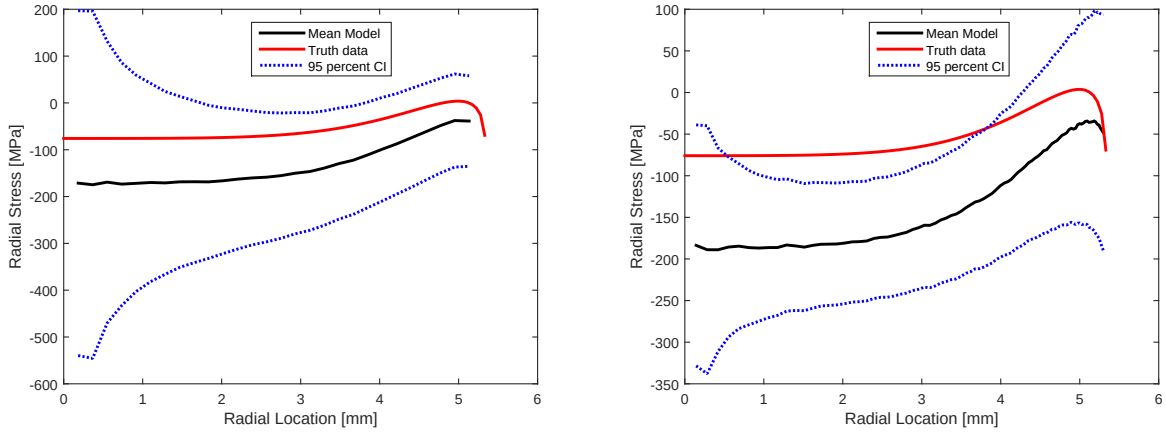

(a) linear Mesh *(b)* logarithmic Mesh

Figure 4.16: 95% Confidence Interval

the same MC analysis is performed with the logarithmic mesh. This uses the same dispersion parameter and the same number of MC samples. The result from this MC analysis can be seen in Figure 4.16b.

The first noticeable feature of Figure 4.16b is that the truth data does not fully lie within the confidence interval. This is an effect of the model being calibrated using the linear mesh and then extrapolated to the logarithmic mesh. It is expected that if the calibration is performed on the logarithmic mesh, the truth data would be encompassed within the confidence interval. This was not performed due to the time requirements for this project and available computational time. The shape of the interval is more of what is expected and provides some good information. For the majority of the profile, the stochastic model predicts that the stress will remain compressive. Near the interface, there is a portion that predicts tensile stress.

The process used in this analysis is primarily used for structural dynamics problem with ROMs that uses modal information to perform the reduction. This ensures that the ROM is fairly accurate for a specified range of frequency since it contains the information from the modal domain projected into physical space. The modal information is a characteristic of the structural dynamics

linear equations of dynamic motion. Since this type of information is not available for this system where the ROM consists of a model with simplified physics. This does not guarantee accuracy and only provides a rough estimate. The inaccuracies experienced is believed to be due to the large difference between the stochastic mean model and the nonlinear model. From the results of this analysis, it can be concluded that the method is not poised well for a static stress analysis. This is primarily due to the assumption that the mean model is fairly accurate. The linear model used here matches the trend of the truth data, but does not match the magnitudes. This method might be of more use in the full dynamic model, but would require a large amount of time and consideration.

Another issue that can cause this inaccuracy is the model itself. The MEA makes the assumption that the mean stochastic model is the nominal system. In the analysis performed, the inverse of the stiffness matrix is used. The statistics do not guarantee that the mean of the inverse is the same as the inverse of the mean. Adhikari investigated this inversing process in [87, 88]. These show that applying the random matrix onto the inverse of the stiffness matrix might be able to produce a more accurate stochastic model, but it is not a guaranteed trend since the systems studied by Adhikari are dynamical. This type of approach is recommended for any future analysis on this linear system.

4.5 Remarks

This chapter showed the use of a stochastic model in order to determine model form error. The MEA is able to randomize a symmetric, positive-definite matrix for the use in structural dynamics with the variance govern by a scalar value. Two different systems are presented. The frame system investigates the modal truncation error when using substructuring. This investigated two types of reductions/synthesis methods: fixed-interface and free-interface. Both of these reductions showed the trend that with more information, the more accurate the model becomes. This is reflected

in a smaller optimal dispersion parameter corresponding to less model form error. This analysis also shows the propagation of subsystem uncertainty to the combined system. Propagating the substructure uncertainty resulted in a more conservative estimate compared to treating the full system in the MEA.

The second system, the GTMS, investigated the effect of modeling choice. This compared a linear, static, axisymmetric system to the more accurate nonlinear, dynamic, full system model. Using the stress profile from the full system, an optimal dispersion value was found for a linear spaced mesh. When a confidence interval was calculated, there was a high probability of failure. Using a more refined mesh gives a more accurate model, but was not able to be fully investigated within the allocated time due to the larger system size.

One of the most powerful uses of the MEA is the ability to describe the model form error with a scalar value. This determination can be done when the nominal model is either deterministic, as shown in this chapter, or stochastic. When the nominal system is stochastic, the analysis becomes more complex and requires more computational power, but is feasible. Treating the nominal model as stochastic is able to characterize parametric error, then the methodology can be applied to determine the model form error. Chapter 5 gives an example and some further explanation on determining the model form error for a stochastic nominal model.

5. IMPLEMENTING PROM INTO THE MEA

5.1 Introduction

One of the most important characteristics of the MEA is that the random germ does not incorporate any physical information about the system. It only requires information such as the definiteness and size of the matrix. This is purposeful in order to evaluate model form error. Since the system and the random germs are independent, this allows for the evaluation of model form error and parametric errors in the same analysis with distinct stochastic characterization.

The use of this separate characterization of uncertainty is not novel when using the MEA. In [83], Soize details the possibility of utilizing this analysis for determining both parametric and model form errors. Since the introduction, this method has been used on a couple different systems by the author. In [84], a simple spring-mass system is evaluated. This shows some interesting characteristics since the parametric errors are insufficient to describe a change in the natural frequencies. For that system, the second mode of vibration does not change with different values of the uncertain parameter. Using the MEA for both parametric and model form gives a better representation of the hypothetical system.

In [81], the Ampair 600 wind turbine is investigated. This analysis utilized a modal model of the system. For additional modeling choices, the frictional interface is modeled as rigid. This is thought of as a preliminary modeling choice, as it is the simplest and quickest to evaluate. The analysis presented an optimal dispersion value that could be compared to other models, such as other ROMs or different interfaces. This would be able to give a quantitative decrease in the model

form error due to the choices made by the analyst.

5.1.1 Expanded Theory

In Chapter 4, the theory of the MEA is introduced. This explanation assumed that the nominal model is deterministic, which is relaxed in order to evaluate parametric errors. This assumption is relaxed in order to evaluate parametric errors. There are two main adjustments that are made in order to incorporate parametric errors. The first change is in the mean model. This is described for the mass matrix as

$$[\boldsymbol{M}(\boldsymbol{X})] = [\boldsymbol{L_M}(\boldsymbol{X})]^T[\boldsymbol{L_M}(\boldsymbol{X})], \tag{5.1}$$

with X being a vector of input parameters with a joint probability distribution. The distribution can be determined either by the analyst or non-parametrically. One possible determination is with the use of maximum entropy on the support of the parameter. For example, a bounded distribution yields a uniform distribution and a non-bounded distribution yields a normal distribution.

The second change when considering parametric errors is the work flow of the analysis. There are two possible changes. The first possibility is if the distribution on the parameters is completely known. This information can be generated from experimental results or expert knowledge. Using the information of the parameter distributions, the Cholesky decomposition has a specified distribution that can easily be sampled. This implies that during the MC sampling, the Cholesky decomposition must also be sampled along with the random germ. This would typically require a higher number of sample evaluations since the effective joint distribution is being sampled, but also tends to require more computational time per evaluation since both the nominal model and random germ need to be created. In order to sample the Cholesky decomposition, either the nominal model can be regenerated or a PROM can be used.

The other possible change in the work flow is used for determining the distribution of the input parameters. This is the work flow that is used for the remainder of this chapter as well as in [81, 84]. Since this methodology is used to determine both types of errors, the analysis essentially doubles: once for parameter error, and once for the model form error. The general work flow is described as follows:

- Generate parameterized model
- Sweep variance of inputs to create maximum likelihood estimates with first set of truth data
- With variances for inputs fixed, sweep dispersion parameters to create estimate with second set of truth data
- Use optimal distributions to determine quantities of interest, such as failure probability.

This analysis, as well as in [81, 84], makes the simplifying assumption that the input parameters are independent and that the mean of the distributions are the nominal values. Doing this assumes that the nominal model is a reasonable approximation of the system. Making this assumption allows for a single characteristic, the variance, to be determined per input parameter. In order to determine the variance of each input parameter, the type of distribution and one set of truth data is required. The distribution can be determined based on engineering judgment or via a maximum entropy method that evaluates the support of the parameter and assigns a distribution. This analysis uses the distributions determined via the maximum entropy method. The second addition to the process is the extra set of truth data. In general this can be gathered from any source, either from a high-fidelity model or from an experiment. This data should be independent to the other truth data that will be used. One commonly used selection technique is to use the natural frequencies as one set of data and the frequency response function as the other set of data. The "Z" parameters in Equation 4.8 are independent of the natural frequencies. One advantage

of using this information is that the data can be generated from a single impact hammer test or swept sine shaker test. Another possibility is to use the lower frequency modes for the parameter estimation and the higher frequency modes for the model form estimation.

5.2 Example System

The system that is evaluated in this chapter is the panel system that was utilized in Chapter 3. This system can be seen in Figure 5.1 with the computational model using the HDM as the PROM for all the calculations presented in this chapter. For this investigation, the range of the uncertain variable, the height of the bumps, is considerably smaller than the previous analysis. This was done to ensure an accurate system level model. The results form Chapter 3 have shown that the HDM is accurate for interpolation between the evaluation points. This is particularly true for systems with small variability. This assumption is verified in Section 5.3.

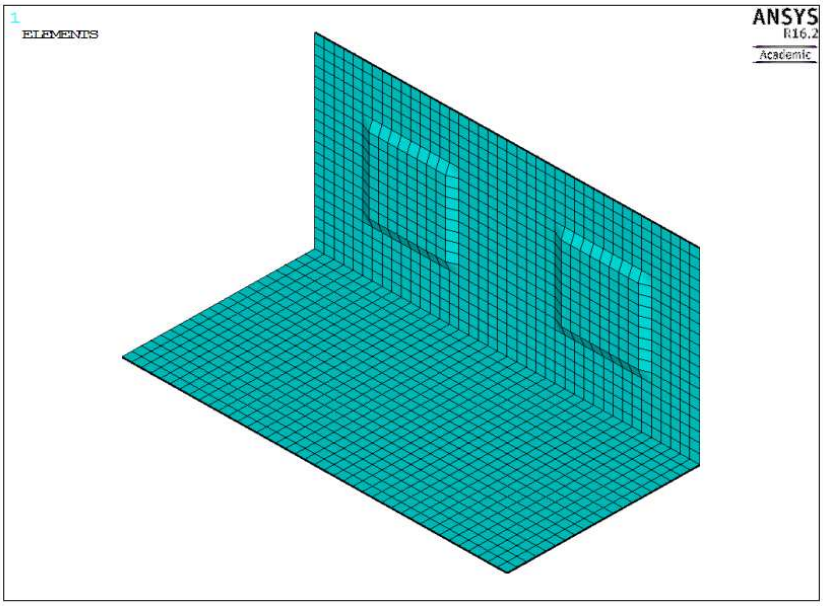

Figure 5.1: Panel System

5.2.1 Truth Data

The truth data is generated by a modification of one high-fidelity simulation evaluation. This evaluation uses a height of the bumps that is closest to the nominal value. This validates the assumption that the nominal model is an approximate solution to the true system. Using the HDM to generate the truth data would lead to an inability to quantify model form error. In order to add some randomness to the system, five random non-zero elements of the stiffness matrix are modified. This modification is a 0.1% increase in the stiffness of that element. This was performed with a check that the natural frequencies of the system do not vary by a large amount. Another possible method to generate truth data is to create a slightly inhomogeneous material property and use that to create the truth data. This is similar to the method used by Adhikari in [87, 88]. Due to limitations in time and availability of the model, this was not used. The model form error using this data would be primarily due to the inhomogeneous material properties.

As previously discussed, characterizing both parameter and model form errors requires two sets of accepted truth data. The selection of data is dependent of the uncertain parameters. For this analysis, the parameter error that is characterized is the height of the bumps. This geometric variation changes both the mass and stiffness of the system, but for simplification, the truth data only uses the stiffness matrix. For the parameter error truth data, the Frobenius norm of the stiffness matrix is used. This is essentially a RMS of each element of the matrix. One possible issue of using this norm as the truth data is the numerical issues that arise. Using any piece of truth data is viable and possible, but the main issue comes in with how well the model can differentiate between values to calculate the likelihood function. While this is potentially an issue, this analysis is still performed in order to test the effect of using this as truth data. To the author's knowledge, this is the first utilization of the Frobenius norm as the truth data. For the model form determination, the first ten natural frequencies are used. These natural frequencies are treated as

independent with equal weighting in the joint distribution.

5.3 Surrogate Model Accuracy

In order to perform the MEA, a model must be evaluated many times via a MC method. Running the high-fidelity FE model is impracticable for any real system, the panel included. So, in order to perform this analysis, a PROM or surrogate model must be used. The surrogate model used in this particular analysis is the HDM as presented in Chapter 3. Even though the HDM was applied to the same system, a new model is generated due to the difference in expected range of the uncertain variable. The range for these random variations is much smaller than that explored in Chapter 3. This expected range for the height of the bump in this analysis is $h \in [2, 4]mm$. To collect the system matrices, a high-fidelity code was evaluated. The high-fidelity model was evaluated by Jeff Fike at Sandia National Laboratories with evaluations performed at specific values for the bump. In the generation of the surrogate model, three values of the bump, $h = \{2, 3, 4\}\, mm$, are used with up to the first three derivatives available. Using this information, three different surrogate models are generated and compared for a parameter sweep.

In order to verify the model, three main criteria are used, (1) elements of the stiffness matrix, (2) elements of the mass matrix, and (3) the natural frequencies. These are selected since the elements of the stiffness matrix and natural frequencies are the quantities used for the truth data in the MEA thus requiring accurate results. The first results are shown in Figures 5.2a-b. These show a diagonal term for the mass and stiffness matrix.

One advantage of using this range for the HDM is that there are two verification points at $h = \{2.5, 3.5\}\, mm$ that are not used in the model generation, and can be seen in Figures 5.2a-b to demonstrate the accuracy of the surrogate model. From these figures, it appears that all the orders of the HDM will produce accurate results. Since the elements of the matrix are not the

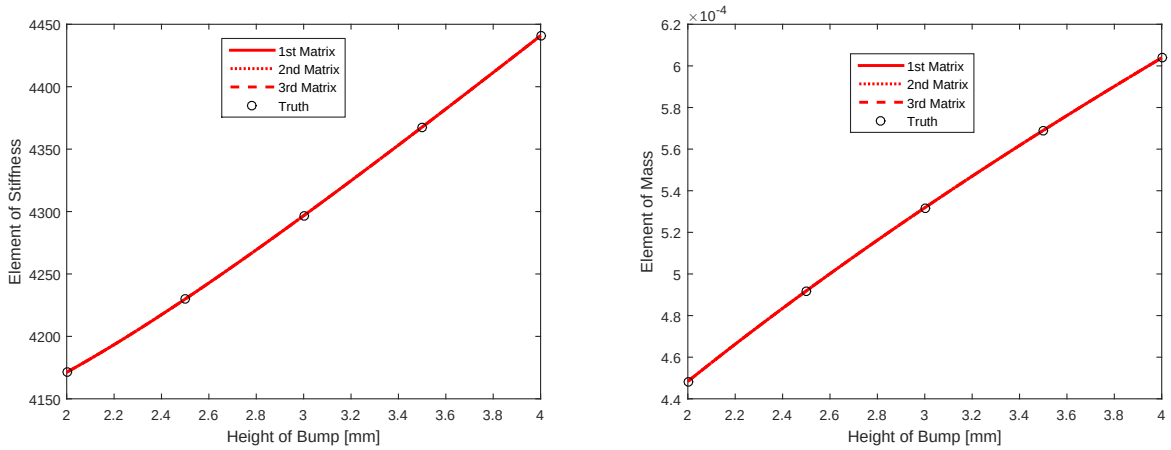

(a) Stiffness Matrix *(b)* Mass Matrix

Figure 5.2: Diagonal Element

only quantities used in this analysis, the natural frequencies need to be verified as well and show what orders of HDM produce accurate results. The verification of the natural frequency is shown in Figure 5.3.

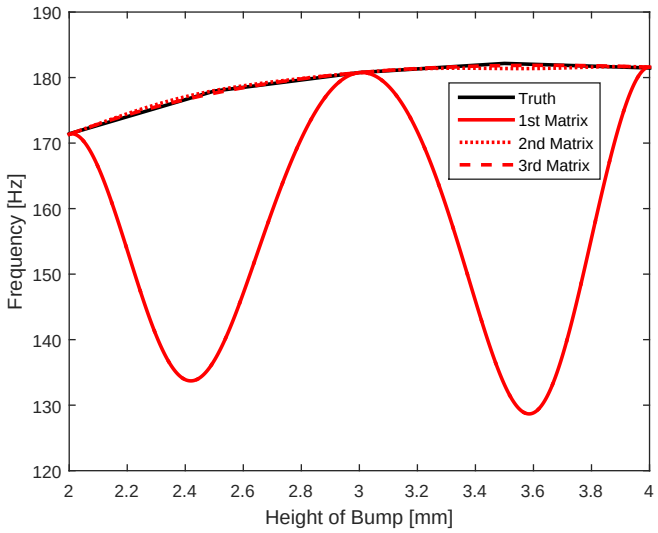

Figure 5.3: Fundamental Frequency

The first take away from Figure 5.3 is that the first order HDM is not very accurate when looking at the natural frequencies, but both the second and third order HDM are very accurate. Since there is not much validation data available, one of the main take aways in the convergence of

the model. The second and third order HDM produce nearly identical results for both the elements of the system matrices and the natural frequencies. Due to this convergence, the second order HDM is used for the remainder of the analysis. This uses the nominal values and the first two derivatives for the three evaluation points at the system matrix level with a polynomial basis function.

5.4 Results

One major issue that arose during this analysis is the size of the system. This system is much larger than the ones previously presenting for using the MEA. The system has $15,480$ DOF for each the mass and stiffness matrix. This mesh was created by Fike in order to have accurate FE results. Previous systems contained on the order of 100 DOF. While there is a reduction in computational cost by using the HDM as a surrogate model, there is still a large burden due to the size alone. Due to this size difference, the number of MC samples and EL evaluations are different than the values used in the previous analysis due to time and computational constraints.

5.4.1 Parameter Error

The first part of this analysis is to determine the maximum likelihood estimate for the unknown parameter, the height of the bump. In order to do this, the length is treated as a matrix with unity size. This enforces a gamma distribution with a mean at the nominal value of $3mm$. Doing this matches the support of the parameter, since the length is a physical measurement must remain positive. This also allows for the variance to be described using the scalar dispersion parameter δ_h. Along with the dispersion parameter, the effective distribution parameters, a and b, will be presented for the optimal distribution.

In order to determine the maximum likelihood estimate, the same procedure to determine the optimal dispersion parameter for model form error is used. This is comprised of refining sweeps at

different ranges. These refined sweeps consists of three different ranges. The first range is a course sweep to get an approximate range for the estimate. This range for the sweep of the dispersion values is $\delta_h \in [0, 0.57]$ incremented at 0.01 with $1,000$ MC samples and 2 EL evaluations at each value of the dispersion parameter. One important thing to note is that the dispersion parameter is a bounded value. Since a scalar is treated as a 1 DOF matrix, the maximum value for the dispersion is $\sqrt{1/3}$ or 0.577. This sweep is essentially a blind sweep with no preconceived idea on what the optimal value is. The results from this sweep can be Figure 5.4. This shows that the optimal dispersion parameter is slightly below 0.20.

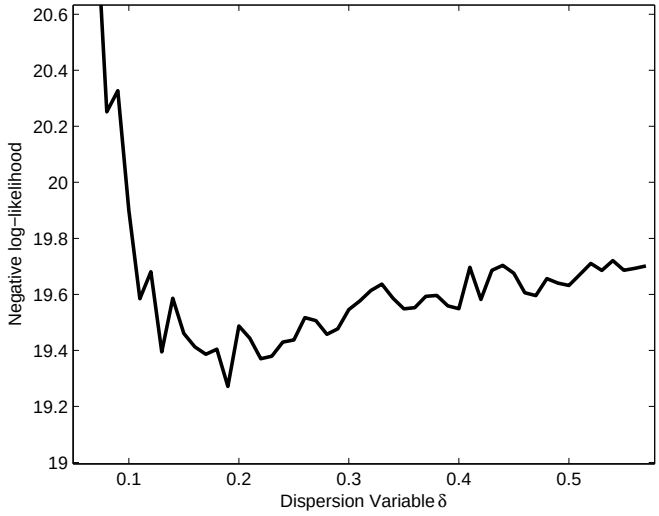

Figure 5.4: Course Sweep for Parametric Error

From the results in Figure 5.4, the next sweep has a smaller range, but with a more refined increment. The range decreases to $\delta_h \in [0.100, 0.260]$ with increments of 0.001. This sweep uses the same number of MC samples, but increases the number of EL evaluations to 10 evaluations for each dispersion value. Figure 5.5 shows the results from the refined sweep. Previous experience with the MEA has shown that when the resolution increases on the sweep, more EL evaluations are needed to reduce the jaggedness for the negative log-likelihood function. When computational resources are scarce, it has previously trended that more EL evaluations produce better results than adding

more MC samples. An example of this will be presented in the final sweep.

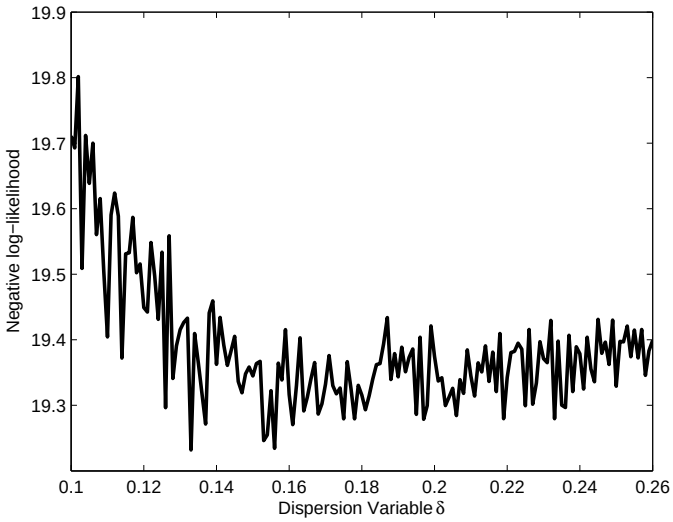

Figure 5.5: Refined Sweep for Parametric Error

One of the first things to note from Figure 5.5 is the jaggedness of the curve. In order to reduce this jaggedness, two options are explored, (1) increase the number of MC samples and (2) increase the number of EL evaluations. To reduce the computational burden, the range on these new sweeps are reduced to $\delta_h \in [0.12, 0.182]$. This sweep that used $5,000$ MC samples and 10 EL evaluations is presented in Figure 5.6a, and the sweep that used $1,000$ MC samples and 30 EL evaluations is presented in Figure 5.6b.

By comparing Figures 5.6a-b, two slightly different optimal dispersion parameters can be determined. In order to differentiate and determine which value is going to be reported, the value of the negative log-likelihood is used. The chosen optimal dispersion value is $\delta_h^{opt} = 0.148$. This occurred with using $1,000$ MC samples and 30 EL evaluations, which produced a lower negative log-likelihood value. The distribution that the optimal dispersion parameter creates is shown in Figure 5.7. Using the method of moments technique, the effective distribution parameters can be determined. For this gamma distribution, the effective parameters are $a = 45.7382$ and $b = 0.065602$. This produces a mean of $3mm$ and a standard deviation of $0.445mm$.

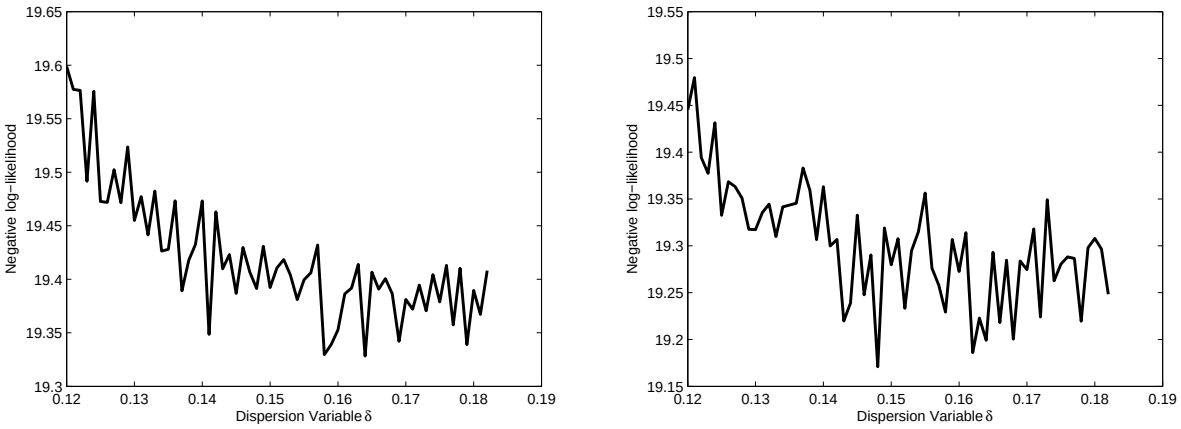

(a) 5,000 MC samples *(b)* 30 EL evaluations

Figure 5.6: Refined Sweep with Nominally 1,000 MC Samples and 10 EL Evaluation

5.4.2 Model Form Error

Once the distribution of the input parameter is determined, the model form error can determined. Similar to the parameter error, the determination of the optimal dispersion parameter uses a sweep with different truth data. This is determined to be the first ten elastic natural frequencies. These values are treated as independent variables with the assumption that the mode shapes remain the same for all combinations of input variables and stochastic instances.

Another major change between the parameter and the model form sweep is the computational requirements. The main reason for this is with the randomization and how it is applied. For the parameter sweep, a scalar is randomized. This does not require much memory and can be done either before the MC analysis or during each MC simulation. One advantage of generating the samples before the MC analysis is the possibility of using a reduced sampling technique, such as LHC, but this requires more memory to store. While this difference is small and reasonable for a scalar, when a matrix is randomized, it can require a large amount of memory in order to store all the samples of the random matrix. There are $15,480$ DOF in the panel system and thus is equivalent to about 240 million scalar values making the storage requirements non-trivial.

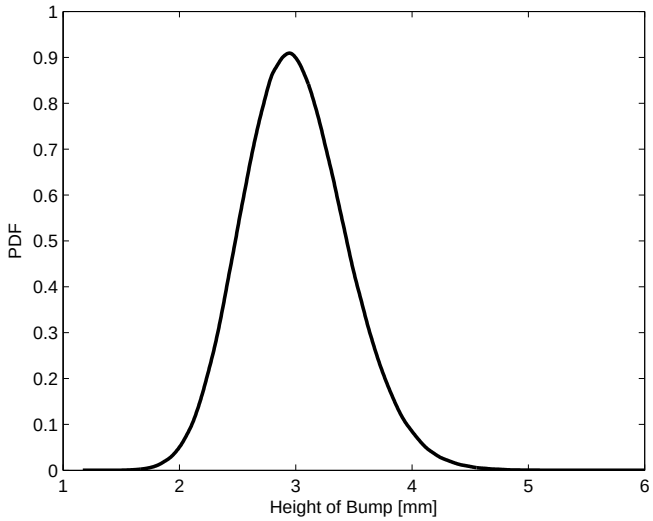

Figure 5.7: Optimal Distribution for Height of Bump

To account for this increase in computational requirements, two changes are made to the method. The first change is that each random matrix sample is generated within the MC simulation and is not externally stored, which prevents the use of LHC sampling. Secondly is how the random matrix is applied. In this analysis, the mass matrix is chosen to be stochastic. It was decided that the stochastic height has a larger effect on the stiffness compared to the mass matrix, thus the more robust mass matrix is chosen to be stochastic. Due to the size of the mass matrix, generating a random sample from the distribution takes around 12 minutes. When performing large number of samples for the MC simulations, this time becomes impracticable within the allotted time frame. In order to reduce this time, the SVD of the mass matrix is performed. Through investigation, only the primary 50 singular values are used. With the reduced set of singular values, each value is randomized as if they are a scalar with the same dispersion parameter. Doing this reduction decreases the computational time to 40 seconds per simulation on the same computer. This is a large reduction allowing for this simulation to be performed within the allotted time.

In order to determine the model form error, a two sweep approach is used. Due to the increase in computational time, the resolution and range of these sweeps are different compared to

the parameter sweep. The first sweep is from $\delta_M \in [0, 0.3]$ with a resolution of 0.05. Each of these values use $1,000$ MC samples and 5 EL evaluations. This decrease in EL evaluation is primarily due the increased computational time compared to the parameter sweep. The results from this sweep can be seen in Figure 5.8a.

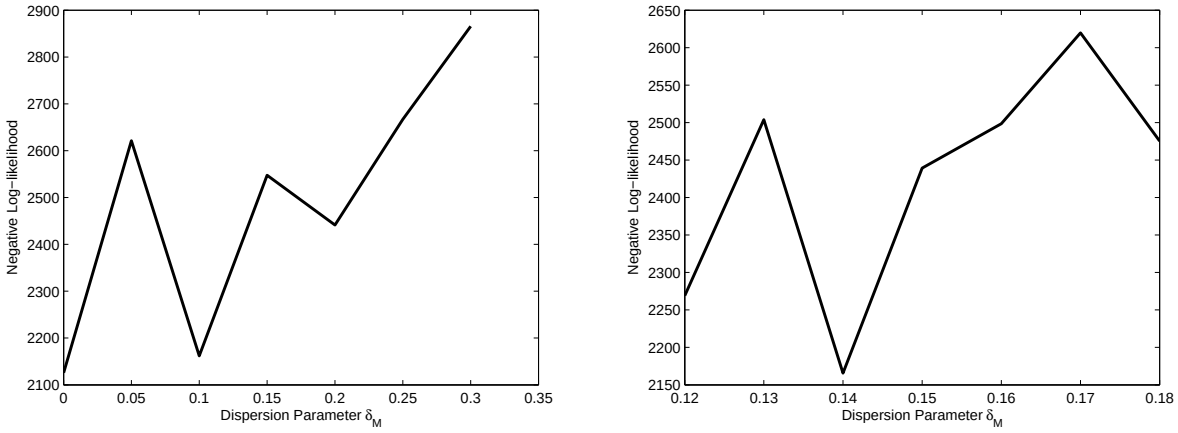

(a) Course *(b)* Refined

Figure 5.8: Sweeps

While the resolution on Figure 5.8a is course, it gives some insight into the approximate range for the optimal value. For the next sweep, the number of samples and EL evaluations remain the same, but the resolution is increased for a smaller range. The new sweep has a resolution of 0.01 and the range is decreased to $\delta_M \in [0.12, 0.18]$. Results from the sweep can be seen in Figure 5.8b.

By investigation, the optimal dispersion parameter is given as $\delta_M^{opt} = 0.14$. As a verification, the first sweep is repeated with a resolution of 0.01. One reoccurring issue with this analysis is the computational requirements. In order to run this large sweep within a reasonable time, the number of MC samples is decreased to 500 samples while maintaining 5 EL evaluations on the range of $\delta_M \in [0, 0.20]$. This sweep in presented in Figure 5.9. Even with the reduced number of MC samples, the optimal dispersion parameter is repeatable compared to the sweep with the higher MC samples.

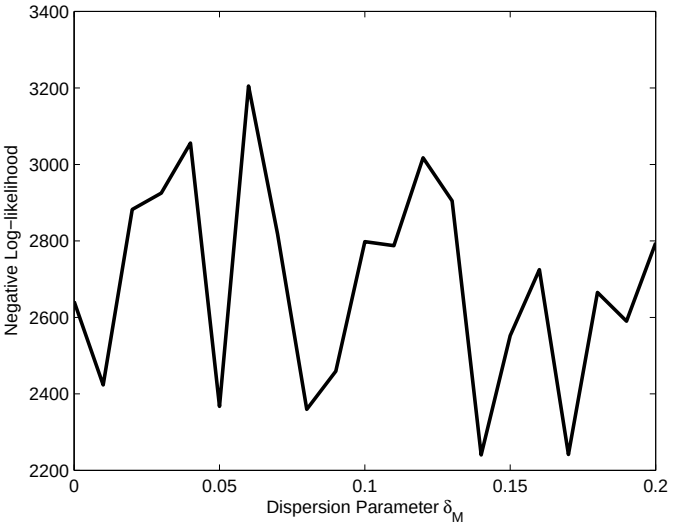

Figure 5.9: Refined Model Form Sweep

5.5 Remarks and Expected Future Work

The work presented in this chapter utilizes a surrogate model, the HDM, into the MEA. This is used in order to determine both the distribution on the uncertain height of the bump and the stochastic mass matrix in order to give insight into the model form error. Performing this analysis resulted in optimal parameters of $\delta_h^{opt} = 0.148$ and $\delta_M^{opt} = 0.14$. One difficulty that this analysis experienced was the size of the system. Previous research using the MEA focused on the model form error due to a ROM or simplified system. This system is conceived of as a realistic system that could be physically tested and the results being used as the truth data. Even thought this was not performed, the methodology shows that it is possible. The information generated from this analysis can be used as a baseline for future analysis. If an analysis uses a ROM, such as CB, in a substructuring analysis, the optimal dispersion parameter can be used to show the decrease in accuracy by the implementation of the ROM.

6. CONCLUSIONS AND FUTURE WORK

6.1 Conclusions

During the traditional aerospace design process, large variability is commonly experienced due to design optimization techniques such as topology optimization. These changes can have a large effect on both the system design and the production. One particular aspect of interest is the effect of machining precision on the desired output. Large aerospace systems tend to have thin nominal values, thus making the machining tolerance more important. Machining tolerance build-up can lead to possible failures and thus requires the quantification of the uncertainty to ensure a safe design and to determine the probability of possible failure.

One way to characterize and quantify the uncertainty of the design is in the use of numerical models. Using these numerical models use both physical parameters as well as mathematical adjustment factors to account for the unknown physics of the system. One possible method to increase the accuracy is to perform a model calibration for the particular system for a physically testable case. These types of tests include modal characterization and ground vibration tests. One commonly used algorithm in this model calibration is the use of gradient based optimization. The calculation of these gradients is a very computationally expensive procedure. Using hyper-dual numbers to determine these numerical derivatives is able to calculate these exactly with a single code evaluation. This is compared to the approximation of the finite difference, which introduces multiple types of errors through the use of multiple code evaluations. Three of the most commonly used methods to generate numerical derivatives are compared for a simple mathematical function

as well as a simple finite element model. The mathematical function shows that the hyper-dual step is the most accurate method among those tested for the first two derivatives. This trend is expected to be true for higher order derivatives but was not tested. Due to the novelty of the hyper-dual step, some special considerations are needed when implemented into a finite element model. These considerations are shown and the results are also shown for both material variations and geometric variations.

In order to perform uncertainty quantification, typically multiple code evaluations is required. One way to reduce this large computational burden is with the used of parameterized reduced order models, or surrogate models. These models are able to provide accurate results at a fraction of the time. Typically, these are generated with high-fidelity code evaluations that incorporate information about the response space in order to be parameterized. This is done by including information about the derivatives or by the use of multiple evaluations in the design space. One novel model of interest is the hyper-dual meta-model. This uses the exact derivative information at multiple design space locations to provide an information rich surrogate model with very few model evaluations. These methods are compared for three different systems with both material variations as well as geometric variation. The models are very useful for model calibration, as well as uncertainty distribution propagation to greatly reduce the computational cost for these methods.

During the design process, many engineering judgments are introduced. One of the major considerations is the type of numerical model to use. These choices can include type of finite element or how to model the material or joints. Since these choices can lead to very different results, a quantitative measure on how the choices affect the accuracy is desired. One possible method to characterize this model form error is presented and utilized. This method incorporates random matrices into the mechanical system to produce a stochastic model that has physically significant bounds, such as positive mass. These random matrices are generate non-parametrically

by a maximum entropy approach. The determination of these matrices are only constricted to physical bounds, such as positive mass, and the assumption that the nominal model is the mean of the random matrix. Using experimental data, the variance of the random matrix can be calibrated to give an estimate on the model form error. The more accurate the model, the lower the expected value of the variance for the random matrices. This method to determine the model form error is performed on four systems: one is a concentric glass-to-metal seal, while the other three are related to a substructured system where two component and the full system that those two create. The glass-to-metal seal uses temperature dependent, linear elastic material properties and is compared to experimentally derived material properties. This analysis uses the residual stress profile on the surface as validation data. The substructuring system uses the first 11 natural frequencies as validation data. This analysis is used to investigate the model reduction/synthesis technique and modal truncation.

Using the non-parametric maximum entropy approach can determine both the model form error along with a separate determination for parametric errors. This requires a large amount of computational resources due to the multiple MC simulations required. In order to reduce this burden, the use of a surrogate model is almost necessary. This final chapter implements the hyper-dual meta-model for the panel system to determine both parametric variance and model form error. The main difficulty is the additional truth data that is required. Independent data sets are required and can be either a scalar value or a vector of scalars. For this analysis, the Frobenius norm of the stiffness matrix and the first ten natural frequencies are used. This analysis shows a preliminary attempt of this specific analysis. Further work must be done on this analysis to ensure validity of the results.

The work presented in this dissertation presents a collection of work that has introduced novel advancements to established techniques and discovers new methodologies. This work utilizes

hyper-dual numbers for the use in uncertainty quantification of structural dynamics. These have been used for various other uses by other researchers, but the use within structural dynamics is novel and unique. The main new technique introduced in this work is the hyper-dual meta-model. This takes the advantages of other various parameterized reduced order modeling techniques and combines them into a single method to greatly increase the accuracy over a large variability range. Along with the parametric uncertainty, the study of model form error is also investigated. This study looked at the modeling choices of a reduced order model and in particular for substructuring type analysis. To the author's knowledge, no previous study has been done to propagate this model form error from a substructures into a synthesized system. Along with the propagation, this work also introduces the use of the empirical likelihood function into the determination of the optimal dispersion parameter in order to increase the repeatability and reduce the effect of the sampling technique.

6.2 Future Work

During the work in this dissertation, several suggested future work projects has been identified. The main two projects involve the implementation of hyper-dual numbers into a commercial finite element program, and an improvement on the calibration of the dispersion parameter in the non-parametric maximum entropy approach. The author's thoughts about each of these topics and some anticipated difficulties are explained in this section.

As a change in scale, there are also several smaller musings that require some investigation. One of these smaller projects is the investigation of the accuracy and cost of calculating higher-order derivatives using hyper-dual numbers. The increase in dimensions for the hyper-dual numbers comes with a large increase in terms. For the first derivative, only two terms are required, while the second and third derivative requires four and eight respectively. This major increase in terms comes

mainly in as all the required cross terms, such as ϵ_{12}. In terms of accuracy, there is no subtractive or truncation errors when calculating the derivatives. While these errors do not contribute, there is a phenomena where the computer precision decreases with the higher order derivatives. An initial thought of this cause is due to the precision on the multiplication and addition. When higher order terms are included, the scalar coefficients require more computer processes. In [59], Fike gives an analytical expression that the computer calculates on a simple problem. It can be seen that the ϵ_{12} term has more computational evaluations to perform, aka more multiplications, than the first derivative term. This increases greatly with more terms and thus has an effect of the higher order derivatives.

Another small project that would be very interesting is comparing the hyper-dual meta-model to a well established uncertainty method such as polynomial chaos. One interesting aspect is that the Hyper-Dual Meta-Model can use the exact same orthogonal polynomials and give a direct comparison and a good reason why the Hyper-Dual Meta-Model should be used. A lesson learned from looking into the NX-ROM is that it is a better comparison if there are two people working on the project. This ensures that the method is being performed at the highest level, and thus the best case for the method. The proposal of this round-robin is a good length and skill level for the Nonlinear Mechanics and Dynamics workshop at Sandia National Labs.

An interesting aspect of the non-parametric maximum entropy approach is the accuracy of the optimal dispersion parameter. One of the main goals of this analysis is to create a scalar value to describe the model form error of the system that can be compared to other models. Since this value is computed numerically, a tolerance interval on this dispersion parameter can give the customer an idea on how robust the model is to random variations. The current implementation is able to give a tolerance interval on the empirical likelihood function. Since the curve is generated by taking the minimum of the negative log-likelihood, the output distribution can be derived analytically

if the distribution on the negative log-likelihood is known. For the current implementation, the joint probability distribution is assigned a beta distribution. This distribution has a support of $[0, 1]$, which is the same support as the probability value. The distribution is then propagated through the analysis to give a tolerance interval for the empirical likelihood. For the future work, an investigation of relating the distribution on the empirical likelihood function to the tolerance interval of the dispersion parameter is suggested. Some extra work can be done in order to get a better distribution on the empirical likelihood. Assuming a beta distribution is a reasonable first approximation, but future work can include a better way to get this distribution, either non-parametrically or assigning a more accurate distribution.

The last smaller project that is identified involves the sampling of the random matrices used in the non-parametric maximum entropy approach. For large systems, such as the paneling system, the size of the random matrix makes an accurate Monte-Carlo analysis difficult computationally. These matrices have non-zero values at every index, thus reducing the memory requirement for this matrix is difficult. An investigation into reduced sampling methods for these matrix would greatly increase the usability of this technique. A preliminary attempt of the reduced sampling was presented by using an effective Latin Hypercube sampling. This method used in this work used the reduced sampling on the gamma and Gaussian random variables that are used in the generation of the random germ. While this was able to give an accelerated convergence compared to the traditional sampling. Further investigation into the reduced sampling methods for random matrices would provide a large computational decrease in the analysis and thus making it feasible for real-world systems.

6.2.1 Hyper-Dual Numbers

This major proposed project involves the advanced implementation of hyper-dual numbers to be used by a larger user-set. The implementation of hyper-dual numbers has two major required paths: commercial implementation and nonlinear implementation. Commercial implementation refers to using hyper-duals as a method of sensitivity analysis in a commercial code, such as Nastran. Similar implementation has been performed by Millwater's research group at the University of Texas at San Antonio. This uses the multi-complex step, which is similar to the hyper-dual step but less accurate, within Ansys for crack propagation with material variations. The main focus of this proposed work is on dynamic analysis for the field of structural dynamics and for geometric variations.

The implementation has two possible methods in order to perform the desired analysis. One method uses a matrix representation. This replaces a real number with a real matrix with a special form that is able to calculate derivatives exactly. One downfall of this method is that for hyper-dual numbers, this matrix is a lower tridiagonal matrix, which requires a different solver compared to the symmetric solvers traditionally used in commercial finite element codes. The other implementation is an object overload methodology. This replaces the basic operations, such as add and multiply, with the hyper-dual formulation. The current implementation within Matlab uses this object overload methodology. One downfall to this implementation is that the number of derivatives must be preprogrammed or programmed as a recursive evaluation.

The next work is to expand hyper-dual numbers into nonlinear analysis and time integration. A typical work flow of a nonlinear analysis uses a commercial code to extract linear information and post-process the information in a user-defined function within a program such as Matlab. One particular implementation of interest is in a jointed structure analysis. This typically uses a Newmark integrator in order to determine the interface forces at each time step. While implementation in Matlab, or a custom program, is the primary goal, the use of commercial codes for this solution

will also be investigated. Utilization of this method can be useful for several agencies such as: Sandia National Laboratories, NASA, and ATA engineering.

Another implementation of interest is in the generation of the nonlinear reduced order model, presented by Hollkamp, that uses multiple forcing cases from a commercial finite element code as data-points. Using hyper-dual numbers can produce additional information for each simulation run, thus reducing the total number of simulations needed to generate an accurate reduced order model. Besides the generation, the use of hyper-dual numbers can also give a robustness measure on the nonlinear model. This also allows for perturbation analysis that can be used for parameter distribution propagation. Using the sensitivities of the output, a Taylor series or meta-model can be used to generate either time history perturbation or stationary response perturbation, such as nonlinear normal modes. Doing this can show the robustness of a design or show how natural variations will change the system output.

6.2.2 Random Matrix Calibration

Another major project that is proposed for future work is the inclusion of an optimization routine into the calibration of the dispersion parameter in the non-parametric maximum entropy approach. The current methodology is to perform multiple parameter sweeps to find the optimal value. This can be very computationally expensive and unnecessary if the range on the sweep is far from the optimal dispersion value. The main suggested project is to create an optimization routine for the dispersion parameter.

One of the main problems that is experienced is that each evaluation is a MC simulation that calculates the joint probability. This objective function, the likelihood function, does have variations between simulations with the same input parameters. Due to this variation, using a gradient based optimization routine is difficult. A suggested routine is the Nelder-Mead algorithm,

which was developed to determine a maximum likelihood estimate for a distribution. Traditional uses of this algorithm uses an analytical distribution. By using the numerical distribution, this value become non-unique and difficult to determine a true value.

One possible course of action is to assign a distribution to the numerical samples. This would allow a smoother curve for the likelihood, but requires the engineering intuition of the selection of the distribution, but can be reasonable for certain systems and output data. This becomes especially difficult to determine a joint distribution when there are multiple outputs.

Acknowledgments

Portions of the work presented in this dissertation are conducted with support from Sandia National Laboratories. Sandia National Laboratories is a multi-mission laboratory managed and operated by National Technology and Engineering Solutions of Sandia, LLC., a wholly owned subsidiary of Honeywell International, Inc., for the U.S. Department of Energy?s National Nuclear Security Administration under contract DE-NA0003525.

APPENDIX

PUBLICATION LIST

Technical Journal Papers

- Bonney, M.S. and Kammer, D.C., Parameterization of Large Variability using the Hyper-Dual Meta-Model. Journal of VVUQ (In Submission)

Conference Papers

- Bonney, M.S. and Kammer, D.C., Parameterization of Large Variability using the Hyper-Dual Meta-Model. Proceedings of the 35th International Modal Analysis Conference, 2017
- Bonney, M.S., Kammer, D.C. and Brake, M.R.W., Numerical Investigation of Probability Measures Utilized in a Maximum Entropy Approach. Proceedings of the International Conference on Uncertainty in Structural Dynamics, 2016.
- Bonney, M.S., Kammer D.C. and Brake, M.R.W., Determining Model Form Uncertainty of Reduced Order Models. Proceedings of the 34rd International Modal Analysis Conference, 2016.
- Bonney, M.S., Robertson, B.A., Schempp, F., Mignolet, M. and Brake, M.R.W., Experimental Determination of Frictional Interface Models. Proceedings of the 34rd International Modal Analysis Conference, 2016.
- Bonney M.S., Kammer D.C., and Brake M.R.W., Fully Parameterized Reduced Order Models Using Hyper-Dual Numbers and Component Mode Synthesis. Proceedings of the ASME 2015 International Design Engineering Technical Conferences & Computers and Information in Engineering Conference, 46029, 2015.
- Kammer D.C., and Bonney M.S., Improved Estimation of Frequency Response Covariance. Proceedings of the 33rd International Modal Analysis Conference, 2015.
- Robertson, B.A., Bonney, M.S., Gastaldi, C., and Brake, M.R.W., Quantifying Epistemic and Aleatoric Uncertainty in the Ampair 600 Wind Turbine. Proceedings of the 33rd International Modal Analysis Conference, 2015.

Peer Reviewed SAND Reports

- Bonney, M.S., Calibration of Rolamite to Historical Centrifuge Data. Technical Report, Sandia National Laboratories, Albuquerque, NM, 2017. (In Review)

- Bonney, M.S., et al., Implementation of Stochastic Modeling and Hyper-Dual Meta-Model for the Concentric Glass-to-Metal Seal Model. Technical Memo, Sandia National Laboratories, Albuquerque, NM. 2017

- Bonney M.S., and Brake M.R.W., Determining Reduced Order Models for Optimal Stochastic Reduced Order Models. Technical Report SAND2015-6896, Sandia National Laboratories, Albuquerque, NM, 2015.

- Bonney M.S., and Brake M.R.W., Utilizing Soize's Approach to Idetify Parameter and Model Uncertainties. Technical Report SAND2014-19209, Sandia National Laboratories, Albuquerque, NM, 2014.

BIBLIOGRAPHY

[1] Bendsoe M.P. and Sigmund O. *Topology Optimization: Theory, Methods, and Applications*. Springer Science & Business Media, 2013.

[2] Craig R.R. and Bampton M.C.C. Coupling of Substructures for Dynamic Analysis. *AIAA Journal 6*, pages 1313–1319, 1968.

[3] Klerk D., Rixen D.J., and Voormeeren S.N. General Framework for Dynamic Substructuring: History, Review and Classification of Techniques. *AIAA journal*, 46(5):1169–1181, 2008.

[4] Craig R.R. Substructure Methods in Vibration. *Journal of Vibration and Acoustics*, 117(B):207–213, 1995.

[5] Kammer D.C. and Triller M.J. Selection of Component Modes for Craig-Bampton Substructure Representations. *ASME J. Vib. Acoust.*, 188(2):264–270, 1996.

[6] MacNeal R.H. A Hybrid Method of Component Mode Synthesis. *Computers & Structures*, 1(4):581–601, 1971.

[7] Rubin S. Improved Component-Mode Representation for Structural Dynamic Analysis. *AiAA Journal*, 13(8):995–1006, 1975.

[8] Craig R.R. and Chang C.J. On the Use of Attachment Modes in Substructure Coupling for Dynamic Analysis. *18th Structural Dynamics and Materials Conference, Structures, Structural Dynamics, and Materials and Co-located Conferences*, 1977.

[9] Rixen D.J. A Dual Craig–Bampton Method for Dynamic Substructuring. *Journal of Computational and applied mathematics*, 168(1):383–391, 2004.

[10] Craig R.R. and Kurdila A.J. *Fundamentals of Structural Dynamics*. John Wiley and Sons, Inc., 2nd edition, 2006.

[11] Afriat S.N. Orthogonal and Oblique Projectors and the Characteristics of Pairs of Vector Spaces. In *Mathematical Proceedings of the Cambridge Philosophical Society*, volume 53, pages 800–816. Cambridge Univ Press, 1957.

[12] Kammer D.C. A Hybrid Approach to Test-Analysis-Model Development for Large Space Structures. *Journal of Vibration and Acoustics*, 113(3):325–332, 1991.

[13] Chatterjee A. An Introduction to the Proper Orthogonal Decomposition. *Current science*, 78(7):808–817, 2000.

[14] Stewart G.W. Perturbation Theory for the Singular Value Decomposition. 1998.

[15] Bonney M.S. and Brake M.R.W. Determining Reduced Order Models for Optimal Stochastic Reduced Order Models. Technical Report SAND2015-6896, Sandia National Laboratories, Albuquerque, NM, 2015.

[16] Castanier M.P., Tan Y., and Pierre C. Characteristic Constraint Modes for Component Mode Synthesis. *AIAA journal*, 39(6):1182–1187, 2001.

[17] Kuether R.J. and Allen M.S. Substructuring with Nonlinear Reduced Order Models and Interface Reduction with Characteristic Constraint Modes. In *55th AIAA/ASMe/ASCE/AHS/SC Structures, Structural Dynamics, and Materials Conference*, page 1518, 2014.

[18] Metropolis N. and Ulam S. The Monte Carlo Method. *Journal of the American Statistical Association*, 44(247):335–341, 1949.

[19] Shapiro A. and Homem de Mello T. On the Rate of Convergence of Optimal Solutions of Monte Carlo Approximations of Stochastic Programs. *SIAM Journal on Optimization*, 11(1):70–86, 2000.

[20] McKay M.D., Beckman R.J., and Conover W.J. Comparison of Three Methods for Selecting Values of Input Variables in the Analysis of Output From a Computer Code. *Technometrics*, 21(2):239–245, 1979.

[21] Helton J.C., Johnson J.D., Sallaberry C.J., and Storlie C.B. Survey of Sampling-Based Methods for Uncertainty and Sensitivity Analysis. *Reliability Engineering & System Safety*, 91(10):1175–1209, 2006.

[22] Helton J.C. and Davis F.J. Latin Hypercube Sampling and the Propagation of Uncertainty in Analyses of Complex Systems. *Reliability Engineering & System Safety*, 81(1):23–69, 2003.

[23] Warner J.E., Grigoriu M., and Aquino W. Stochastic Reduced Order Models for Random Vectors: Application to Random Eigenvalue Problems. *Probabilistic Engineering Mechanics*, 31:1–11, 2013.

[24] Emery J.M., Field R.V., Foulk J.W., Karlson K.N., and Grigoriu M.D. Predicting laser weld reliability with stochastic reduced-order models. *International Journal for Numerical Methods in Engineering*, 2015.

[25] Moens D. and Vandepitte D. A Survey of Non-Probabilistic Uncertainty Treatment in Finite Element Analysis. *Computer methods in applied mechanics and engineering*, 194(12):1527–1555, 2005.

[26] Hasselman T.K., Chrostowski J.D., and Ross T.J. Propagation of Modeling Uncertainty Through Structural Dynamic Models. In *35th Structures, Structural Dynamics, and Materials Conference, Hilton Head, SC*, pages 72–83, 1994.

[27] Li Y., Chen J., and Feng L. Dealing With Uncertainty: a Survey of Theories and Practices. *Knowledge and Data Engineering, IEEE Transactions on*, 25(11):2463–2482, 2013.

[28] Zadeh L.A. Fuzzy Sets. *Information and control*, 8(3):338–353, 1965.

[29] Ben-Haim Y. Info-gap Value of Information in Model Updating. *Mechanical Systems and Signal Processing*, 15(3):457–474, 2001.

[30] Ben-Haim Y. Uncertainty, Probability and Information-gaps. *Reliability Engineering & System Safety*, 85(1):249–266, 2004.

[31] Moore R.E. *Interval Analysis*, volume 4. Prentice-Hall Englewood Cliffs, 1966.

[32] Moore R.E., Bierbaum F., and Schwiertz K. *Methods and Applications of Interval Analysis*, volume 2. SIAM, 1979.

[33] Koyluoglu H.U. Interval Algebra to Deal with Pattern Loading and Structural Uncertainties. In *Proc. ASCE*, volume 121, pages 1149–1158, 1995.

[34] Ferson S. and Tucker W.T. Sensitivity Analysis Using Probability Bounding. *Reliability Engineering & System Safety*, 91(10):1435–1442, 2006.

[35] Muhanna R.L. and Mullen R.L. Uncertainty in Mechanics Problems-Interval-Based Approach. *Journal of Engineering Mechanics*, 127(6):557–566, 2001.

[36] Swiler L.P., Paez T.L., and Mayes R.L. Epistemic Uncertainty Quantification Tutorial. In *Proceedings of the 27th International Modal Analysis Conference*, 2009.

[37] Eldred M.S., Swiler L.P., and Tang G. Mixed Aleatory-Epistemic Uncertainty Quantification with Stochastic Expansions and Optimization-Based Interval Estimation. *Reliability Engineering & System Safety*, 96(9):1092–1113, 2011.

[38] Wiener N. The Homogeneous Chaos. *American Journal of Mathematics*, 60(4):897–936, 1938.

[39] Xiu D. and Karniadakis G.E. The Wiener–Askey Polynomial Chaos for Stochastic Differential Equations. *SIAM journal on scientific computing*, 24(2):619–644, 2002.

[40] Sandu A., Sandu C., and Ahmadian M. Modeling Multibody Systems with Uncertainties. Part I: Theoretical and Computational Aspects. *Multibody System Dynamics*, 15(4):369–391, 2006.

[41] Sandu C., Sandu A., and Ahmadian M. Modeling Multibody Systems With Uncertainties. Part II: Numerical Applications. *Multibody System Dynamics*, 15(3):241–262, 2006.

[42] Kewlani G., Crawford J., and Iagnemma K. A polynomial chaos approach to the analysis of vehicle dynamics under uncertainty. *Vehicle System Dynamics*, 50(5):749–774, 2012.

[43] O'Hagan A. Polynomial Chaos: A Tutorial and Critique From a Statisticians Perspective. *SIAM/ASA J. Uncertainty Quantification*, 20:1–20, 2013.

[44] Kammer D.C. and Krattiger D. Propagation of Uncertainty in Substructed Spacecraft Using Frequency Response. *AIAA Journal*, 51(2):353–361, 2013.

[45] Kammer D.C. and Bonney M.S. Improved Estimation of Frequency Response Covariance. *Proceedings of the 33rd International Modal Analysis Conference*, 2014.

[46] Falsone G. and Impollonia N. A New Approach for the Stochastic Analysis of Finite Element Modelled Structures with Uncertain Parameters. *Computer Methods in Applied Mechanics and Engineering*, 191(44):5067–5085, 2002.

[47] Falsone G. and Ferro G. A method for the Dynamical Analysis of FE Discretized Uncertain Structures in the Frequency Domain. *Computer methods in applied mechanics and engineering*, 194(42):4544–4564, 2005.

[48] Falsone G. and Ferro G. An Exact Solution for the Static and Dynamic Analysis of FE Discretized Uncertain Structures. *Computer Methods in Applied Mechanics and Engineering*, 196(21):2390–2400, 2007.

[49] Winkler R.L. *An Introduction to Bayesian Inference and Decision*. Holt, Rinehart and Winston New York, 1972.

[50] Box G.E.P. and Tiao G.C. *Bayesian Inference in Statistical Analysis*, volume 40. John Wiley & Sons, 2011.

[51] Dempster A.P. A Generalization of Bayesian Inference. *Journal of the Royal Statistical Society. Series B (Methodological)*, pages 205–247, 1968.

[52] Box G.E.P. Sampling and Bayes' Inference in Scientific Modelling and Robustness. *Journal of the Royal Statistical Society. Series A (General)*, pages 383–430, 1980.

[53] Park I., Amarchinta H.K., and Grandhi R.V. A Bayesian Approach for Quantification of Model Uncertainty. *Reliability Engineering & System Safety*, 95(7):777–785, 2010.

[54] Riley M.E. *Quantification of Model-Form, Predictive, and Parametric Uncertainties in Simulation-Based Design*. PhD thesis, Wright State University, 2011.

[55] Gamerman D. and Lopes H.F. *Markov Chain Monte Carlo: Stochastic Simulation for Bayesian Inference*. CRC Press, 2006.

[56] Beck J.L. and Katafygiotis L.S. Updating Models and Their Uncertainties. I: Bayesian Statistical Framework. *Journal of Engineering Mechanics*, 124(4):455–461, 1998.

[57] Katafygiotis L.S. and Beck J.L. Updating Models and Their Uncertainties. II: Model Identifiability. *Journal of Engineering Mechanics*, 124(4):463–467, 1998.

[58] Fike J.A., Jongsma S., Alonso J.J., and Van Der Weide E. Optimization with Gradient and Hessian Information Calculated using Hyper-Dual Numbers. *AIAA paper*, 3807:2011, 2011.

[59] Fike J.A. and Alonso J.J. The Development of Hyper-Dual Numbers for Exact Second-Derivative Calculations. *AIAA paper*, 886:124, 2011.

[60] Fike J.A. *Multi-Objective Optimization using Hyper-Dual Numbers*. PhD thesis, Stanford university, 2013.

[61] Martins J.R.R.A., Sturdza P., and Alonso J.J. The Connection Between the Complex-Step Derivative Approximation and Algorithmic Differentiation. *AIAA paper*, 921:2001, 2001.

[62] Fornberg B. Generation of Finite Difference Formulas on Arbitrarily Spaced Grids. *Mathematics of computation*, 51(184):699–706, 1988.

[63] Martins J.R.R.A., Sturdza P., and Alonso J.J. The Complex-Step Derivative Approximation. *ACM Transactions on Mathematical Software (TOMS)*, 29(3):245–262, 2003.

[64] Lai K.L. and Crassidis J.L. Extensions of the First and Second Complex-Step Derivative Approximations. *Journal of Computational and Applied Mathematics*, 219(1):276–293, 2008.

[65] Lantoine G., Russell R.P., and Dargent T. Using Multicomplex Variables for Automatic Computation of High-Order Derivatives. *ACM Trans. Math. Softw.*, 38(3):16:1–16:21, April 2012.

[66] Garza J. and Millwater H. Sensitivity Analysis in Structural Dynamics using the ZFEM Complex Variable Finite Element Method. In *54th AIAA/ASME/ASCE/AHS/ASC Structures, Structural Dynamics, and Materials Conference*, page 1580, 2013.

[67] Garza J. and Millwater H. Multicomplex Newmark-Beta Time Integration Method for Sensitivity Analysis in Structural Dynamics. *AIAA Journal*, 53(5):1188–1198, 2015.

[68] Fike J.A. and Alonso J.J. Automatic Differentiation Through the Use of Hyper-Dual Numbers for Second Derivatives. In *Recent Advances in Algorithmic Differentiation*, pages 163–173. Springer, 2012.

[69] Bonney M.S., Kammer D.C., and Brake M.R.W. Fully Parameterized Reduced Order Models Using Hyper-Dual Numbers and Component Mode Synthesis. *Proceedings of the ASME 2015 International Design Engineering Technical Conferences & Computers and Information in Engineering Conference*, 46029, 2015.

[70] Craig R.R. Coupling of Substructures for Dynamic Analyses - An overview. *41st Structures, Structural Dynamics, and Materials Conference and Exhibit, Structures, Structural Dynamics, and Materials and Co-located Conferences*, 2000.

[71] Brake M.R.W., Fike J.A., and Topping S.D. Parameterized Reduced Order Models from a Single Mesh Using Hyper-Dual Numbers. *Journal of Sound and Vibration*, in press.

[72] Brake M.R.W., Fike J.A., and Topping S.D. Parameterized Reduced Order Models from a Single Mesh Using Hyper-Dual Numbers. Technical report, Sandia National Laboratories (SNL-NM), Albuquerque, NM (United States), 2014.

[73] Fox E. The Pratt & Whitney Probabilistic Design System. In *35th Structures, Structural Dynamics, and Materials Conference*, page 1442, 1994.

[74] Hong S.K., Epureanu B.I., and Castanier M.P. Next-Generation Parametric Reduced-Order Models. *Mechanical Systems and Signal Processing*, 37(1):403–421, 2013.

[75] Brake M.R.W., Reuss P., Schwigshackl C.W., Salles L., Negus M.E., Peebles D.E., Mayes R.L., Bilbao-Ludena J.C., Bonney M.S., Catalfamo S., Gastaldi C., Gross J., Lacayo R.M., Robertson B.A., Smith S., Swacek C., and Tiedemann M. The 2014 Sandia Nonlinear Mechanics and Dynamics Summer Research Institute. Technical Report SAND2015-1876, Sandia National Laboratories Livermore, CA; Sandia National Laboratories (SNL-NM), Albuquerque, NM (United States), 2015.

[76] Brake M.R.W, Reuss P., Segalman D.J., and Gaul L. Variability and Repeatability of Jointed Structures with Frictional Interfaces. In *IMAC XXXII A Conference and Exposition on Structural Dyanimcs*, February 2014.

[77] Bonney M.S., Robertson B.A., Mignolet M., Schempp F., and Brake M.R.W. Experimental Determination of Frictional Interface Models. In *Dynamics of Coupled Structures, Volume 4*, pages 473–490. Springer International Publishing, 2016.

[78] Emery J.M., Field R.V., Foulk J.W., and Grigoriu M.D. Stochastic Reduced-Order Models for Multi-Scale Simulation of Laser Weld Failure. Technical report, Sandia National Laboratories Livermore, CA; Sandia National Laboratories (SNL-NM), Albuquerque, NM (United States), 2013.

[79] Michael S. Large Sample Properties of Simulations Using Latin Hypercube Sampling. *Technometrics*, 29(2):143–151, 1987.

[80] Bonney M.S., Kammer D.C., and Brake M.R.W. Numerical Investigation of Probability Measures Utilized in a Maximum Entropy Approach. In *Uncertainty in Structural Dynamics*, pages 4307–4321, 2016.

[81] Robertson B.A., Bonney M.S., Gastaldi C., and Brake M.R.W. Quantifying Epistemic and Aleatoric Uncertainty in the Ampair 600 Wind Turbine. *Proceedings of the 33rd International Modal Analysis Conference*, 2014.

[82] Soize C. Random Matrix Theory for Modeling Uncertainties in Computational Mechanics. *Computer Methods in Applied Mechanics and Engineering*, 194:1333–1366, 2004.

[83] Soize C. Generalized Probabilistic Approach of Uncertainties in Computational Dynamics Using Random Matrices and Polynomial Chaos Decompositions. *International Journal for Numerical Methods in Engineering*, pages 1–32, 2009.

[84] Bonney M.S. and Brake M.R.W. Utilizing Soize's Approach to Idetify Parameter and Model Uncertainties. Technical Report SAND2014-19209, Sandia National Laboratories, Albuquerque, NM, 2014.

[85] Soize C. Maximum Entropy Approach for Modeling Random Uncertainties in Transient Elastodynamics. *Journal of Acoustical Society of America*, 5:1979–1994, 2001.

[86] Batou A., Soize C., and Audebert S. Model Identification in Computational Stochastic Dynamics Using Experimental Modal Data. *Mechanical Systems and Signal Processing*, 50-51:Pages: 307–322, 2014.

[87] Adhikari S. Matrix Variate Distributions for Probabilistic Structural Dynamics. *AIAA journal*, 45(7):1748–1762, 2007.

[88] Adhikari S. Wishart Random Matrices in Probabilistic Structural Mechanics. *Journal of engineering mechanics*, 134(12):1029–1044, 2008.

[89] Jamison R.D., Gorman P.H., Rodelas J., MacCallum D.O., Neidigk M., and Dempsey J.F. Analysis of Laser Weld Induced Stress in a Hermetic Seal. In *Residual Stress, Thermomechanics & Infrared Imaging, Hybrid Techniques and Inverse Problems, Volume 9*, pages 199–207. Springer, 2016.

[90] Chambers R.S., Tandon R., and Stavig M.E. Characterization and Calibration of a Viscoelastic Simplified Potential Energy Clock Model for Inorganic Glasses. *Journal of Non-Crystalline Solids*, 432, Part B:545 – 555, 2016.

[91] Qi H.J., Antoun B., Hall R., Lu H., Arzoumanidis A., Silberstein M., Furmanski J., Amirkhizi A., and Gonzalez-Gutierrez J. *Challenges in Mechanics of Time-Dependent Materials, Volume 2*. Springer, 2016.